

AD-A151 835

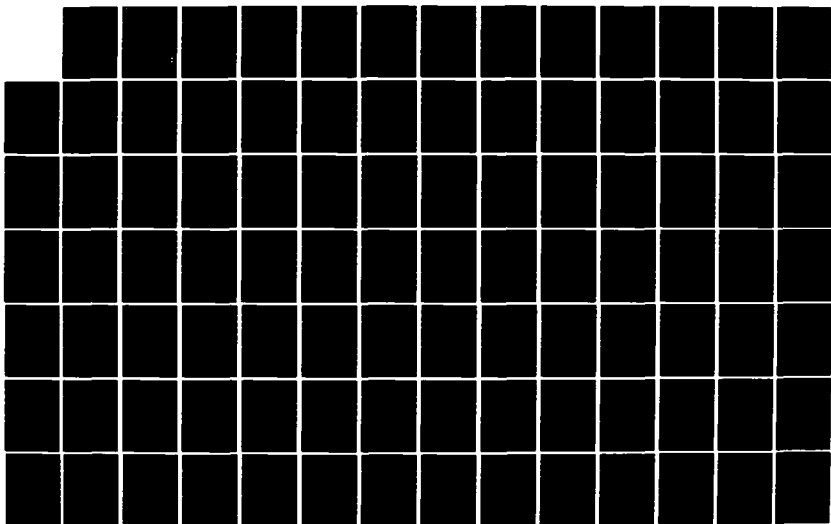
TRANSITION REGION FOR CORNER CRACKS AT HOLES(U) AIR
FORCE INST OF TECH WRIGHT-PATTERSON AFB OH SCHOOL OF
ENGINEERING P A CHANSLER DEC 84 AFIT/GAE/AA/84D-4

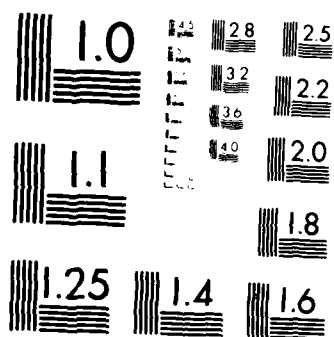
1/2

UNCLASSIFIED

F/G 11/6

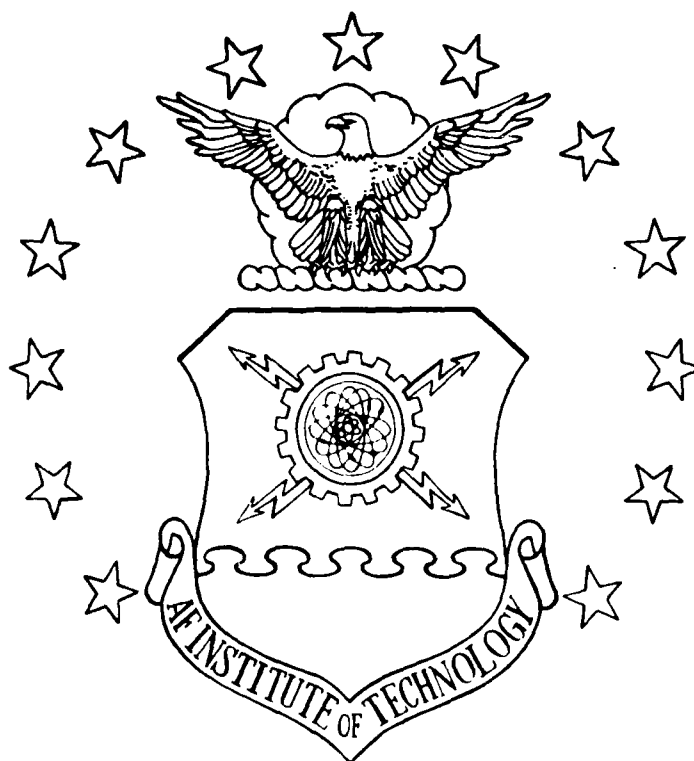
NL





MICROCOPY RESOLUTION TEST CHART
NATIONAL BUREAU OF STANDARDS-1963-A

AD-A151 835



TRANSITION REGION FOR CORNER
CRACKS AT HOLES

THESIS

Phillip A. Chansler
Captain, USAF

AFIT/GAE/AA/84D-4

DTIC FILE COPY

This document has been approved
for public release and sale; its
distribution is unlimited.

DEPARTMENT OF THE AIR FORCE
AIR UNIVERSITY

AIR FORCE INSTITUTE OF TECHNOLOGY

DTIC
ELECTE

APR 01 1985

E

Wright-Patterson Air Force Base, Ohio

85 03 13 086

AFIT/GAE/AA/84D-4

TRANSITION REGION FOR CORNER
CRACKS AT HOLES

THESIS

Phillip A. Chansler
Captain, USAF

AFIT/GAE/AA/84D-4

Approved for public release; distribution unlimited

TRANSITION REGION FOR CORNER CRACKS AT HOLES

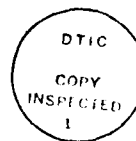
THESIS

Presented to the Faculty of the School of Engineering
of the Air Force Institute of Technology
Air University
In Partial Fulfillment of the
Requirements for the Degree of
Master of Science in Aeronautical Engineering

Phillip A. Chansler, B.S.M.E., M.S.S.M.

Captain, USAF

December 1984



Accountant for
R. H.
R. H.
U.S.
District Court

District
Court

A-1

TABLE OF CONTENTS

Acknowledgements	iv
List of Figures	v
List of Tables	viii
Abstract	x
I. Introduction	1
Motivation	1
Background	2
Scope	10
Approach	12
II. Experimental Program	15
Material Characterization Tests	15
Corner Crack at a Hole Tests	26
III. Experimental Stress Intensity Factors	32
Stress Intensity Factors for the Front and Back Surfaces	32
IV. Analytical Stress Intensity Factors	45
Newman-Raju Solution for Corner Cracks at a Hole	45
Grandt's Linearization of Bowie's Solution	52
Opel's Correction Factors	52
V. Development of Transition Criteria	55
The Transition Region	55
Analytical/Experimental Correlations	62
Correction Factor Development	63
Summary of Transition Region	70
VI. Evaluation of Transition Criteria	71
Life Prediction Models Used	71
Results	72
Discussion of Results	85
VII. Conclusions and Recommendations	93
Appendix: Computer Programs Used for Life Predictions	96
Bibliography	113
Vita	118

Acknowledgements

First and foremost, I would like to gratefully acknowledge the sponsorship of Jim Rudd and the Fatigue and Fracture Group of the Flight Dynamics Laboratory, Air Force Wright Aeronautical Laboratories. The Group provided the test facilities, equipment and the money. Jim Rudd provided the expertise, patience and friendship. It was not only a challenge working with Jim, but fun as well. It was refreshing to work with someone who is an expert in his field and willing to share his knowledge. Next, I would like to thank my advisor, Major Haritos. Without his patience, understanding and guidance I would have never completed this work. He told me to panic when I should and relax when all was well. That kept me sane. Speaking of sanity, the group in room 142 helped me keep my motivation. Casey, Neil and Bruce. Without your friendship, comraderie and computer expertise I'd be at AFIT for years! Thanks. And last but not least, I want to thank my typist, Sue Davis. (This was a bigger project than we both expected, wasn't it!!) I was a real slave driver, and you still fed me when I was hungry. You're wonderful, thanks.

List of Figures

Figure	Page
1. Crack Configurations as it Transitions from Corner Crack to a Through-the-Thickness Crack	12
2. Center Crack Tension (CCT) Specimen Geometry for Specimens used in Material Characterization	16
3. Material Characterization Data: Crack Length vs. Life (cycles), $R = 0.1$	17
4. Material Characterization Data: Crack Length vs. Life (cycles), $R = 0.5$	18
5. Material Characterization Data: Crack Length vs. Life (cycles), $R = -0.5$	19
6. Schematic of James-Anderson Backtracking Technique	21
7. Material Characterization Data: Maximum Stress Intensity Factor vs. Crack Growth Rate, $R = 0.1$	22
8. Material Characterization Data: Maximum Stress Intensity Factor vs. Crack Growth Rate, $R = 0.5$	23
9. Material Characterization Data: Maximum Stress Intensity Factor vs. Crack Growth Rate, $R = -0.5$	24
10. Specimen Geometry for Specimens used for Mechanical Property Tests	27
11. Corner-Crack-at-a-Hole Test Specimens Geometry	28
12. Corner-Crack-at-a-Hole Test Data: Front Surface Crack Length vs. Crack Growth Rate; $\sigma_{max} = 18$ ksi, $R = 0.1$	33
13. Corner-Crack-at-a-Hole Test Data: Front Surface Crack Length vs. Crack Growth Rate; $\sigma_{max} = 18$ ksi, $R = 0.3$	33
14. Corner-Crack-at-a-Hole Test Data: Front Surface Crack Length vs. Crack Growth Rate; $\sigma_{max} = 18$ ksi, $R = 0.5$	34

15.	Corner-Crack-at-a-Hole Test Data: Front Surface Crack Length vs. Crack Growth Rate; $\sigma_{\max} = 15$ ksi, $R = 0.1$	35
16.	Corner-Crack-at-a-Hole Test Data: Front Surface Crack Length vs. Crack Growth Rate; $\sigma_{\max} = 15$ ksi, $R = 0.3$	36
17.	Corner-Crack-at-a-Hole Test Data: Front Surface Crack Length vs. Crack Growth Rate; $\sigma_{\max} = 15$ ksi, $R = -0.5$	37
18.	Corner-Crack-at-a-Hole Test Data: Back Surface Crack Length vs. Crack Growth Rate; $\sigma_{\max} = 18$ ksi, $R = 0.1$	38
19.	Corner-Crack-at-a-Hole Test Data: Back Surface Crack Length vs. Crack Growth Rate; $\sigma_{\max} = 18$ ksi, $R = 0.3$	39
20.	Corner-Crack-at-a-Hole Test Data: Back Surface Crack Length vs. Crack Growth Rate; $\sigma_{\max} = 18$ ksi, $R = -0.5$	40
21.	Corner-Crack-at-a-Hole Test Data: Back Surface Crack Length vs. Crack Growth Rate; $\sigma_{\max} = 15$ ksi, $R = 0.1$	41
22.	Corner-Crack-at-a-Hole Test Data: Back Surface Crack Length vs. Crack Growth Rate; $\sigma_{\max} = 15$ ksi, $R = 0.3$	42
23.	Corner-Crack-at-a-Hole Test Data: Back Surface Crack Length vs. Crack Growth Rate; $\sigma_{\max} = 15$ ksi, $R = -0.5$	43
24.	Effects of Mesh Refinement Near the Free Surface on the Distribution of Boundary-Correction Factors for Surface Cracks at a Hole	48
25.	Transition Regions Considered	53
26.	Comparison of the Opet Transition Region for Specimens of Different Thickness	60
27.	Correlations of Stress Intensity Factors Along the Front Surface for 2024-T651 Aluminum Tests	64

28.	Correlations of Stress Intensity Factors Along the Front Surface for 7075-T651 Aluminum Tests	65
29.	Correlations of Stress Intensity Factors Along the Back Surface for 2024-T651 Aluminum	66
30.	Correlations of Stress Intensity Factors Along the Back Surface for 7075-T651	67
31.	Correlations of Stress Intensity Factors Along the Back Surface for 2024-T351 and 7075-T651 Aluminum Tests (Correction Factor Plotted)	67
32.	Correlations of Stress Intensity Factors Along the Front Surface for 2024-T351 and 7075-T651 Aluminum Tests (Correction Factor Plotted)	69
33.	The Collipriest-Ehret Transition Region	86

List of Tables

Table	Page
1. Comparison of Results. Instantaneous vs. Opel's Model for 2024-T351 Aluminum	13
2. 2024-T351 Aluminum Test Condition (a_i , c_i are average of duplicate specimens)	29
3. Parametric Angle Effect for 2024-T351 Aluminum Using Newman-Bowie (Uncorrected)	50
4. Parametric Angle Effect for 7075-T651 Aluminum Using Newman-Bowie (Uncorrected)	51
5. Comparison of Life to Back Surface Penetration for Different Parametric Angles Using Newman-Raju (Uncorrected) for 2024-T351 Aluminum	57
6. Comparison of Life to Back Surface Penetration for Different Parametric Angles Using Newman-Raju (Uncorrected) for 7075-T651 Aluminum	58
7. 7075-T651 Aluminum Test Condition (a_i , c_i are average of duplicate specimens) from Opel [5]	73
8. Experimental Life for 2024-T351 Aluminum (Averages of Duplicate Specimens)	74
9. Experimental Life for 7075-T651 Aluminum (Averages of Duplicate Specimens) from Opel [5]	75
10. Life Prediction (Corrected Newman-Bowie) for 2024-T351 Aluminum	77
11. Life Prediction (Corrected Newman-Bowie) for 7075-T651 Aluminum	78
12. Life Prediction (Instantaneous/Newman-Bowie Uncorrected) for 2024-T351 Aluminum	79
13. Life Prediction (Instantaneous/Newman-Bowie Uncorrected) for 7075-T651 Aluminum	80
14. Life Prediction, Opel's Model for 7075-T651 Aluminum	81
15. Life Prediction (Brussat) for 2024-T351 Aluminum	83

16.	Life Prediction (Brussat) for 7075-T651 Aluminum	84
17.	Life Prediction (Collipriest-Ehret) for 2024-T351 Aluminum	87
18.	Life Prediction (Collipriest-Ehret) for 7075-T651 Aluminum	88
19.	Percent Total Life Ratios for All Models Considered for 2024-T351 Aluminum	89
20.	Percent Total Life Ratios for All Models Considered for 7075-T651 Aluminum	90

ABSTRACT

This study develops correction factors for currently used stress intensity factor equations to more accurately predict stress intensity factors for a corner-crack emanating from a hole as it transitions to a uniform through-the-thickness crack. These correction factors resulted in an increase in accuracy for total life prediction and much better correlation between analytical stress intensity factor predictions and experimental results in the transition region for 2024-T351 and 7075-T651 aluminum alloys. An experimental program was undertaken to generate all 2024-T351 aluminum test data used in this investigation. The 7075-T651 aluminum test data was generated during earlier work. Correction factors developed by Opel for 7075-T651 aluminum were evaluated for 2024-T351 aluminum and found to be excessively conservative.

Hartranft and Sih suggested the stress intensity factors be evaluated at an imaginary surface at an angle ϕ away from the front and hole-bore surfaces. These stress intensity factors could then be used in the life prediction models for life from a corner-crack until back surface penetration. Evaluating stress intensity factors at $\phi = 10^\circ$ and 80° eliminate surface boundary effects caused by fabrication processes like cold rolling and hole drilling, thereby improving life predictions to back surface penetration significantly. It is shown that with $\phi = 10^\circ$ and 80° , no other corrections are necessary for life

prediction to back surface penetration.

A transition region is postulated to effect life prediction from back surface penetration until final fracture. Correlations were made between experimental results for 2024-T351 and 7075-T651 aluminum test data and the Grandt linearization of the Bowie solution for a through-the-thickness crack. These correlations were plotted from back surface penetration until final fracture. The plot yields the end of the transition region and the required correction factors. The life prediction model incorporating these transition correction factors are shown to be the most accurate and versatile of all models investigated.

Life predictions were made using the new model, an instantaneous model (which assumes a through-crack at back surface penetration), Opel's model, Brussat's model and the Collipriest-Ehret model.

1.0 INTRODUCTION

1.1. Motivation

Cracks in aerospace structural components continue to cause problems ranging from premature retirement of parts to catastrophic failures. These problems result in the loss of millions of dollars annually to the aerospace industry and have caused loss of life in certain cases. A good deal of progress has been made over the past several years to eliminate the conditions leading to crack initiation and growth. However, flaws due to material defects, manufacturing methods, and in-service conditions will always be present. Therefore, in order to correctly predict component fatigue life, a life-prediction method which assumes the presence of flaws at the onset of the component operational usage is required.

In 1971, the United States Air Force (USAF) sponsored an in-depth review of aerospace structural failures (Gran et al,[1]). This review showed that the predominate failure mechanism was cracks emanating from fastener holes. In fact, over one-third of all failures studied were due to cracks emanating from fastener holes. As a result of this review the USAF recently adopted a damage-tolerant design philosophy to ensure that catastrophic failures are not caused by cracks emanating from fastener holes. This philosophy was introduced by Wood and Engle [2] and is based on Linear Elastic Fracture Mechanics (LEFM).

This fracture mechanics analysis of cracks at fastener holes requires knowledge of the stress intensity factor, K , for all crack geometries of interest. Since the crack length within the bore of the hole cannot be accurately measured, a combination of analytical crack solutions must be used. Exact analytical expressions for stress intensity factors have been derived for cases involving very small flaws in infinite (very large) elastic bodies (e.g., Williams [3], [4]). These solutions have to be modified for finite problems by the inclusion of correction factors. These correction factors are generally derived using experimental data and backtracking techniques, finite element approximations, or any of various other approximate methods (see e.g. see references [5]-[11], which are used in this work). The stress intensity factors are functions of the test-specimen geometry, loading, and crack geometry. Many works published over the past several years have dealt with estimating and/or calculating stress intensity factors, and the most significant of these works are discussed in the next section.

1.2 Background

1.2.1. Previous Work on Stress Intensity Factors for Corner-Cracks Emanating from a Hole. In 1956, Bowie [12] made the first major contribution to the problem of cracks emanating from holes, specifically, cracks emanating from open holes in plates. Using complex variable methods, Bowie solved the two dimensional problem of

single and double through-cracks at an open hole. Bowie's work is significant in that although it is not an exact solution, it is universally used as a basis for comparison with other studies of cracks emanating from holes. More importantly, Bowie's solution is also widely used to establish the accuracy of other methods which attempt to solve more complicated crack problems.

Bowie's solution was improved upon in 1972 by Liu [13]. He studied the quarter-elliptical crack at a hole in a plate and superimposed a number of solutions for his approximation. He used the Smith et al. solution [14] to account for the hole surface and the front surface of the specimen and Kobayashi's solution [15] as a correction for the back surface. These approximations were superimposed on Bowie's [12] two dimensional approximation of the three-dimensional hole effect. This did not, however, result in a solution and only gave stress intensity estimates at a point on the periphery of the crack, midway between the front of the specimen and the surface of the hole.

A unique approach to the solution of the single through-crack problem was presented by Tweed and Rooke in 1973 [16]. They derived stress-intensity factor relations using a Mellin integral transform technique. This method provided a substantial improvement over the Bowie solution, especially for small crack lengths.

Grandt [10] used the principle of superposition to develop a stress intensity factor solution for large plates containing radial holes with through-the-thickness cracks loaded with arbitrary crack-face pressure. Grandt's method is based on work by Rice [17], who showed that once the displacement field and stress intensity factor are known for one geometry and loading, K_I the stress intensity factor for mode I deformation may be obtained for any other symmetric loading applied to the same crack geometry. Grandt [10] used a remote, uniform tensile stress as the known loading, crack-tip stresses obtained by Bowie [12], and stress intensity factor results by Paris and Sih [13] to develop his solution for through-the-thickness cracks at holes. Grandt developed solutions for a number of different fastener configurations.

In 1978, Kullgren et al. [19] extended and refined the numerical solution introduced by Browning and Smith [20] that was based on a modification of the Schwartz-Neumann alternating method for obtaining stress-intensity factors for a semi-circular crack at a hole. Kullgren's technique, labeled the finite element alternating method, is based on finite element approximations. Kullgren considered quarter-elliptical cracks emanating from open holes in plates. Kullgren and Smith [21] extended this method to single semi-elliptical and double quarter-elliptical cracks emanating from fastener holes. This work has demonstrated that the finite element alternating method is versatile. It can be adopted for many different complex

geometries, loading conditions and crack orientations. The only drawback of this method seems to be the difficulty involved in modifying the computer codes.

A rather significant contribution to the area of three-dimensional cracks subjected to uniform tension was made by Newman and Raju [9] in 1981. They studied several crack configurations and considered several parameters such as crack depth, crack length, specimen thickness and hole radius. They considered solutions due to Howland [22] for stress concentration at a hole and Tada et al. [23] for crack eccentricity corrections as a basis for their finite width correction factors. Newman and Raju also evaluated Shah's conversion factors that were applied to approximate double-crack solutions using single-crack results. These factors, which were derived by using Green's function to find stress intensity factors at a hole in a plate under uniaxial tension, were found to be in good agreement with the results of Kullgren and Smith [21].

Solutions for analytical stress intensity factors for corner cracks at a hole due to Newman and Raju [9], Shah [24] and [25] were evaluated by Heckel and Rudd [25] using correlations with experimental stress intensity factors obtained using the Line-Anderson backtracking technique [26]. They found that Newman and Raju's solution provided excellent analytical/experimental correlations of the stress intensity factor, crack growth rates and crack shape changes. Shah's solution produced excellent stress

intensity factor correlations and life predictions. They also determined that both of Liu's one-dimensional and two-dimensional solutions yielded unconservative stress intensity factors and crack growth rates.

In 1983, Schijve [27] used data collected by Raju and Newman [28, 29] for semi- and quarter-elliptical corner cracks at holes to develop interpolation techniques for cracks with other dimensions. He noted that real cracks will not always have elliptical shapes, but as a first approximation the semi- and quarter-elliptical crack front assumption is a valid one. However, Schijve noted that in general, the geometric ratios, a/c , a/t , R/t (where a is crack depth, c is crack length, t is specimen thickness and R is hole radius) will differ from those used by Raju and Newman. Schijve remedied this by using various interpolation methods judiciously chosen for given crack geometries. The results were compared to the Raju-Newman solutions and found to agree to within 2%.

... Transition of a Corner Crack at a Hole to a Through-the-hole Crack. The transition region starts when the corner crack reaches the edge of the hole nearly reaches the point of back stress concentration and ends when the crack becomes a uniform through-the-hole crack. (Determining the boundaries of this region is a significant part of this work and will be discussed in detail in a subsequent paper.) Currently, procedures for dealing with this transition region range from establishing various approximations and

correction factors to compensate for transition effects to totally ignoring the transition region. The American Society for Testing and Materials (ASTM) is trying to remedy this rather inconsistent approach by sponsoring "round-robin" competitions for predicting the life of specimens to determine the accuracy of current procedures. These round-robin competitions have aided greatly in the rapid advances in the development of transition region criteria. ASTM published some of these results dealing strictly with part-through crack fatigue life predictions in 1979, (see Chang [30]).

Peterson and Vroman [31] developed a computational scheme to determine stress intensity factors for initial part-through crack defects. Instead of using the number of loading cycles as the independent variable, as in most current solutions, their computer code uses very small increments of crack size to calculate the number of loading cycles required for each increment of crack growth. The code uses equations developed by Forman [32] to calculate stress intensity factors at the surface and along the crack front. K , the stress intensity factor, is determined as a function of crack depth to specimen thickness ratio, crack aspect ratio, crack depth, and crack half-length. Crack growth rates were calculated by substituting the stress intensity factors into a Paris-type equation [33]. When Peterson and Vroman first presented their approach in 1972, it was found to be more conservative than the Kobayashi-Moss solution [15]. Further investigation in 1974 concluded that the Kobayashi-Moss

solution was more accurate. However, it was also concluded that the Peterson-Vroman procedure was attractive due to its ease of application. A 1976 modification to the Peterson-Vroman approach provided a good approximation, and made this method even more attractive.

The common procedure for dealing with the transition of a corner crack at a hole to a through-crack is to assume a corner crack until back-surface penetration and then assume a through crack until fracture. This procedure is quite conservative. Johnson [34] compensated for this by suggesting that the crack be considered a through-the-thickness crack only after the back-surface crack length is 90% of the front-surface crack length. Johnson based his idea on an imaginary crack depth found by letting the crack grow in the same elliptical shape it had when it penetrated the back surface. This assumption seems to be in good agreement with the trends of experimental data [5, 6].

Brussat and Chiu [8] considered the crack in the transition region to be a combination of a surface flaw and a through-the-thickness crack. Their criterion was based on crack depth, length, and specimen thickness for a quarter-circular corner flaw at a hole. Brussat and Chiu developed transition region correction factors based on engineering judgment rather than on actual mathematical results.

The most commonly used procedure for predicting the life of a specimen considering the transition region of a corner-crack-at-a-hole is the one discussed by Engle in [11]. This procedure has been adopted by the USAF as the current damage-tolerant philosophy and forms the basis and starting point for this thesis. It uses Newman and Raju's corner crack solution until the crack depth is equal to the plate thickness, and then uses Grandt's [10] linearization of Bowie's solution [12] for a through-the-thickness crack near a hole. However, this approach ignores the portion of the transition region extending from back-surface penetration to where the crack becomes a through-the-thickness one. The results are therefore conservative.

In 1983, Opel [5] suggested modifications to the method discussed by Engle. Opel improved the total life predictions by approximately 15%. His work also resulted in a better correlation between the analytical stress intensity factor prediction and the experimental results by developing transition-region correction factors for corner-cracks-at-a-hole tests. Opel's work was performed in three phases. First, correlations were made between experimental results obtained by Grandt and Snow [35] for Polymethylmethacrylate (PMMA) testing and the Newman-Raju [9] three-dimensional stress intensity factor equation for a single corner crack at a hole. These correlations became unconservative when the normalized crack depth (a/t) reached a value of 0.75, and this was defined as the beginning of the transition region. Next, correlations were made between experimental results

obtained by Heckel and Rudd [25, 36] for 7075-T651 aluminum testing and the Grandt linearization of the Bowie solution for a through crack emanating from a hole. These correlations were found to be unconservative until the normalized crack depth (c/R) reached a value of 2.5; beyond that point the correlations became conservative. This point was defined as the end of the transition region. Finally, stress intensity factors for the transition region were developed. Along the bore of the hole, a second-order polynomial regression curve-fit was used for the normalized crack depths (a/t) found in the transition region. The resulting correction factor was multiplied by the stress intensity factors found using the Newman-Raju solution. A first order polynomial regression curve-fit was found to give accurate correction factors for the Newman-Raju stress intensity factors along the front surface. A second-order polynomial regression curve-fit was used to find the transition correction factors for the Grandt linearization of the Bowie solution along the back surface until final fracture. Opel proceeded to make life predictions using his new model, the model referenced by Engle [11], and the Brussat model [8]. Opel's model proved to be the most accurate.

1.3 Scope

An experimental program was undertaken to investigate the crack-growth behavior in corner-crack-at-a-hole specimens of 2024-T351 aluminum alloy. Of particular interest was an assessment of the effectiveness of a procedure introduced by Opel [5] for predicting

crack growth rates in similar specimens of 7075-T651 aluminum alloy to predict crack growth in other materials. He used experimental data obtained from PMMA and 7075-T651 specimens to derive correction factors for existing solutions which were shown to yield better predictions for these materials. Just as in Opel's work, a part-elliptical corner crack at a hole is considered. The corner crack center is located at the intersection of the hole wall and the front surface. The crack lies in a plane perpendicular to the axis of loading. The finite plate geometry and loading conditions are such that the plane of the crack is a plane of symmetry for the open hole problem. The loading is a remote uniaxial constant amplitude loading, and the initial crack eccentricity, a/c , is greater than one.

The specific objectives of this thesis are to:

1. Evaluate the applicability of Opel's [5] correction factors to 2024-T351 aluminum, and should they prove to yield inaccurate predictions, calculate new correction factors for the stress-intensity-factor models.
2. Evaluate the increase in accuracy suggested by Hartranft and Sih [37] for life predictions if the stress intensity factors are calculated at an angle ϕ from the surfaces as indicated in Fig. 1.
3. Determine if transition correction factors for the region from corner-crack until back surface penetration are needed if the Hartranft and Sih suggestion is used as mentioned in 2. above.

4. Determine the transition region and new transition correction factors for the development of an improved life prediction model.
5. Evaluate the ability of existing stress intensity factor models to predict the behavior of a corner-crack-at-a-hole in 2024-T351 aluminum as it transitions into a uniform through-the-thickness crack (Fig. 1).
6. Assess the accuracy of the corrected model by comparing the total life predictions obtained using these models to results of other life-predictions.

1.4 Approach

Stress intensity factor correlations were performed for experimental results obtained at the Air Force Flight Dynamics Laboratory for 2024-T351 and 7075-T651 aluminum, constant-amplitude-loading testing and the Grandt-Bowie [10, 11, 12] stress intensity solution for a through-the-thickness crack. Opel's model has not proved to be adequate for a new, more ductile material (2024-T351 aluminum). Examination of Table 1 reveals that although the Opel model shows a 9% increase in accuracy over instantaneous model for 2024-T351 aluminum, the total life predictions are still 30% conservative. Therefore, a more accurate model will be investigated.

These correlations were plotted from back-surface penetration to final fracture. Correlations were performed for both front and back surfaces. These plots were used to develop transition correction

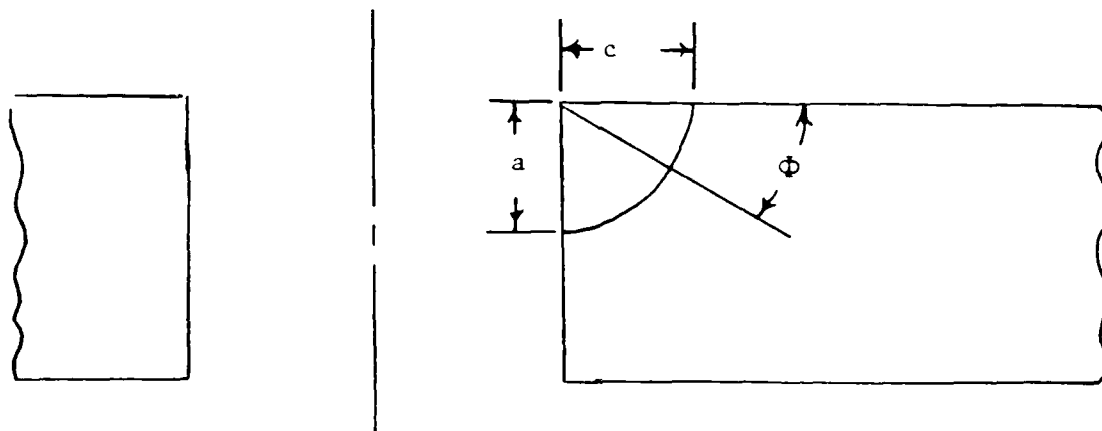


Figure 1a: Crack Configuration Before Transition

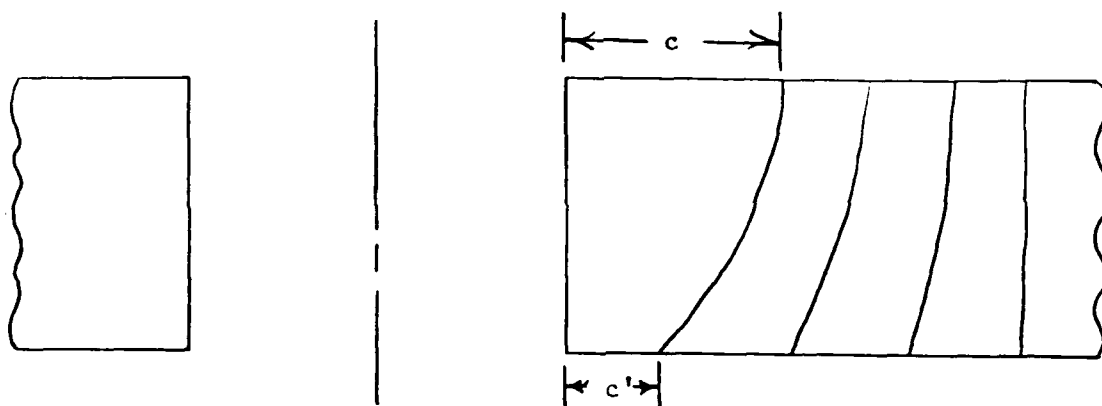


Figure 1b: Crack Configuration During Transition

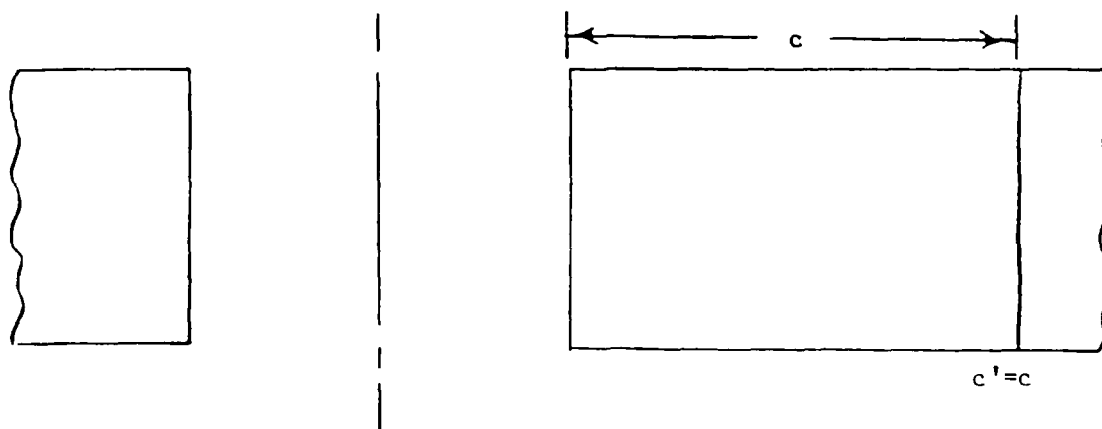


Figure 1c: Crack Configuration After Transition

Instantaneous Model	$\sigma_{max} = 18 \text{ ksi}$			$\sigma_{max} = 15 \text{ ksi}$		
	R = 0.1	R = 0.3	R = -0.5	R = 0.1	R = 0.3	R = -0.5
Average						
a = t	9,053 (37.33)	16,105 (44.24)	5,135 (44.46)	16,561 (35.42)	39,144 (46.32)	12,598 (46.40)
a = t + c = c	12,310 (65.10)	23,746 (71.65)	11,422 (69.22)	24,333 (66.61)	46,748 (91.65)	20,103 (70.06)
c = c	21,363 (49.50)	39,851 (57.31)	16,557 (59.03)	40,894 (49.10)	85,892 (63.39)	32,701 (58.56)
Opel Model						
a = t	8,310 (34.27)	14,672 (40.31)	4,583 (39.68)	15,100 (32.30)	36,306 (42.97)	11,643 (42.88)
a = t + c = c	16,592 (87.74)	32,071 (96.77)	14,478 (87.75)	32,796 (89.78)	62,967 (123.49)	25,121 (87.54)
c = c	24,902 (57.70)	46,743 (67.22)	19,061 (67.95)	47,896 (57.51)	99,273 (73.27)	36,764 (65.83)

Table 1: Comparison of Results. Instantaneous vs. Opel's Model for 2024-T351 Aluminum

factors for the region from back surface penetration to the end of the transition region, i.e., to the point where a uniform through-the-thickness crack develops. The end of the transition region was identified at the point where the back surface crack length is nine-tenths of the front surface crack length (i.e., $c' = .9c$, as in Johnson[34]) (More details on the definition of the transition region will be given in later sections.) These correlations and transition correction factors are compared to those developed and presented by Opel [5] and Opel, Rudd, and Haritos [6].

Finally, total life predictions are made from a specified initial crack length to final fracture using: a) a transition criterion developed in this paper, b) an instantaneous transition criterion presented in Chang [20] c) at the transition criteria developed by Opel [5], d) the criterion developed by Brussat et al [8], and e) the corrections developed by Collipriest and Ehret [7]. The criterion developed in this paper is then evaluated by comparing its predictions to those of Chang, Brussat et al., Opel and Collipriest and Ehret, as well as to the experimental results obtained in the course of this investigation.

2.0 EXPERIMENTAL PROGRAM

The entire experimental program was conducted at the Air Force Wright Aeronautical Laboratories, Flight Dynamics Laboratory, Wright-Patterson Air Force Base, Ohio. Two distinct sets of data were generated for this study: material characterization data and corner-crack-at-a-hole data, both for 2024-T351 aluminum. The material-characterization tests included both crack-growth-rate and fracture-toughness tests. The James-Anderson backtracking technique was applied to these data in order to obtain experimental stress intensity factors. These factors were used in the life predictions for the corner-crack-at-a-hole tests. The corner-crack-at-a-hole test results were used to develop a new transition criterion and evaluate the accuracy of this new criterion by comparing it to the results reported. The details of all tests conducted and the procedures followed are described in the next sections.

2.1 Material-Characterization Tests

Material-characterization tests were conducted using center-cracked tension specimens. (Specimen dimensions are given in Fig. 2) The crack-growth-rate tests used three sets of duplicate specimens, with maximum stress $\sigma_{\max} = 10.0$ ksi and stress ratio $R = 0.1, 0.5, -0.5$. The crack length vs. number of cycles (a vs N) data for the tests are shown in Figs. 3 through 5 (based on R values).

Using the experimental a vs N data, the maximum stress intensity

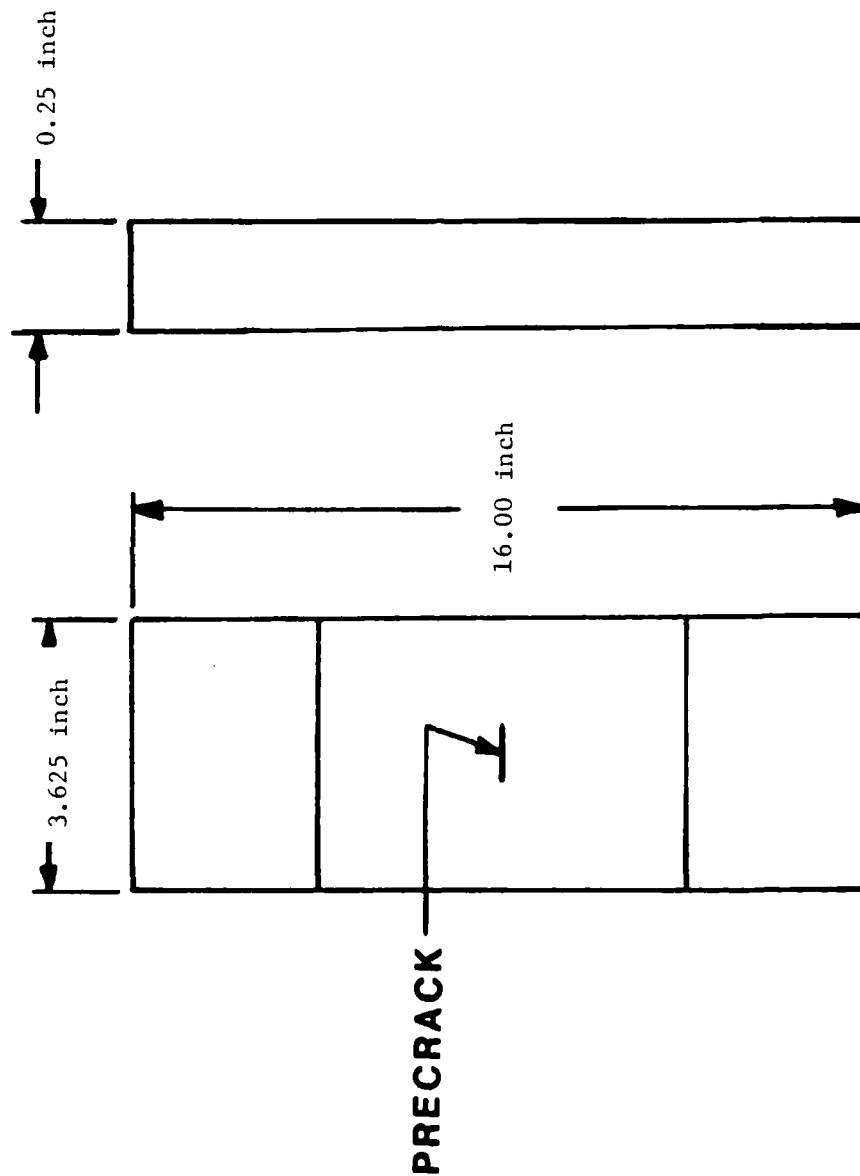


Figure 2 : Center-Cracked Tension Specimen Geometry for Material Characterization Tests (Precrack=0.14") and Fracture Toughness Tests (Precrack=1.4")

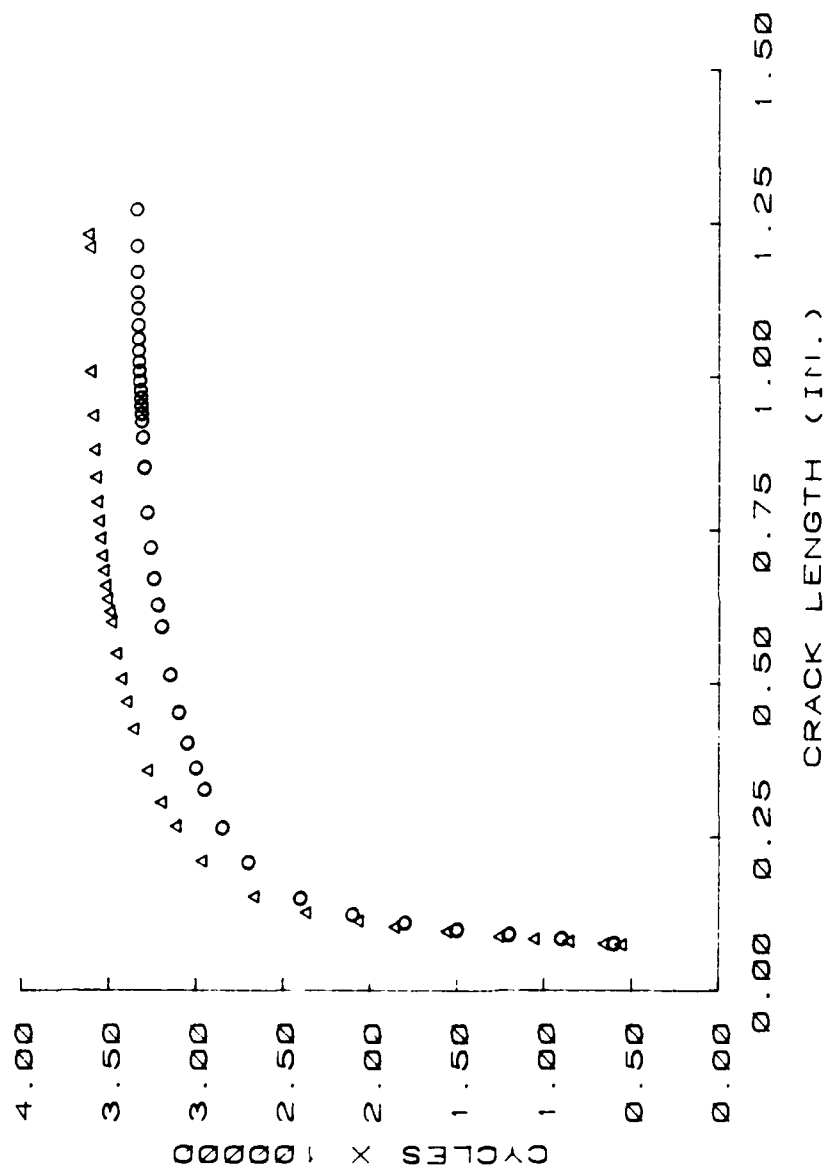


Figure 3: Material Characterization Data. Crack Length vs. Life to Final Fracture.
Maximum Stress - 10 ksi, Load Ratio - R=0.1

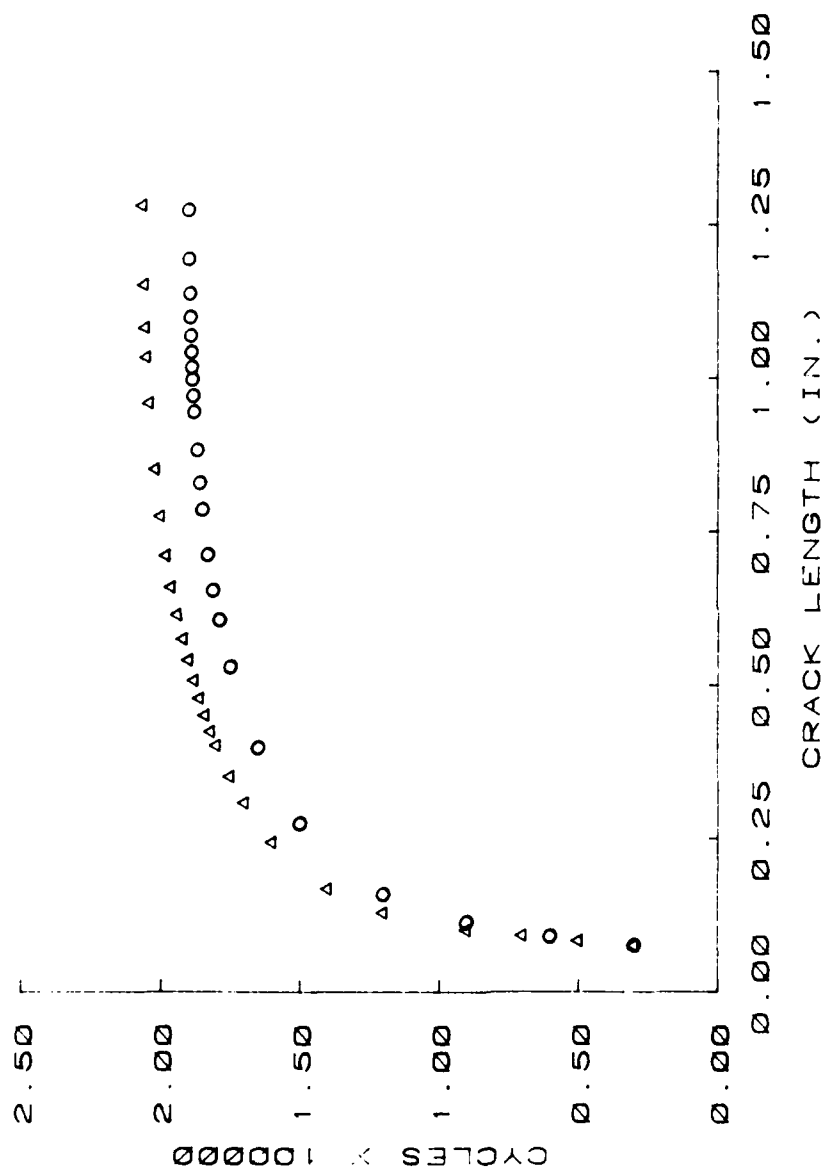
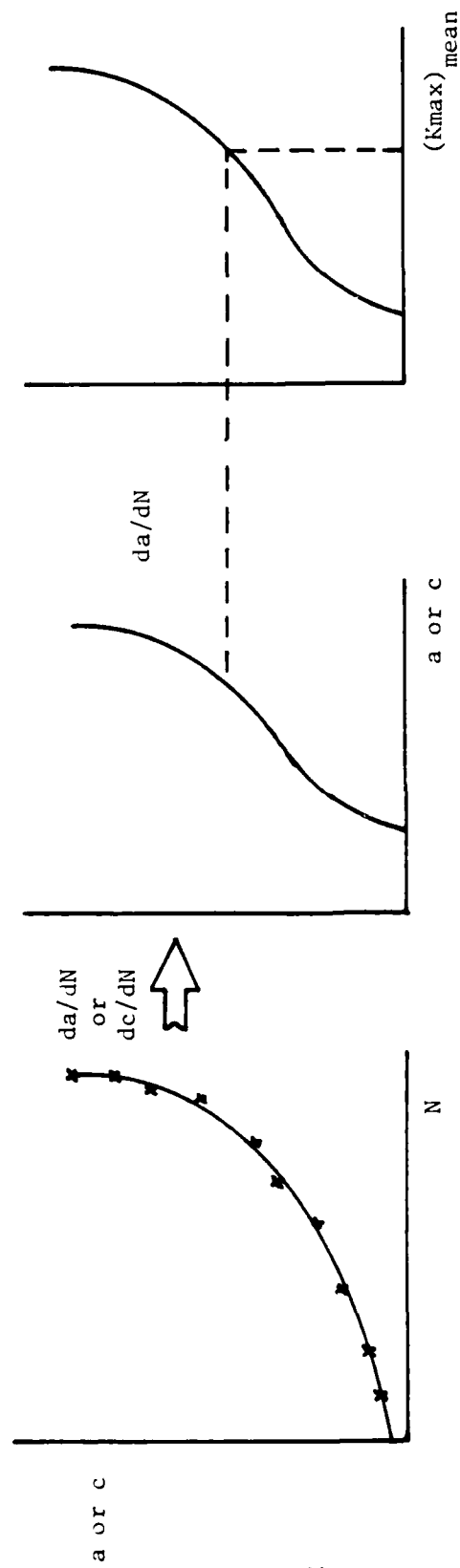


Figure 5: Material Characterization Data. Crack Length vs. Life to Final Fracture.
Maximum Stress - 10 ksi, Load Ratio - R= -0.5

factor (K_{\max}) was calculated and the data was then transformed to crack maximum growth rate vs. maximum stress intensity factor (da/dN vs. K_{\max}) data using a series of computer programs developed by Grimsely [38], which are based on the ASTM-recommended incremental polynomial-technique. The computer programs also curve-fit the crack-growth data with a Walker equation [39]. The Grimsely programs, called the Crack Rate Analysis and Walker Equation Solver using the Method of Least Squares (CRAWLS), provide a major portion of the data and equations used in this study and therefore warrant further discussion.

The CRAWLS programs transform crack-growth test data (a vs N) into crack-growth rates (using the incremental polynomial technique) and then fits those growth rate data with a Walker equation. Conversion of crack-growth data (a vs N) into crack growth rate data (da/dN vs K_{\max}) requires differentiation of the crack-growth curve. This differentiation is performed using a method which fits a parabola to successive subsets of seven data points by the method of least squares (see e.g. by Hudar et al. [40]). The derivative of the fitted curve is then calculated for the middle point of each subset. This procedure, combined with the James-Anderson backtracking technique [26], results in evaluation of the derivative over the entire curve, (see Fig. 6). After obtaining the crack-growth rates, the data are fitted with a Walker equation of the form:

$$da/dN = C[(1 - R)^m K_{\max}]^n \quad (1)$$



Corner-Crack Test

Corner-Crack Test

Basic da/dN Test

Figure 6: Schematic of James-Anderson Backtracking Technique

Note: A method for solving the Walker equation for C,M,N has been proposed by Chang et al. [41]. This method uses a least-squares fit of the data for a series of assumed values of M. Walker-equation plots are generated and chosen based on which best fits the data.

The results of the material-characterization tests are given in Figs. 7 through 9 for the three values of the R ratio.

Data for the center-cracked-tension specimens, including both positive and negative stress ratios, were input into Grimseiy's CRAWLS programs. The positive-stress-ratio data can be represented by the following best-fit Walker equation:

$$da/dN = 1.11616 \times 10^{-9} [K_{\max}(1-R)^{.7}]^{3.71797} \quad (2)$$

where: K_{\max} is in units of Ksi per in and da/dN is inch per cycle

The best-fit Walker equations for the negative stress ratios are:

$$da/dN = 4.31544 \times 10^{-9} (K_{\max})^{3.2116} \quad (3)$$

Four fracture-toughness tests were also performed for the 2024-T351 aluminum. These tests were conducted for center-cracked tension specimens like those shown in Fig. 2. The fracture toughness was determined by a combination of fatigue and static tensile testing. The specimen was subjected to cyclic loading according to ASTM Standards until through-cracks of approximately .005 inches were initiated on both ends of the center notch. Then the specimen was statically loaded by a linearly increasing load until failure

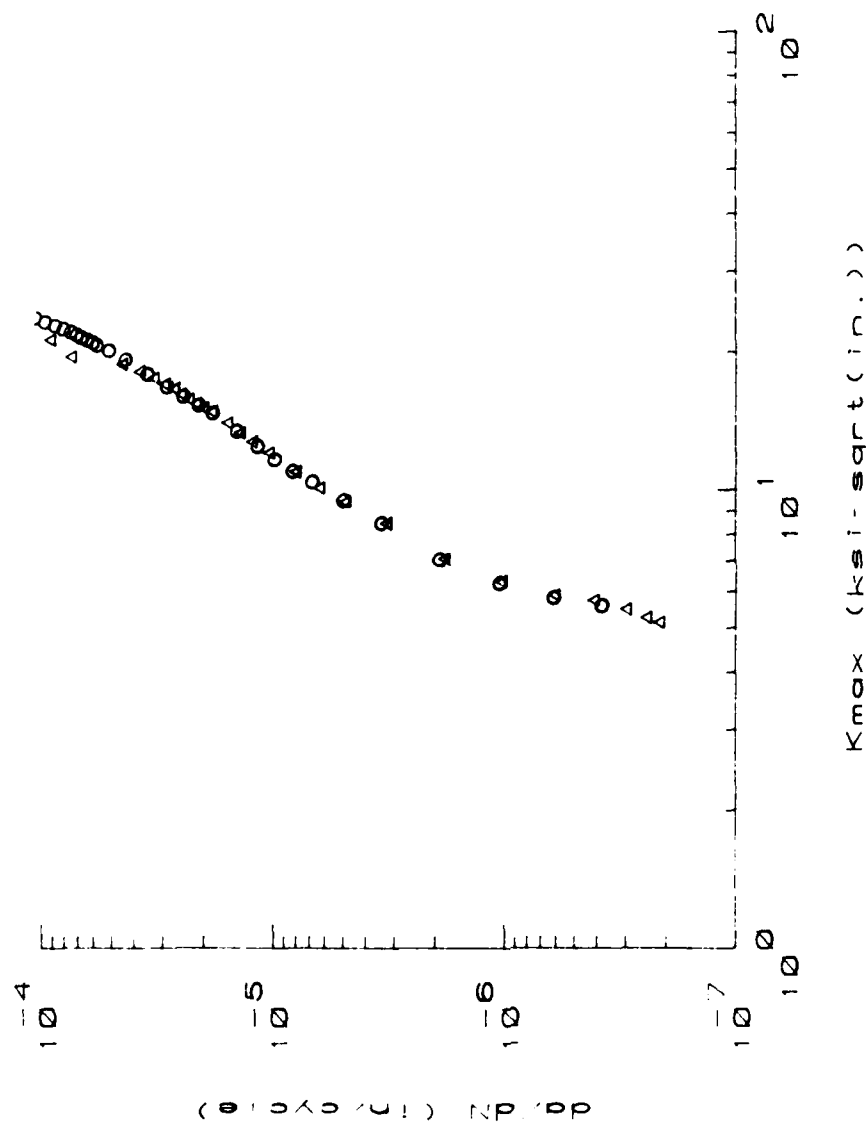


Figure 7: Material Characterization Data.
 Maximum Stress Intensity Factor vs. Crack Growth Rate.
 Maximum Stress - 10 ksi, Load Ratio - $R=0.1$

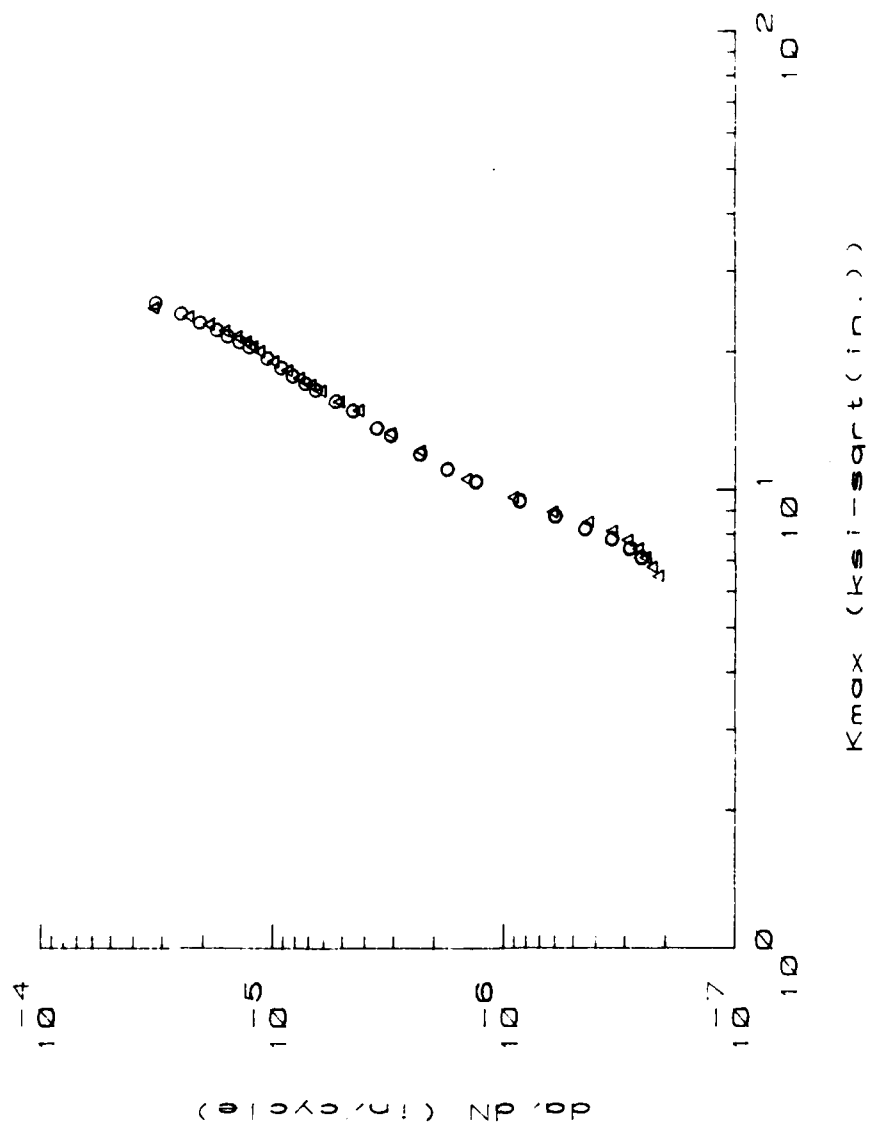


Figure 8: Material Characterization Data.
 Maximum Stress Intensity Factor vs. Crack Growth Rate.
 Maximum Stress - 10 ksi, Load Ratio - $R=0.5$

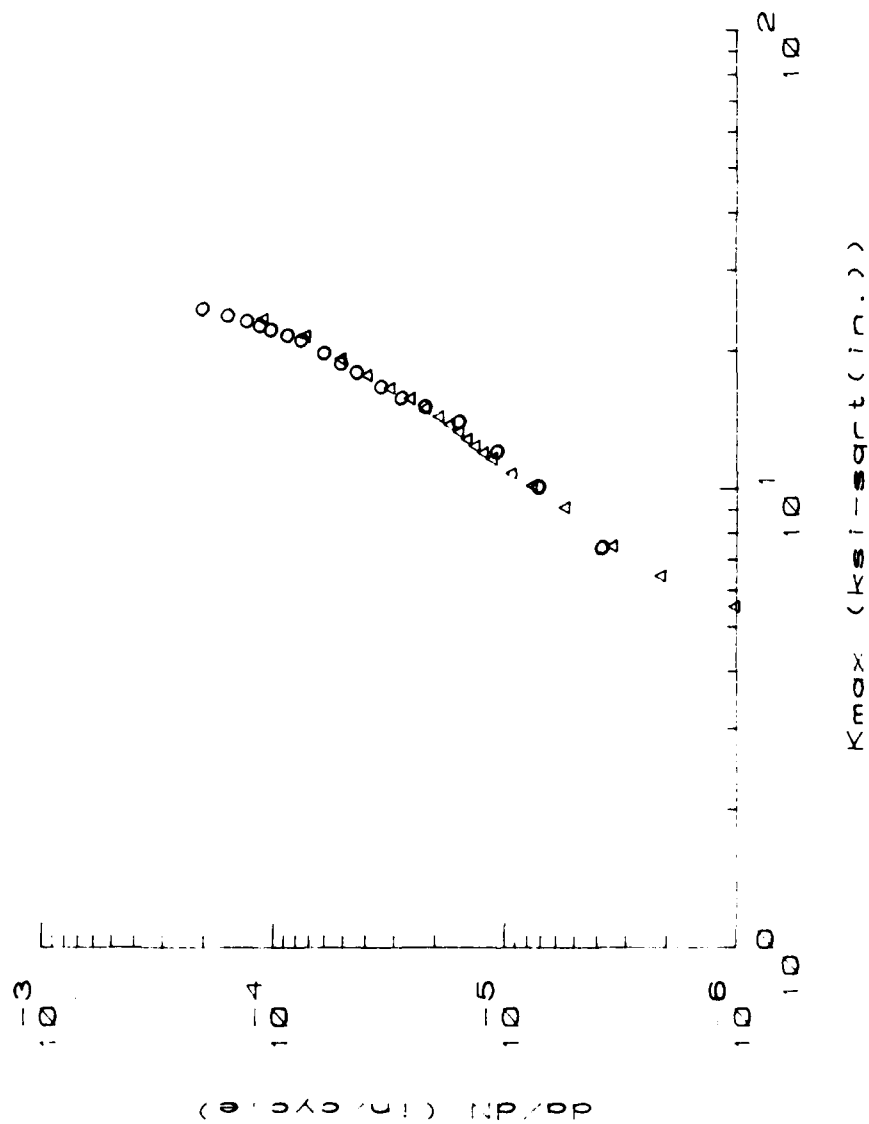


Figure 9: Material Characterization Data.
 Maximum Stress Intensity Factor vs. Crack Growth Rate.
 Maximum Stress - 10 ksi, Load Ratio - $R = -0.5$

occurred. The average fracture toughness was determined using the following equation:

$$K_{IC} = \sigma_c \sqrt{\pi a} \sqrt{\sec(\pi a/w)} \quad (4)$$

Where: σ_c = stress at failure
a = crack length
w = specimen width

The average fracture toughness for these tests was found to be 53.5 ksi $\times \sqrt{\text{in}}$ (48.68 MPa $\times \sqrt{\text{mm}}$).

Standard tensile tests using a "dogbone" type specimen were performed for 2024-T351 aluminum to determine yield strength. The specimen geometry is shown in figure 10. The average yield strength for the two tests performed using 1/2-inch thick 2024-T351 aluminum specimens was 63 ksi (913.59 MPa).

2.2 Corner-Crack-at-a-Hole Tests

Twelve corner-crack-at-a-hole tests were performed using 2024-T351 aluminum alloy specimens. The typical specimen geometry is shown in Fig. 11. The specimens were precracked at the same constant amplitude stress levels used in the crack growth tests ($\sigma_{\text{max}} = 10$ ksi). After precracking, the maximum stress levels used for testing were 18 ksi and 15 ksi. Two positive stress ratios ($R = 0.1$ and 0.3) and one negative ($R = -0.5$) stress ratio were considered. The maximum stress level, stress ratio, and initial crack size and shape for each of the twelve tests are given in Table 2. Duplicate

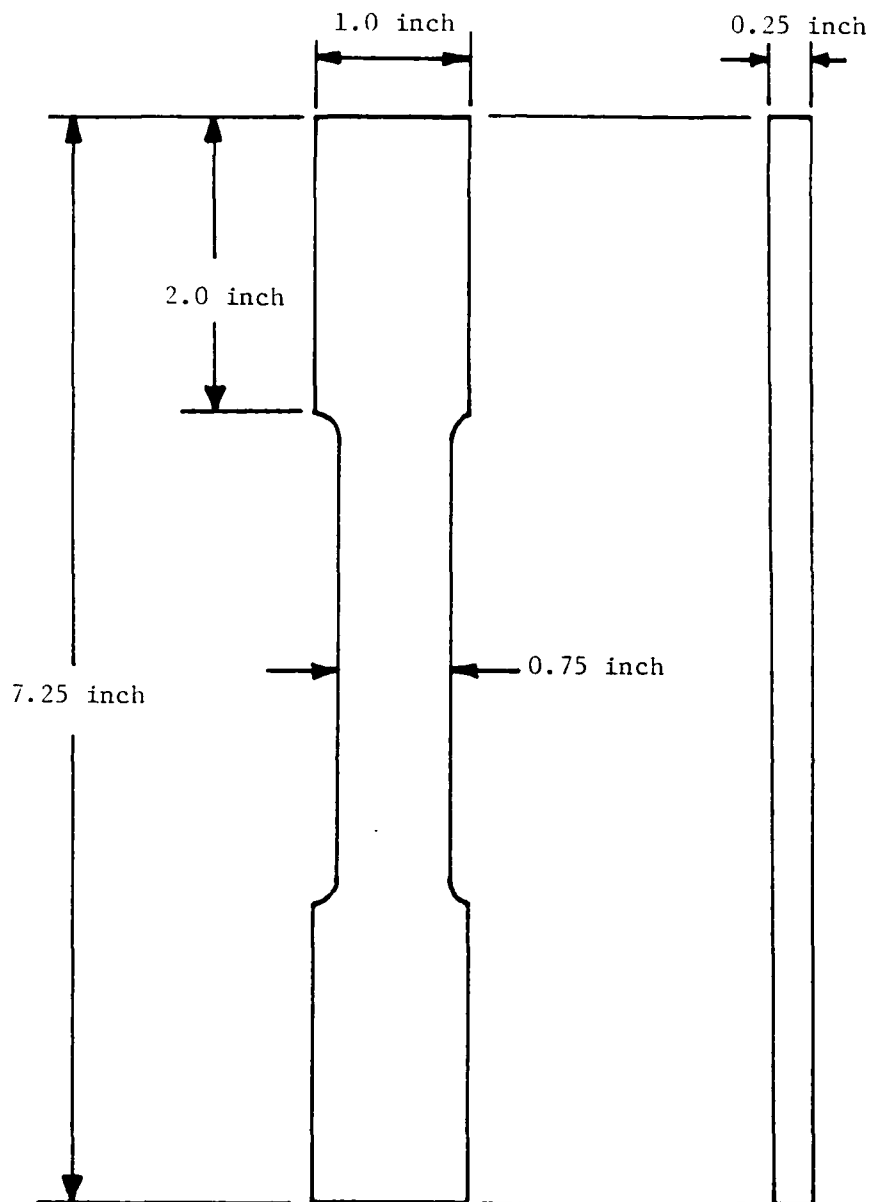


Figure 10: "Dogbone" Specimen Geometry Used for Strength Tests Used to Determine Average Yield Strength

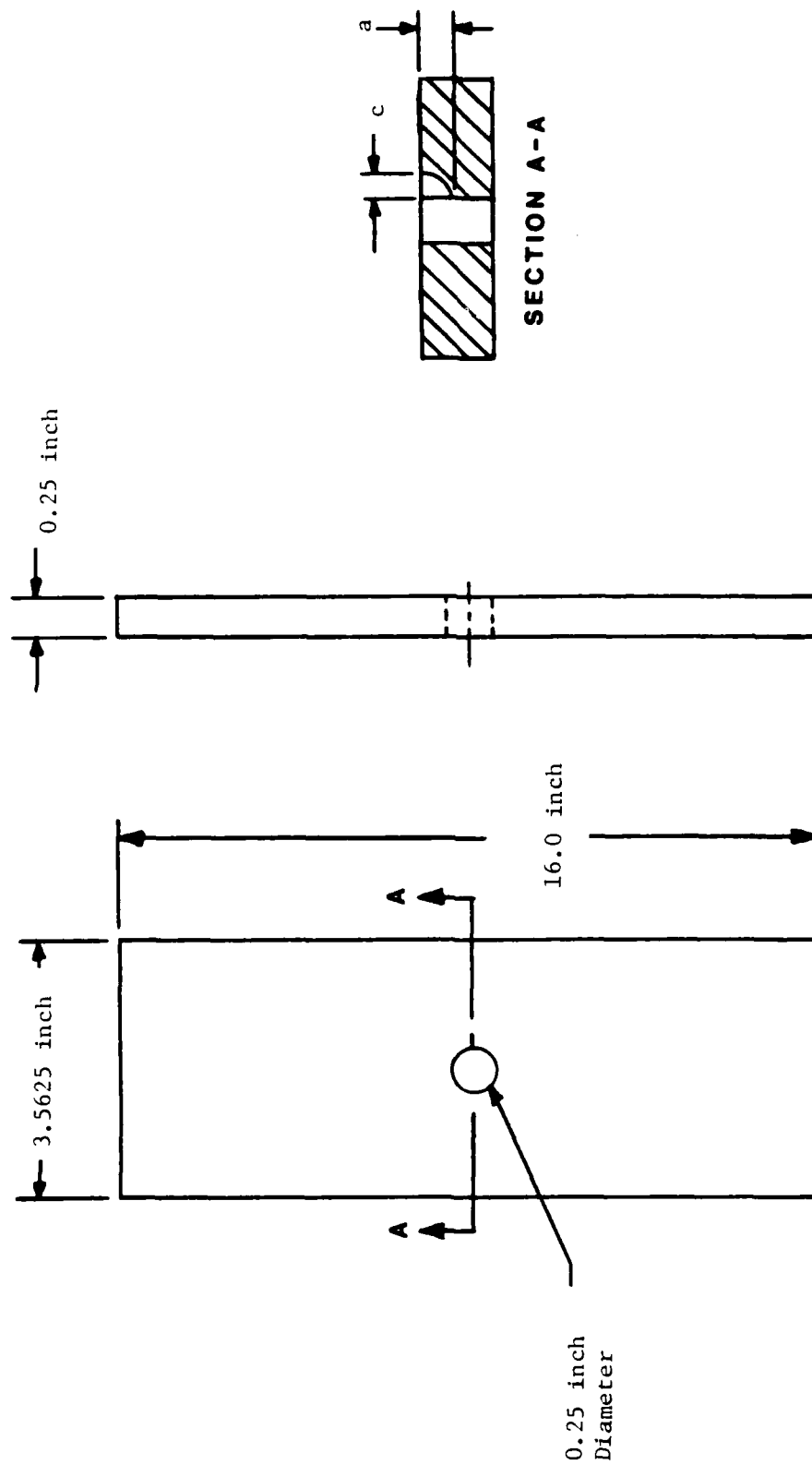


Figure 11: Specimen Geometry for Corner-Crack-at-a-Hole Tests

Specimen Number	Load Ratio (R)	a_i (in)	c_i (in)	σ_{max} , ksi
PC 1/2	0.1	.062	.050	18.00
PC 3/4	0.3	.077	.049	18.00
PC 5/6	-0.5	.115	.050	18.00
PC 7/8	0.1	.072	.052	15.00
PC 4/10	0.3	.049	.045	15.00
PC 11/12	-0.5	.051	.056	15.00

TABLE 2: 2024-T351 Aluminum Test Conditions
(a_i , c_i are average of duplicate specimens)

tests were carried out for each of the six load conditions. The results were averaged to eliminate any bias that might arise due to any possible faulty tests.

To evaluate the stress intensity factors along the bore of the hole for the 2024-T351 aluminum corner-crack-at-a-hole tests, the initial crack length along the bore of the hole (a_i) must be known. Unlike materials such as PMMA, aluminum is not transparent and currently there is no way to measure a_i during the test. Therefore, to obtain values for a_i for the first 8 specimens, a marker load was applied after a crack was observed on the front surface. The marker load had the same maximum constant amplitude stress levels as those used in the tests, but the minimum stress levels were increased to the stress ratio, $R = 0.85$. The marker load produced striations on the fracture surfaces which could then easily be measured with an optical microscope after the completion of the tests. This measurement yielded the value of a_i for each specimen. During testing of the last four specimens, PC-9 through PC-12, the "Fax Film" method was employed. Fax Film is a thin, mylar-type plastic film which becomes very soft when acetone is rubbed on it. The soft film is forced into the small initial crack and then removed, a crack impression is left on the film and with the aid of an optical microscope, the initial crack length can be measured. This method is very accurate if the initial crack length is sufficiently small; it also requires much less time and effort than the marker band technique.

The corner-crack-at-a-hole tests for 2024-T531 aluminum specimens were continued until failure occurred. Crack length measurements were taken throughout the test. Crack length measurements on both the front and back surfaces were taken at random intervals during the tests. All measurements were made using two optical microscopes mounted on the fatigue machine, one at the front surface of the specimen and one at the back surface. Using the crack length measurements and the number of fatigue cycles between each measurement, the crack growth rates for both the front and back surfaces were computed using methods which are described in the next chapter.

3.0 EXPERIMENTAL STRESS INTENSITY FACTORS

3.1. Stress Intensity Factors for the Front and Back Surfaces

Using the data from the fatigue tests experimental stress intensity factors for the front and back surfaces were obtained using the James-Anderson backtracking technique [26]. The technique is shown schematically in Fig. 6 and may be briefly outlined (ref. Opel [5], p.23) as follows:

1. Crack-growth curves were determined at the back surface (c' vs N) and the front surface (c vs N) using raw data from the corner-crack-at-a-hole tests.
2. Using the crack growth curves, crack-growth rates were determined and expressed as a function of crack lengths (i.e., dc'/dN vs c' and dc/dN vs c). Crack growth rates were determined using the standard seven-point polynomial regression technique discussed earlier. This curve-fit allows for the calculation of the crack growth rate at any crack length. Crack length vs. crack growth rate are plotted for the front surface in Figs. 12 through 17 and for the back surface in Figs. 18 through 23.
3. The stress intensity factors, for positive stress ratios, associated with given crack lengths and corresponding crack growth rates were found using the Walker equation. The Walker equation form for the positive stress ratios was found to be:

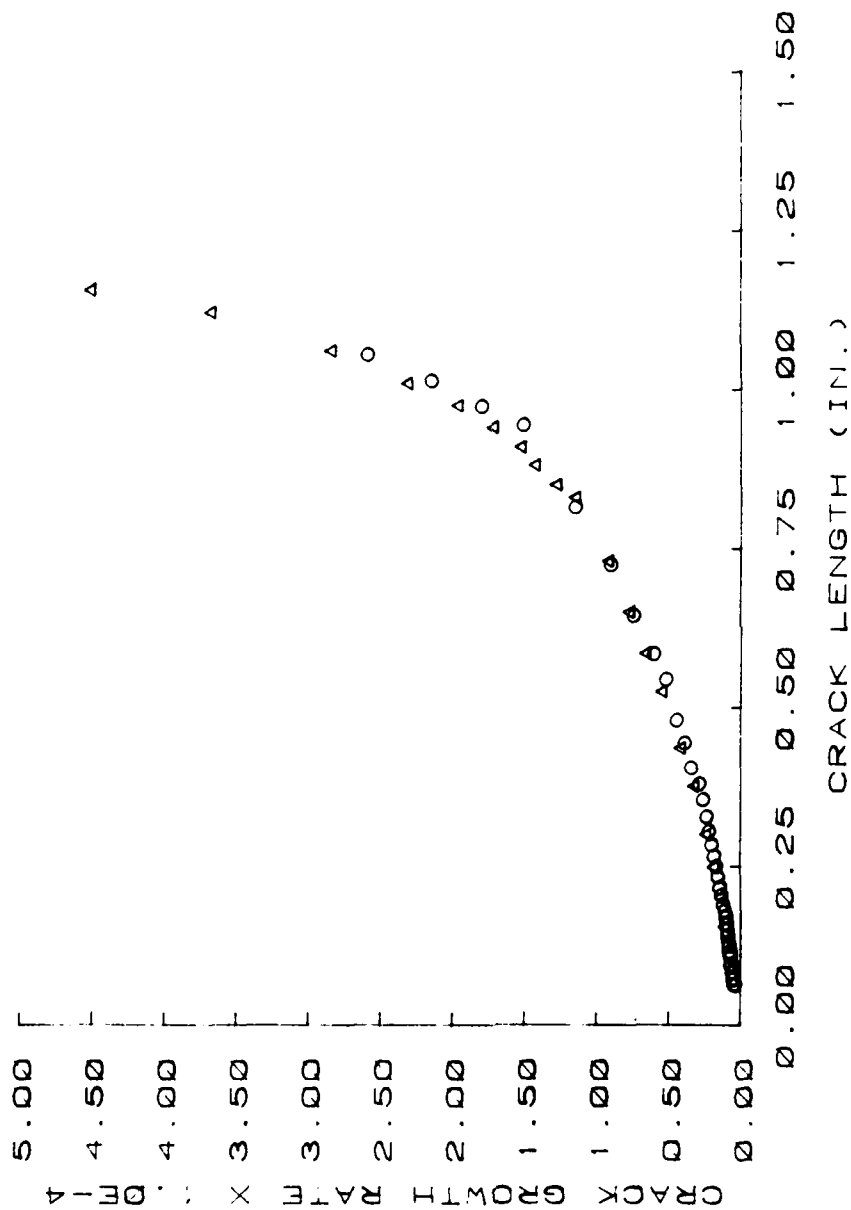


Figure 12: 2024-T351 Aluminum Corner-Crack-at-a-Hole Test Data.
 Front Surface Crack Length vs. Crack Growth Rate.
 Maximum Stress - 18 ksi, Load Ratio - R=0.1

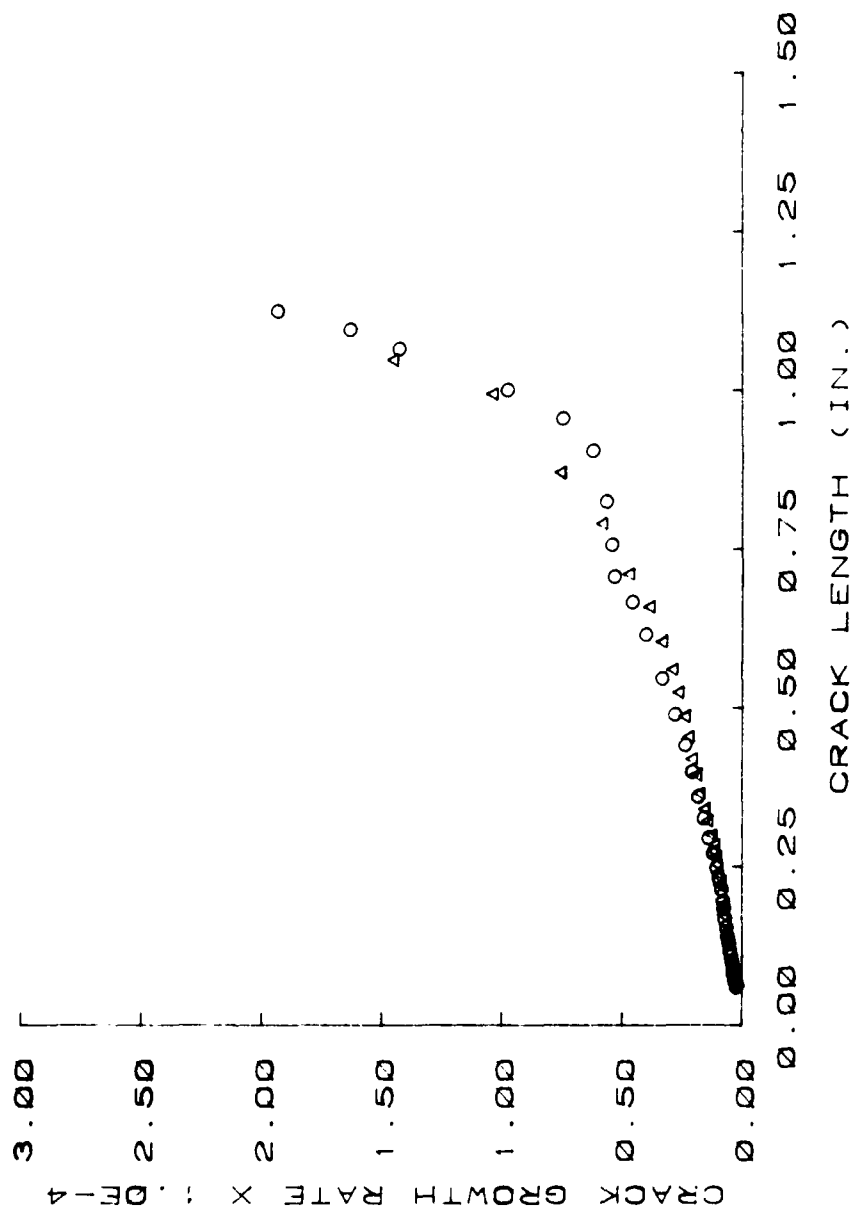


Figure 13: 2024-T351 Aluminum Corner-Crack-at-a-Hole Test Data.
 Front Surface Crack Length vs. Crack Growth Rate.
 Maximum Stress - 18 ksi, Load Ratio - R=0.3

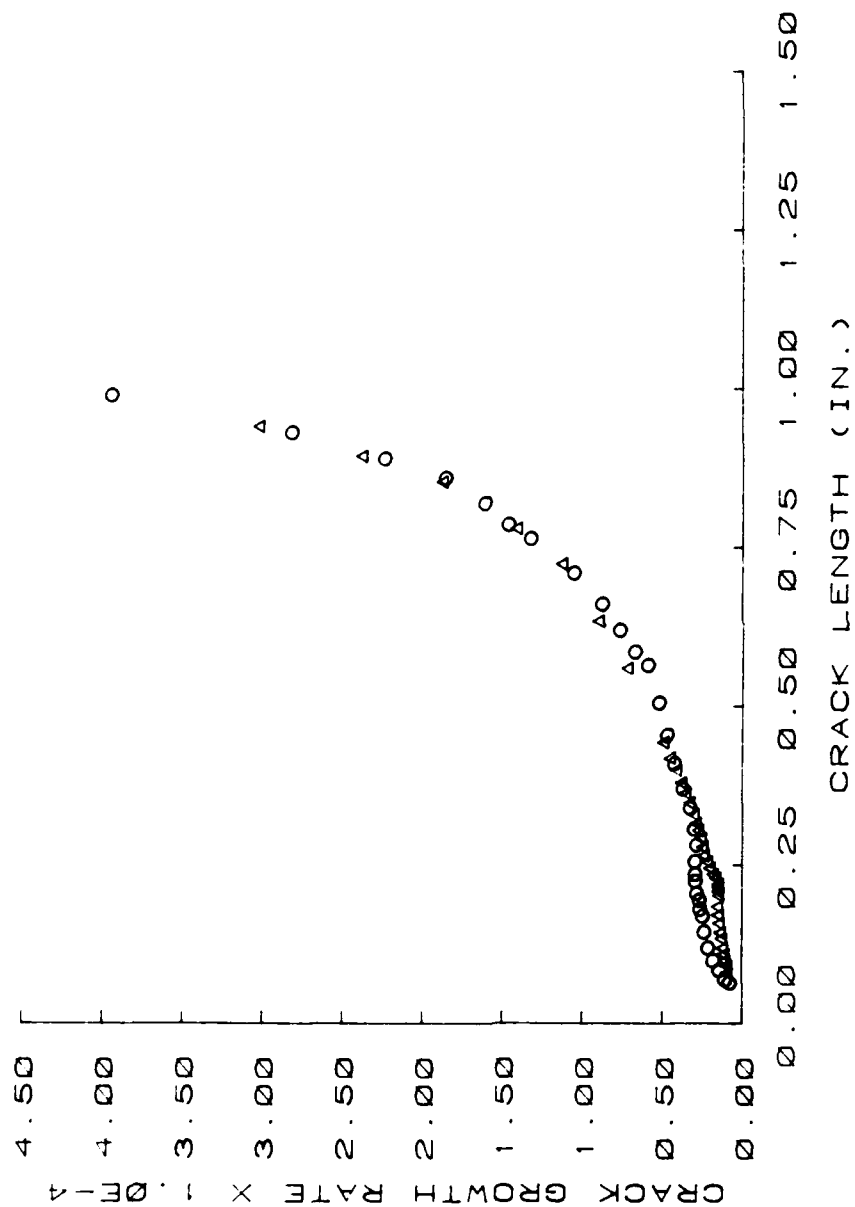


Figure 14: 2024-T351 Aluminum Corner-Crack-at-a-Hole Test Data.
 Front Surface Crack Length vs. Crack Growth Rate.
 Maximum Stress - 18 ksi, Load Ratio - $R = -0.5$

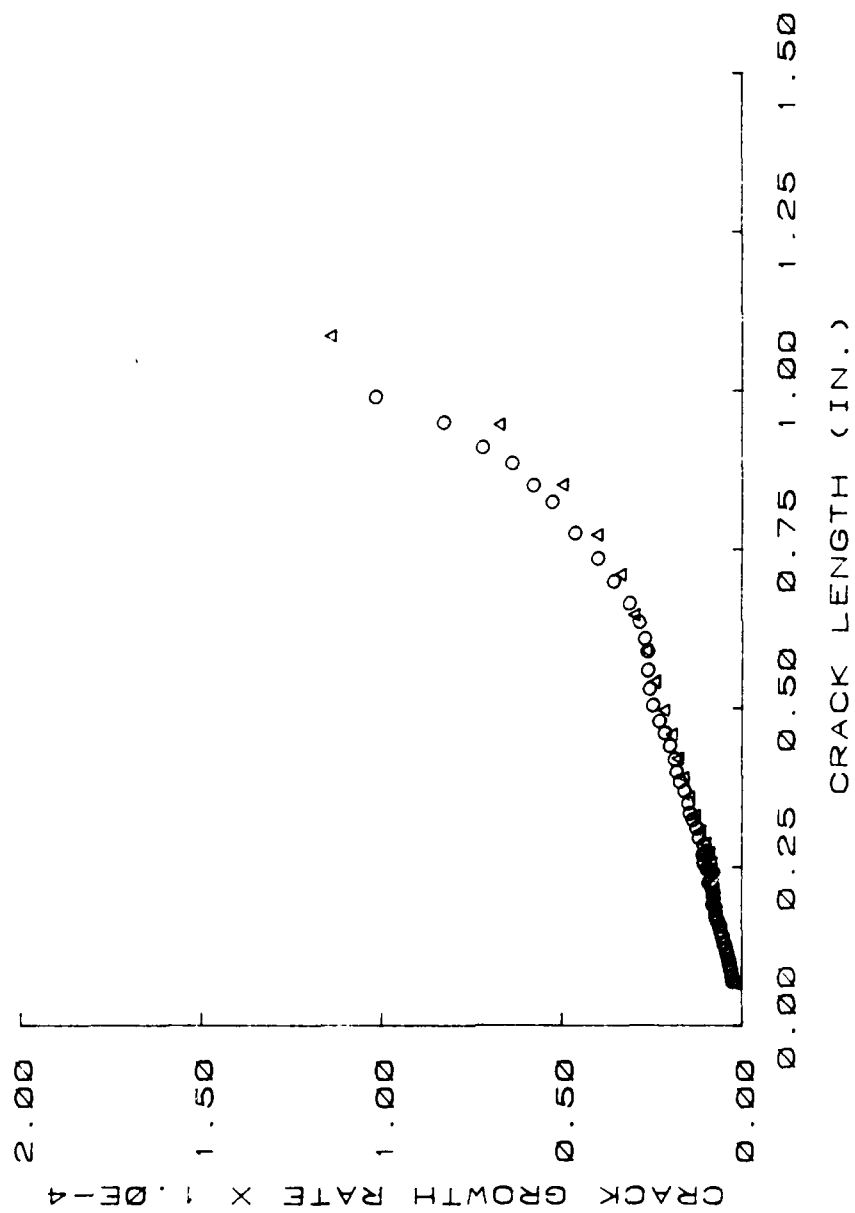


Figure 15: 2024-T351 Aluminum Corner-Crack-at-a-Hole Test Data.
 Front Surface Crack Length vs. Crack Growth Rate.
 Maximum Stress - 15 ksi, Load Ratio - R=0.1

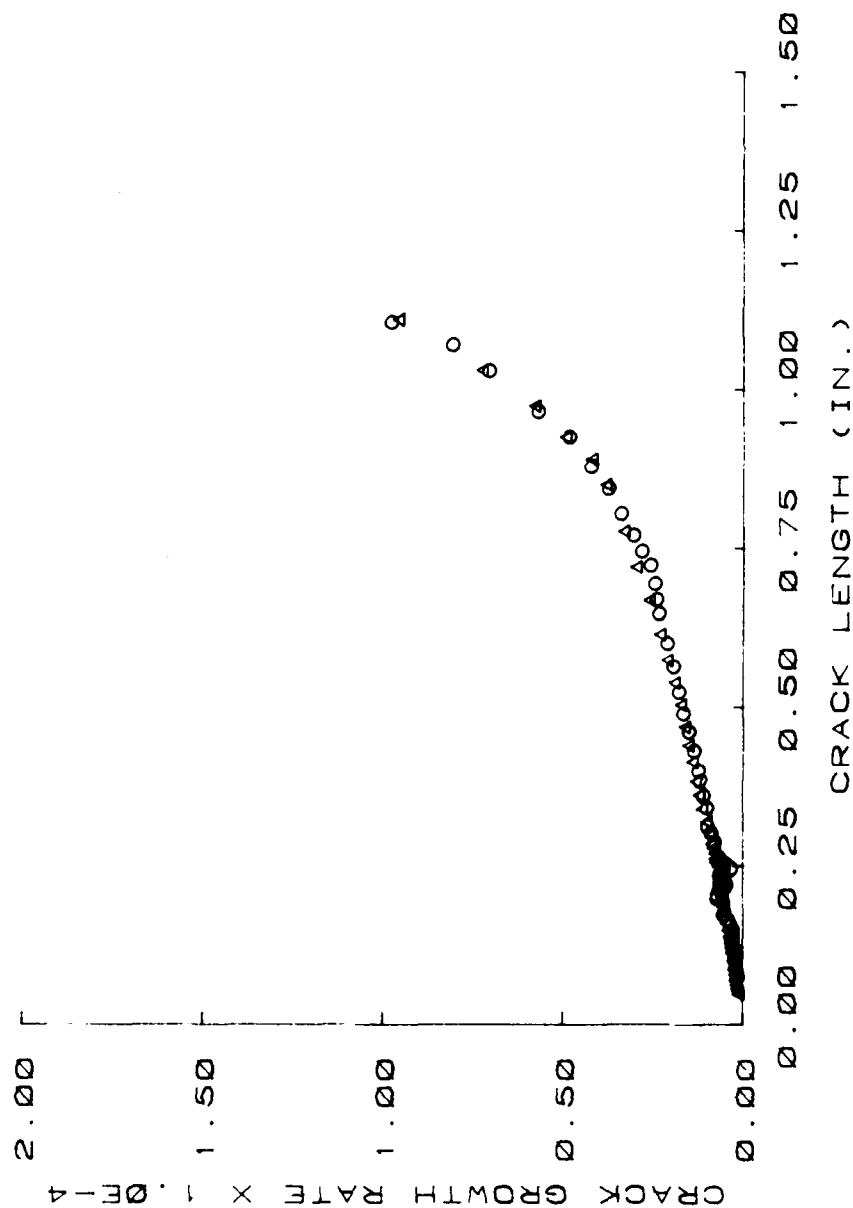


Figure 16 : 2024-T351 Aluminum Corner-Crack-at-a-Hole Test Data.
Front Surface Crack Length vs. Crack Growth Rate.
Maximum Stress - 15 ksi, Load Ratio - R=0.3

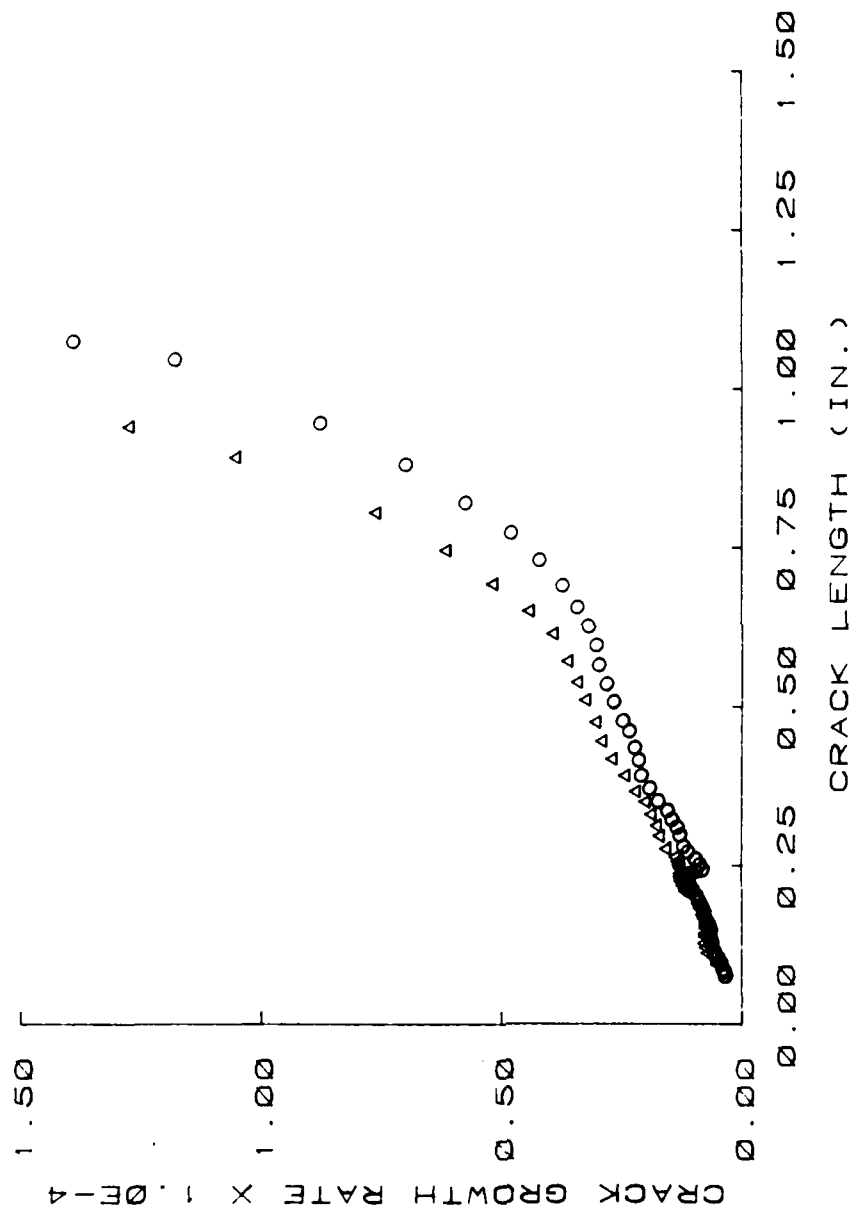


Figure 17 : 2024-T351 Aluminum Corner-Crack-at-a-Hole Test Data.
 Front Surface Crack Length vs. Crack Growth Rate.
 Maximum Stress - 15 ksi, Load Ratio - R= -0.5

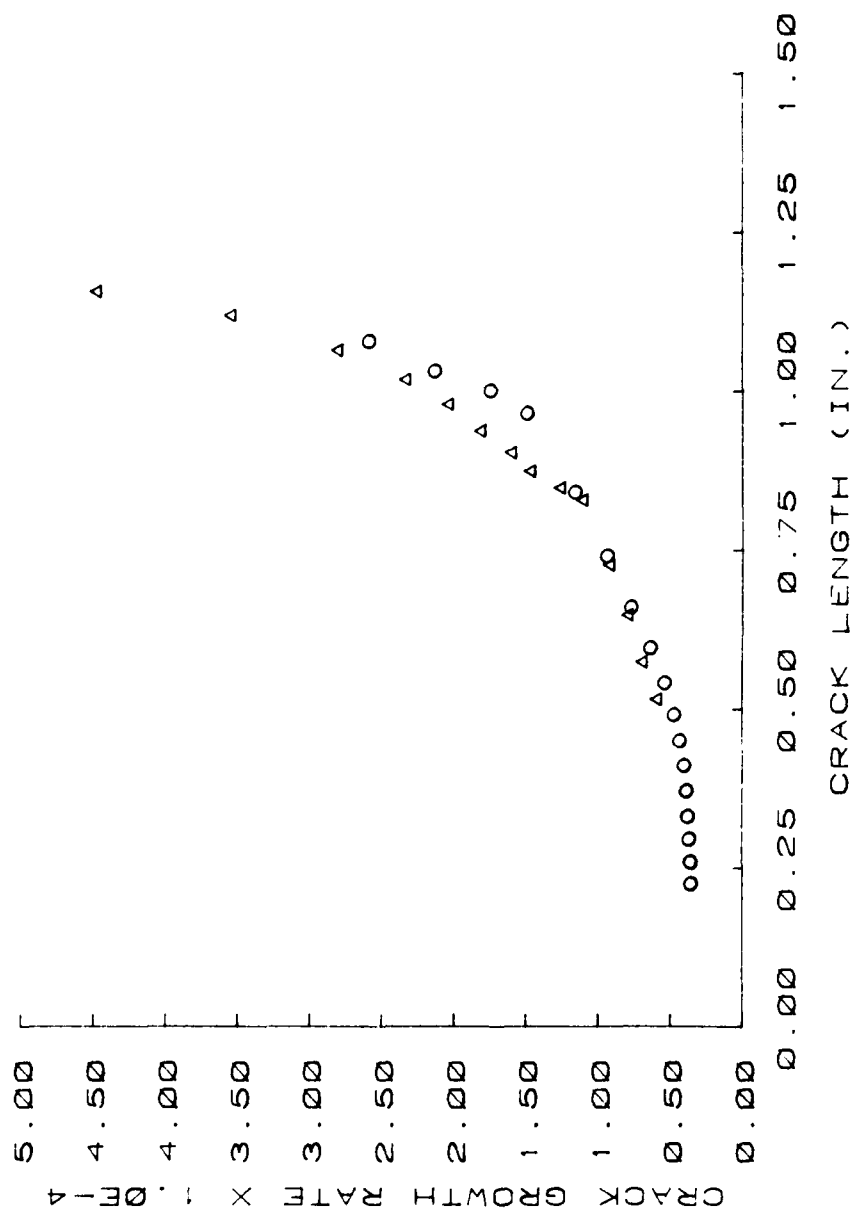


Figure 18: 2024-T351 Aluminum Corner-Crack-at-a-Hole Test Data.
 Back Surface Crack Length vs. Crack Growth Rate.
 Maximum Stress - 18 ksi, Load Ratio - R=0.1

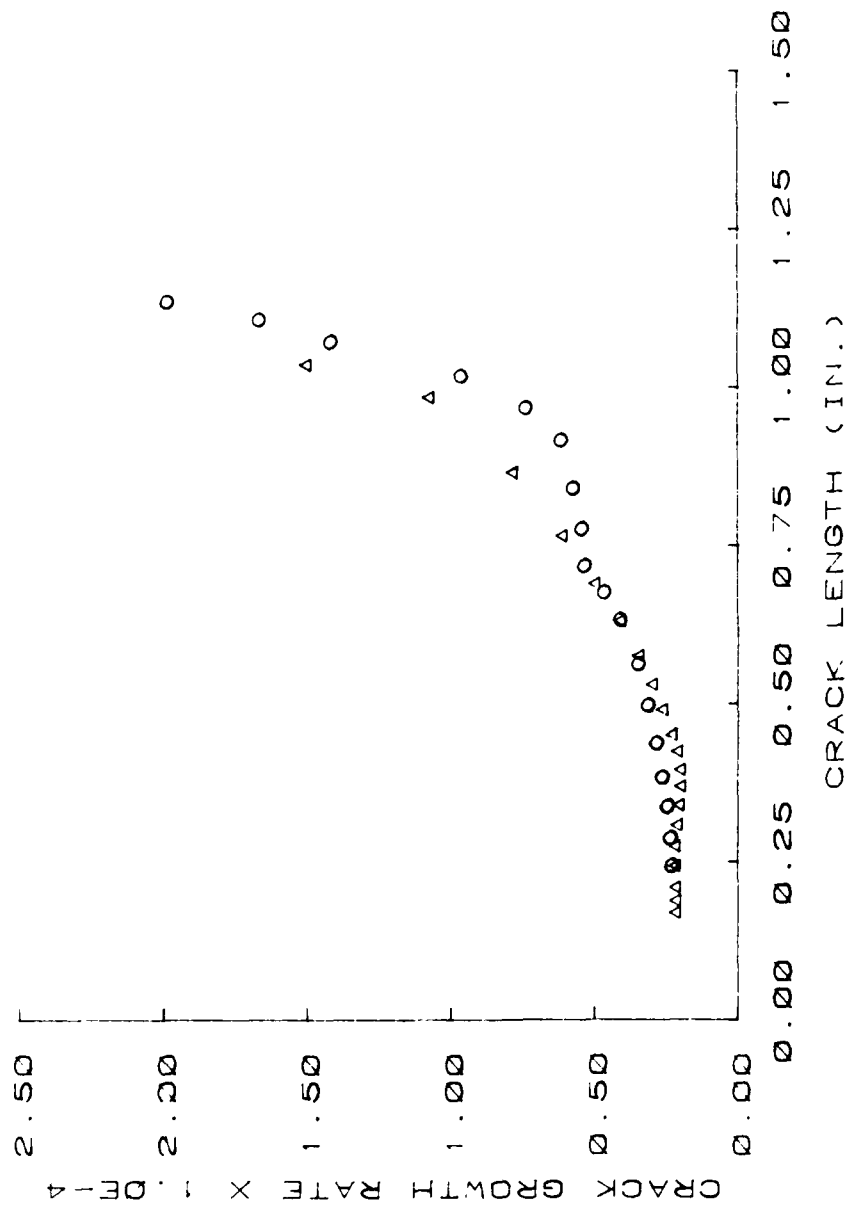


Figure 19: 2024-T351 Aluminum Corner-Crack-at-a-Hole Test Data.
 Back Surface Crack Length vs. Crack Growth Rate.
 Maximum Stress - 18 ksi, Load Ratio - R=0.3

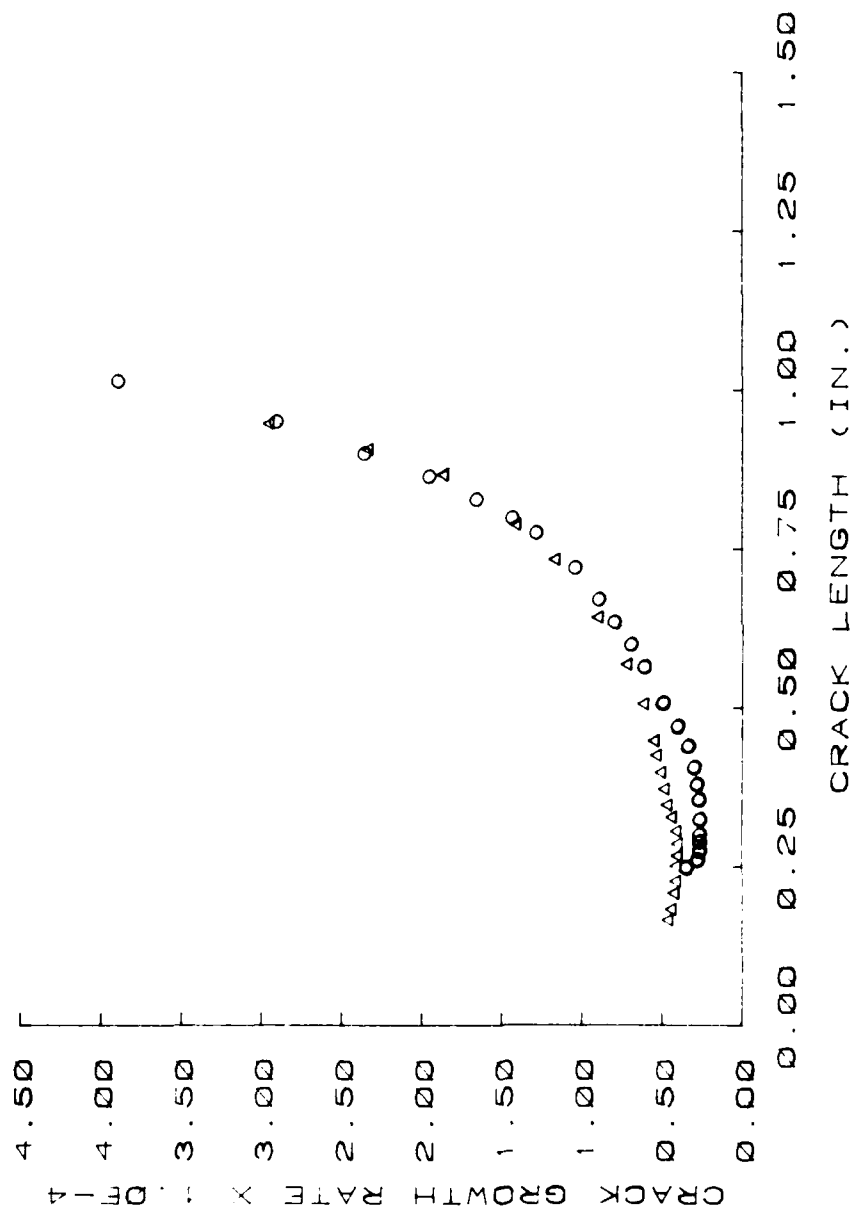


Figure 20 : 2024-T351 Aluminum Corner-Crack-at-a-Hole Test Data.
 Back Surface Crack Length vs. Crack Growth Rate.
 Maximum Stress - 18 ksi, Load Ratio - $R = -0.5$

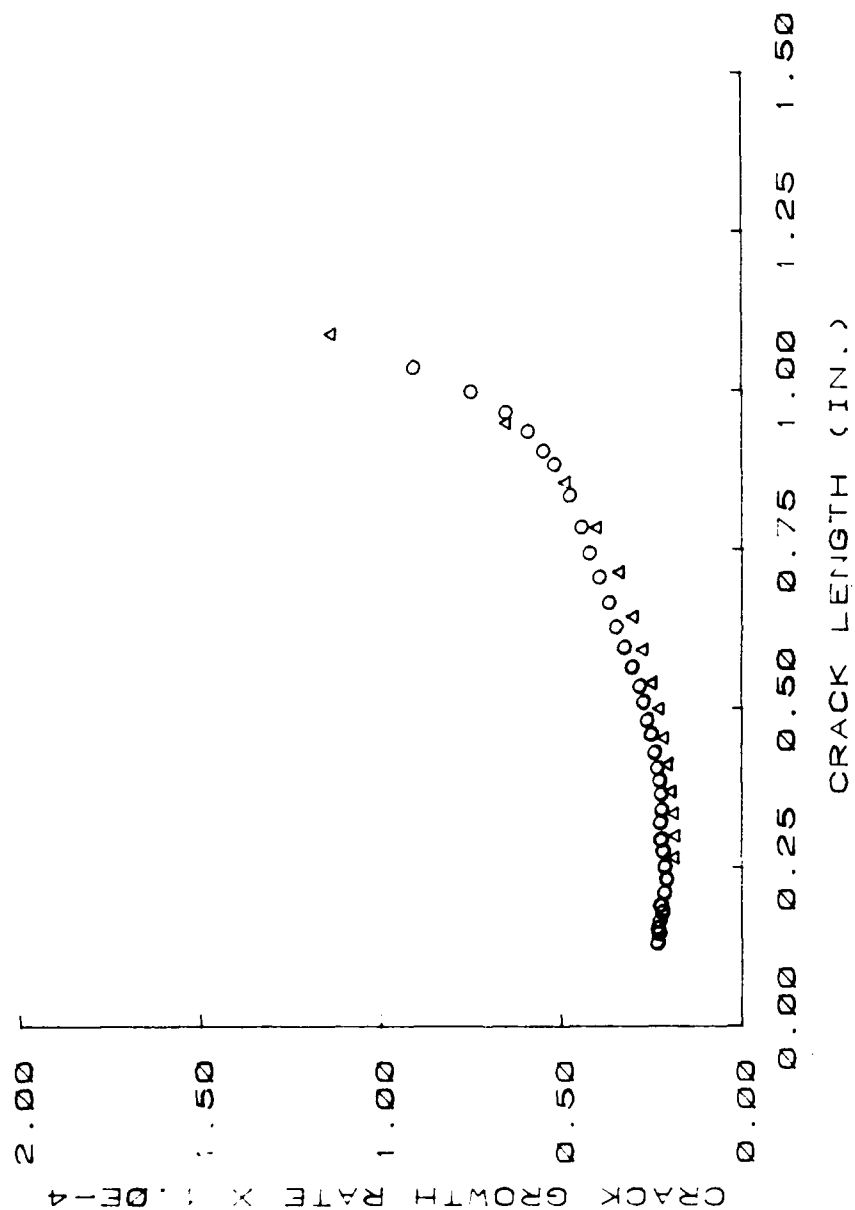


Figure 21: 2024-T351 Aluminum Corner-Crack-at-a-Hole Test Data.
 Back Surface Crack Length vs. Crack Growth Rate.
 Maximum Stress - 15 ksi, Load Ratio - R=0.1

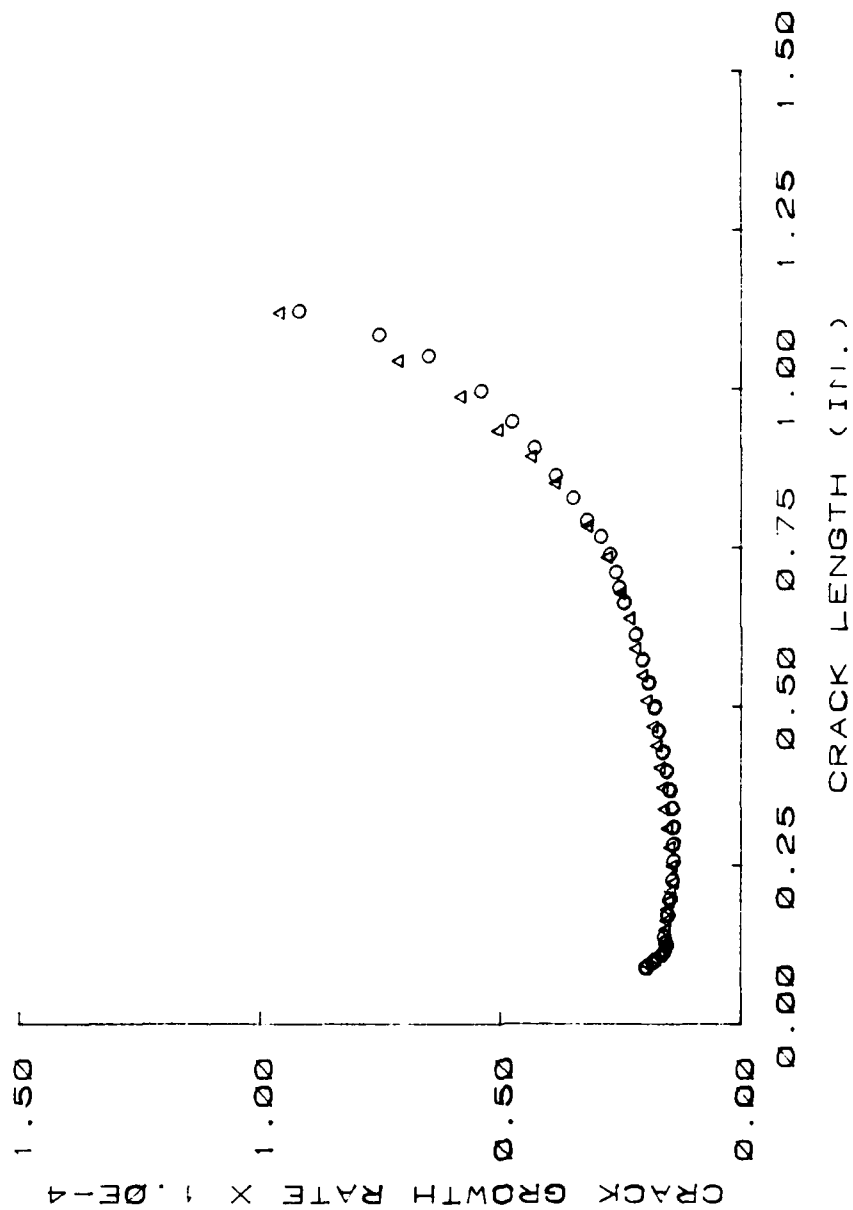


Figure 22: 2024-T351 Aluminum Corner-Crack-at-a-Hole Test Data.
 Back Surface Crack Length vs. Crack Growth Rate.
 Maximum Stress - 15 ksi, Load Ratio - R=0.3

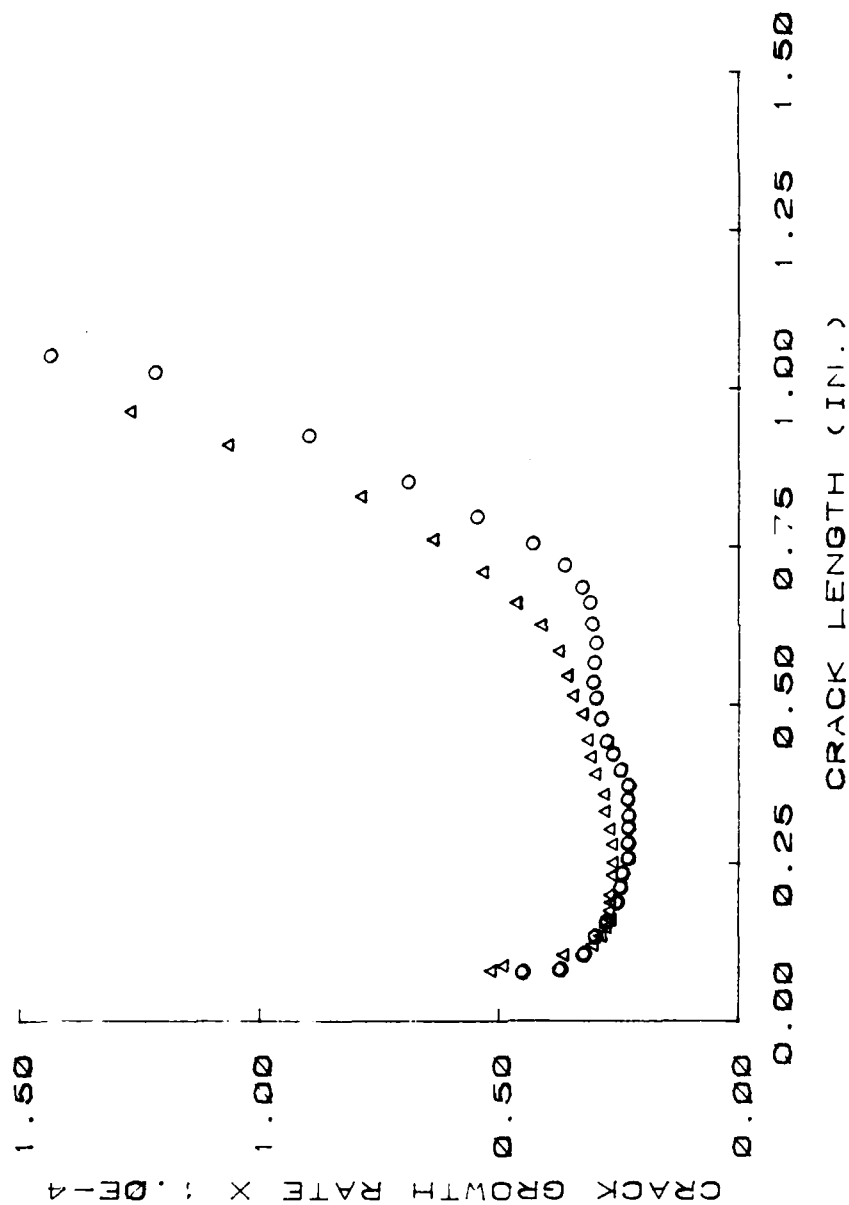


Figure 23 : 2024-T351 Aluminum Corner-Crack-at-a-Hole Test Data.
 Back Surface Crack Length vs. Crack Growth Rate.
 Maximum Stress - 15 ksi, Load Ratio - R= -0.5

$$K_{\max} = [8.9593 \times 10^8 (dc/dN)]^{.26896} (1-R)^{-.7} \quad (5)$$

for the front surface. When dc'/dN is substituted for dc/dN in Equation (5) the K_{\max} for the back surface is obtained. The stress intensity factor equation for the front surface the negative stress ratio was found to be:

$$K_{\max} = [2.31726 \times 10^8 (dc/dN)]^{.31137} \quad (6)$$

Similarly, to obtain K_{\max} for the back surface dc/dN is replaced for dc'/dN in equation (6). Recall that dc/dN and dc'/dN are found using a polynomial regression curve-fit to each duplicate set of data. In this case a 5th-order polynomial seemed to optimize the fit.

NOTE: Experimental stress intensity factors along the bore of the hole could not be found because no measurements could be made along the bore of the hole. The predicted number of cycles to back surface breakthrough and an average K_{\max} will be calculated and used in life predictions in a later section of this work.

4. 0 ANALYTICAL STRESS INTENSITY FACTORS

Three different analytical stress-intensity-factor solutions were considered in this thesis. The first solution was the Newman-Raju three-dimensional finite element solution [9] developed for corner cracks at a hole. The second solution was the Grandt linearization of the Bowie equation [10, 11] used for through cracks after back surface penetration has occurred. Finally, analytical stress intensity factors were calculated using Opel's transition-region correction factors [5] applied to the Newman-Raju solution in the corner crack region and to the Grandt/ Bowie solution for a through crack after back surface penetration. After the stress-intensity-factors were calculated, correlations were made between the experimental results and the Newman-Raju/ Grandt-Bowie solutions without transition corrections and by using Opel's transition region correction factors. (These results will be used in a later section to obtain life predictions in order to assess the accuracy of the analytical stress-intensity-factors.)

4. 1 Newman-Raju Solution for Corner-Cracks-At-A-Hole.

The Newman-Raju solution for stress intensity factors for corner cracks at holes was considered because of its accuracy as outlined by Heckel and Rudd [36] . This solution was also chosen because it is currently one of the most widely used solutions in the aerospace industry. The equation considered was based on an initial crack

eccentricity (a/c : crack depth divided by crack length, see Fig.1, greater than one). The equation is:

$$K_{\max} = \sigma_{\max} \sqrt{\pi a/Q} F_{ch}(a/c, a/t, R/t, c/b, \phi) F_{sh} \quad (7)$$

where:

$$Q = 1 + 1.464(c/a)^{1.65} \quad (8)$$

$$F_{ch} = [M_1 + M_2(a/t)^2 + M_3(a/t)^4] g_1 g_2 g_3 f\phi f_w \quad (9)$$

$$M_1 = \sqrt{c/a} (1 + 0.04(c/a)) \quad (10)$$

$$M_2 = 0.2(c/a)^4 \quad (11)$$

$$M_3 = -0.11(c/a)^4 \quad (12)$$

$$g_1 = 1 + [0.1 + 0.35(c/a)(a/t)^2](1 - \sin\phi)^2 \quad (13)$$

$$g_2 = [1 - 0.15\lambda + 3.46\lambda^2 - 4.47\lambda^3 + 3.52\lambda^4] / [1 + 0.13\lambda^2] \quad (14)$$

$$\lambda = [1 + (c/r)\cos(0.85\phi)]^{-1} \quad (15)$$

$$g_3 = [1.13 - 0.09(c/a)][1 + 0.1(1 - \cos\phi)^2][0.8 + 0.2(a/t)^{2.5}] \quad (16)$$

$$f\phi = [(c/a)^2 \sin^2\phi + \cos^2\phi]^{0.25} \quad (17)$$

$$f_w = [\sec(\pi R/2b) \sec(\sqrt{a/t}(\pi(2R+c))/(4(b-c)+2c))]^{0.5} \quad (18)$$

$$F_{sh} = [(4/\pi + ac/2tR)/(4/\pi + ac/tR)]^{0.5} \quad (19)$$

See reference 9 for details of this solution.

4.1.1 Boundary-Layer Effect On Stress Intensity Factors. Hartranft and Sih [37] suggested that the stress intensity factors in a very thin "boundary-layer" near the intersection of the crack-front with a free surface drop off rapidly and tend to zero at the free surface. This idea suggests a trend opposite to that of Newman and Raju's life prediction solution [9]. Their solution assumes that the stress intensity factors tend towards infinity at the surface. Some reflection on the problem will help to clarify the situation. A large stress intensity factor would lead to a higher value of da/dN , which would predict a shorter life. The Newman-Raju solution has been known to be quite conservative [5, 6, 9] i.e. they seem to over-estimate the stress intensity factor which leads to a prediction of shorter lives than those observed experimentally. Newman and Raju investigated Hartranft and Sih's suggestion using finite element techniques and found that the stress intensity factors tended toward zero at the free surface, as proposed. This implies, theoretically, that no crack would grow at the surface of the specimen (i.e., if K_{max} approaches zero, da/dN approaches zero, da/dN approaches zero). Newman and Raju subsequently investigated the effect of the boundary layer by evaluating stress intensity factors along an imaginary surface at an angle ϕ from the free surfaces (see Fig. 1). A graph showing the trend of the Newman-Raju correction and the result of evaluating the stress intensity factors at an angle ϕ from the free surface is shown in Fig. 24. It can easily be seen that at the free surface (i.e.,

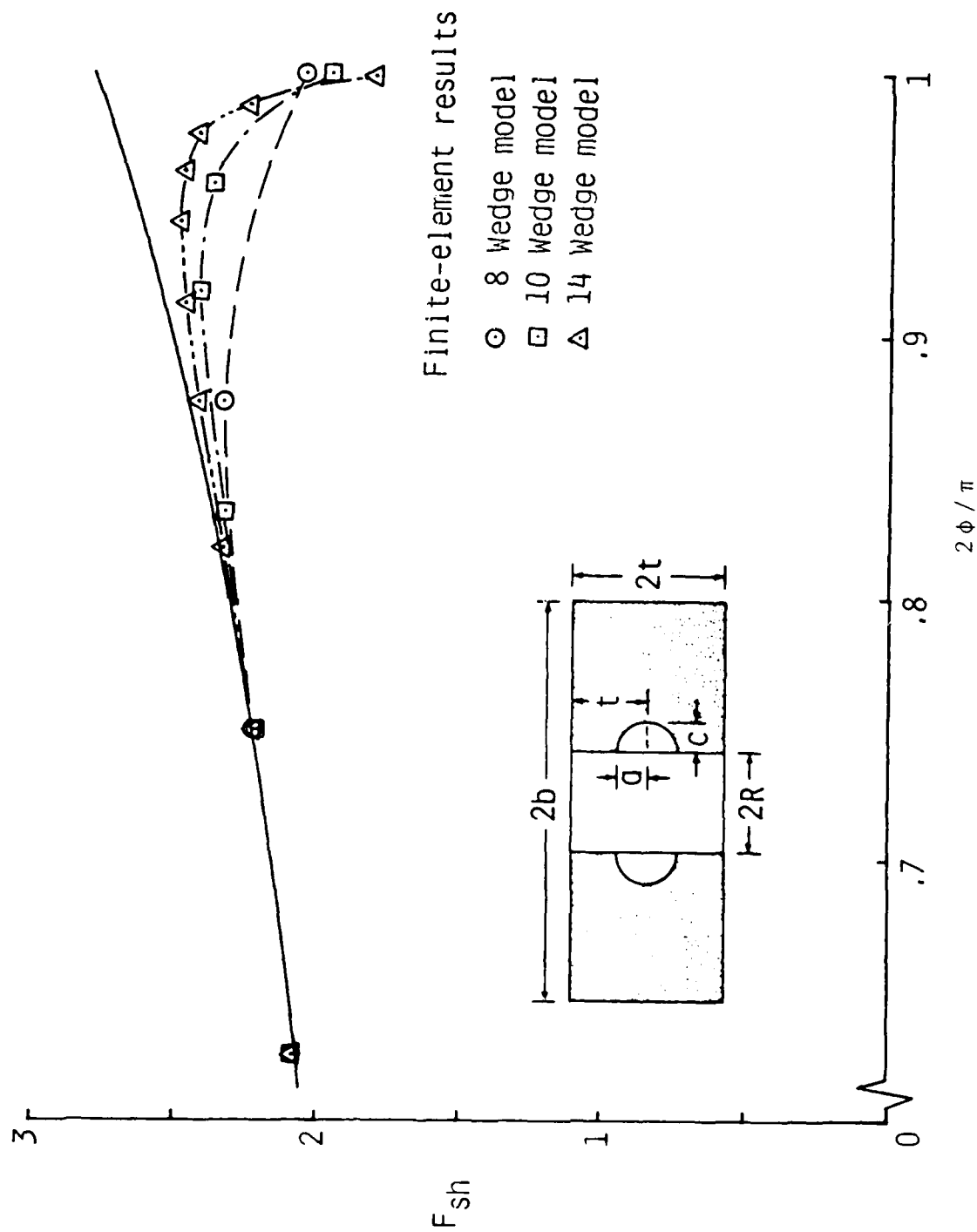


Figure 24. Effects of Mesh Refinement Near the Free Surface on the Distribution of Boundary-Correction Factors for Surface Cracks at a Hole [9]

where $2\phi/\pi = 1$), there is some inconsistency. If the angle ϕ is increased, the solutions become more consistent. (Newman and Raju did find that beyond a value of $\phi > .4\pi$, there was no difference between the two solutions, see Fig. 24).

Recently, an ASTM Task Group was established for the purpose of improving current methods for calculating stress intensity factors. The task group has been sponsoring an annual stress intensity factor solution "round-robin". The participants provide stress intensity factor solutions and these are evaluated by comparing them to other participant solutions for the purpose of finding better solutions. Some participants have used this idea of evaluating the stress intensity factor along a surface at an angle of ϕ (ϕ , is the parametric angle and is equal to 0° at the front surface and 90° at the base of the hole), most notably Chung [43], and have met with a great deal of success. An appropriate value for the angle ϕ , based on results from the round-robin competition, is $\phi = 10^\circ$.

Evaluation of the stress intensity factors along a surface at $\phi = 10^\circ$ (see Fig. 1 for geometry), has lead to improvement in accuracy of life prediction using the Newman-Raju corner-crack-at-a-hole solution. Life Predictions until back surface penetration (the only region where ϕ has an effect) improved an average of 20% for 2024-T351 aluminum and 30% for 7075-T651 aluminum using the Uncorrected Newman-Raju solution (see Tables 3 and 4, respectively). The improvement in life prediction is quite significant and therefore, the solutions for 2024-T351 and 7075-T651 aluminum, studies in this thesis, will include the angle $\phi = 10^\circ$ in all calculations.

$\sigma_{\text{max}} = 18 \text{ ksi}$ $\sigma_{\text{max}} = 15 \text{ ksi}$

R = 0.1 R = 0.3 R = -0.5 R = 0.1 R = 0.3 R = -0.5 Average

$\psi = 0^\circ - 90^\circ$

a = t	9,053 (37.33)	16,105 (44.24)	5,135 (44.46)	16,561 (35.42)	39,144 (46.32)	12,598 (46.40)	(42.36)
a=t -- C=Cc	12,310 (65.10)	23,746 (71.65)	11,422 (69.22)	24,333 (66.61)	46,748 (91.68)	20,103 (70.06)	(72.39)
C = Cc	21,363 (49.50)	39,851 (57.31)	16,557 (59.03)	40,894 (49.10)	85,892 (63.39)	32,701 (58.56)	(56.15)

$\psi = 10^\circ - 80^\circ$

a = t	13,509 (55.71)	23,910 (65.69)	7,247 (62.74)	24,784 (53.01)	57,744 (68.34)	18,248 (67.21)	(62.12)
a=t -- C=Cc	11,430 (60.44)	22,078 (66.62)	10,821 (65.58)	22,615 (61.91)	43,392 (85.10)	18,893 (65.84)	(67.53)
C = Cc	24,939 (57.78)	45,988 (66.13)	18,068 (64.41)	47,399 (56.91)	101,136 (74.64)	37,141 (66.51)	(64.40)

() - indicates percent of experimental life

TABLE 3: Parametric Angle Effect for 2024-T351 Aluminum Using Newman-Bowie Solution (Uncorrected)

		$\sigma_{max} = 20 \text{ ksi}$			$\sigma_{max} = 15 \text{ ksi}$		
		R=0.1	R=0.3	R=-0.5	R=0.1	R=0.3	R=-0.5
$\psi = 0^\circ - 90^\circ$							Average
a=t		4,311 (54.02)	6,626 (48.72)	3,815 (59.70)	10,771 (84.28)	15,373 (105.95)	7,491 (88.65)
							8,374 (62.45)
a=t-c=c		7,192 (64.87)	11,088 (59.94)	6,612 (70.72)	19,295 (66.12)	29,740 (74.63)	16,954 (91.25)
							16,550 (57.31)
c=c		11,503 (59.79)	17,714 (55.18)	10,427 (66.25)	30,066 (71.65)	45,113 (83.00)	24,445 (90.44)
							24,924 (58.94)
$\psi = 10^\circ - 80^\circ$							
a=t		6,282 (78.12)	9,613 (70.63)	5,289 (82.77)	15,551 (121.68)	22,127 (152.49)	10,382 (122.86)
							11,442 (85.52)
a=t-c=c		6,703 (59.53)	10,230 (55.57)	6,925 (74.06)	18,100 (62.03)	27,915 (70.05)	16,351 (85.00)
							16,225 (56.18)
c=c		12,985 (67.50)	19,893 (61.97)	12,214 (77.60)	33,651 (80.20)	50,042 (92.06)	26,733 (98.90)
							27,667 (65.42)

() - indicates percent of experimental life

TABLE 4: Parametric Angle Effect for 7075-T651 Aluminum Using Newman-Bowie Solution (Uncorrected)

4.2 Grandt's Linearization of Bowie's Solution for Through Cracks.

The Grandt linearization of the Bowie equation described by Engle [11] was considered for through cracks from back surface penetration until final fracture. The equation considered was:

$$K_{\max} = \sigma_{\max} \sqrt{\pi c} F_{gr}(c/r) f_w \quad (20)$$

where: $F_{gr} = .6762062 = [.8733015 / (.3245442(c/R))]$

f_w is given by equation (18).

Details for this solution are given in reference 11.

4.3 Opel's Correction Factors. In the third of the solutions considered, in his thesis Opel introduced transition region correction factors for the Newman-Raju and Grandt/Bowie solutions. Opel separated the transition region into two different regions. The beginning of the first transition region was where $a/t = 0.75$ and ended where $a/t = 1.0$ (see Fig. 25 for details). From the initial crack length to where $a/t = 0.75$, the Newman-Raju solution was used without correction factors. From $a/t = 0.75$ to $a/t = 1.0$ Opel applied the correction factor F_{tr} to the Newman-Raju solution. The new stress-intensity-factors (K) new were found using an equation of the form:

$$(K)_{\max} = (K)_{N-R} \times (F_{tr}) \quad (21)$$

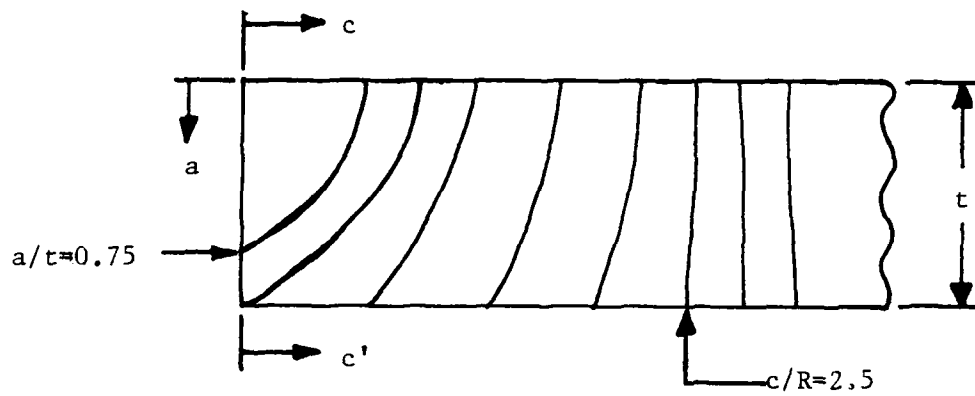


Figure 25a: Opel's Transition Region

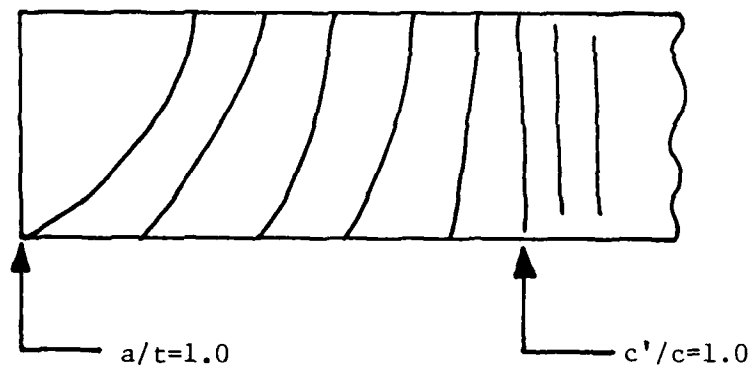


Figure 25b: Chansler's Transition Region

F_{tr} , Opel's correction factor, was found using the James-Anderson backtracking technique and a polynomial regression curve fit, and was determined to be of the form

$$(F_{tr})_b = 1/ [.573924 + 1.468068(a/t) - 1.275787(a/t)^2],$$

for the base of the hole and

$$(F_{tr})_{fs} = 1/[1.31687 - .362863(a/t)], \quad a \leq t$$

for the front surface.

Transition correction factors were also developed for the region from the back surface penetration ($a/t = 1.0$) to the end of the transition region where $c/r = 2.5$. The correction factor for the back surface was found to be:

$$(F_{tr})_{bs} = 1/ [.191601 + .724961(c'/R) - .158451(c'/R)^2]$$

The equation used for the stress-intensity-factors on the back surface transition region was:

$$(K)_{bs} = \sqrt{c' \pi} F_{B-G}(c'/R) F_w(F_{tr})_{bs}$$

where $F_{B-G}(c'/r)$ is the Grandt curve fit [10] to Bowie's tabular hole correction factor [12]. f_w is the finite width correction used by Newman-Raju [9]. The Grandt linearization of the Bowie solution was used for stress intensity factors for the region from the end of the transition region to final fracture.

5.0. DEVELOPMENT OF TRANSITION CRITERIA

5.1. The Transition Region

The transition region for corner-crack-at-a-hole problems has been treated in various ways in a number of life prediction solutions. Current procedures dealing with this transition region range from the development of correction factors to compensate for the region to totally ignoring the transition region by assuming a through-the-thickness crack at back surface penetration. It is suggested here that the transition region be dealt with in the following manner. First, assume there are no transition effects along the base of the hole. Second, assume the transition region extends from back surface penetration ($a=t$) to a point where the front surface crack length (c) is approximately equal to the back surface crack length (c'), i.e. $c'/c = 0.9$. Finally, it will be necessary to develop transition region correction factors for this region from $a = t$ to $c/c' = 0.9$ that are based on the crack shape as it propagates through the transition region. Since the original intent of this work was to derive material-independent transition region correction factors based on the work by Opel [5], the approach outlined above represents a significant departure from the original intent. Therefore, some justification is warranted.

5.1.1. Corner Crack until Back Surface Penetration. Physically, the idea that no correction factors are needed in this region makes sense.

As the crack propagates towards back surface penetration, it retains a quarter-elliptical shape with varying aspect ratio until $a = t$. (See Fig. 1.) Therefore, no correction factor should be necessary. This idea contradicts the work by Opel, but there are good reasons that can be justified analytically.

Opel developed transition correction factors in this region primarily to improve on Newman and Raju's conservative life prediction solution for corner cracks at a hole. The discussion of the boundary layer effects in the previous section suggested by Hartranft and Sih [37] and tested by Newman and Raju [9] provide a means by which to improve the conservative Newman-Raju corner crack solution.

The Newman-Raju solution is a function of the angle ϕ , among other parameters. (See Fig. 1.) Opel's correction factors for stress intensity and life predictions are based on $\phi = 0^\circ$ and 90° , corresponding to the front surface and the surface along the base of the hole respectively. Hartranft and Sih suggest that calculation of stress intensity factors along an imaginary surface at the interior of the specimen would lead to possibly more accurate life predictions. This idea seems to be valid based on finite element solutions made by Newman and Raju. In fact, life predictions are improved drastically if ϕ is 10° and 80° which correspond to imaginary surfaces near the front surface and near the surface at the base of the hole respectively. Tables 5 and 6 show comparisons of solutions for 2024-T351 and 7075-T651 aluminums respectively. The first solution is the

		$\sigma_{\max} = 18 \text{ ksi}$			$\sigma_{\max} = 15 \text{ ksi}$		
		$R = 0.1$	$R = 0.3$	$R = -0.5$	$R = 0.1$	$R = 0.3$	$R = -0.5$
$\phi = 0^\circ - 90^\circ$							
$a = t$		9,053 (37.33)	16,105 (44.24)	5,135 (44.46)	16,561 (35.42)	39,144 (46.32)	12,598 (46.40)
$\phi = 10^\circ - 80^\circ$							
$a = t$		13,509 (55.71)	23,910 (65.69)	7,247 (62.74)	24,784 (53.01)	57,744 (68.34)	28,248 (67.21)
							Average

Table 5: Comparison of Life to Back Surface Penetration for Different Parametric Angles
Using Newman-Raju (Uncorrected) for 2024-T351 Aluminum

		$\sigma_{\max} = 20 \text{ ksi}$		$\sigma_{\max} = 15 \text{ ksi}$			
		R = 0.1	R = 0.3	R = -0.5	R = 0.1	R = 0.3	R = -0.5

uncorrected Newman-Raju solution with $\phi = 0^\circ$ and 90° and the second is the uncorrected Newman-Raju solution with $\phi = 10^\circ$ and 80° . Comparing these two solutions for life until back surface penetration ($a=t$), it can easily be seen that using $\phi = 10^\circ$ and 80° improves the Newman-Bowie model enough to warrant the exclusion of all correction factors used for life until back surface penetration.

5.1.2. Back Surface Penetration Until Final Fracture. Opel chose to use transition region correction factors in this region based on front and back surface crack lengths, normalized by the hole radius (R), c/R and c'/R respectively. These transition region correction factors were applied from back surface penetration ($a = t$) to a point where $c/R, c'/R = 2.5$. (See Opel for discussion on development of the end point for the transition region.) The Opel transition correction factors produced favorable results towards increasing the accuracy of the Grandt linearization of the Bowie solution for through the thickness cracks. However, when examined closely, it turns out that these corrections are highly dependent on specimen thickness. This dependence can easily be seen by considering an example (see Fig. 26). The specimens considered by Opel were fabricated from 7075-T651 aluminum with thickness $t = .25$ inches and a hole radius $R = .125$ inches. After the crack propagates through the back surface at $a = t$, Opel applied the transition correction factors, based on c/R and c'/R , to the Grandt-Bowie solution with favorable results. Opel applied correction factors, based on specimens with $t = .25$, to the region $a = t$

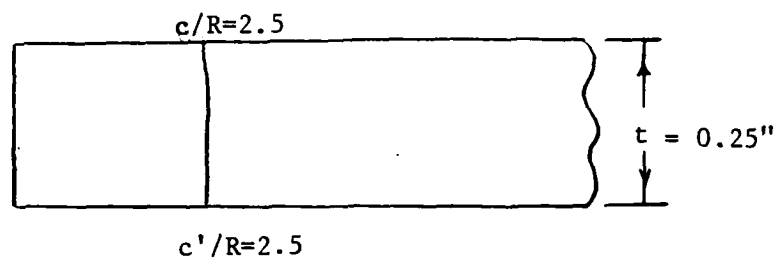


Figure 26a:

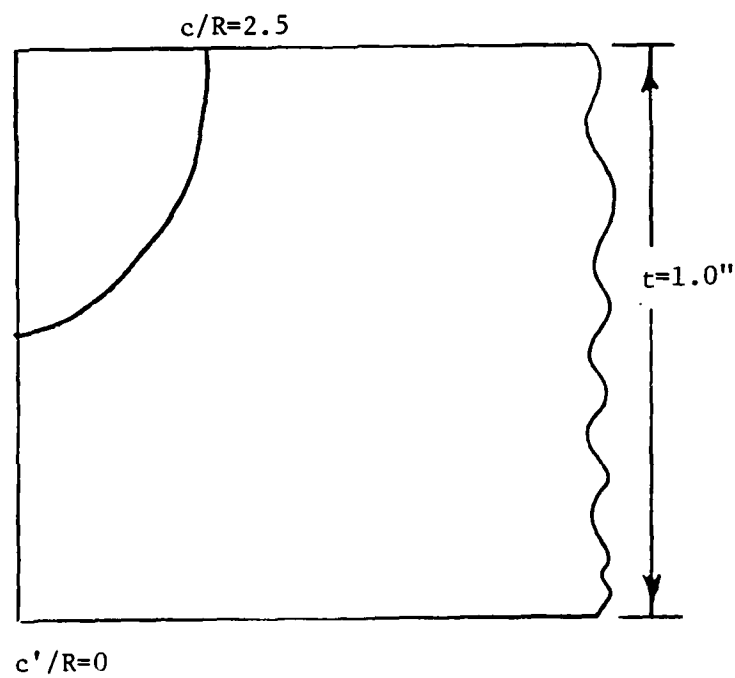


Figure 26b:

Figure 26 : Comparison of End of Opel Transition Region
For Specimens of Different Thickness

(or $c'/R = 0$ to $c'/R = 2.5$. At $c'/R = 2.5$, the crack was considered a through-the-thickness crack and after that point no corrections were necessary to modify the Grandt-Bowie solution. (Note: $c'/R = 2.5$ corresponds to $c' = .3125$ inches and at this point $c = .3125$ inches as well.) If one were to consider a thicker specimen, say $t = 1.0$ inch, with the same hole radius ($R = .125$ "), the crack would not have reached back surface penetration ($a = t$) when $c/R = 2.5$ (i.e. $c' = 0$). Therefore, applying surface correction factors at $c/R = 2.5$ for the thicker specimen would be invalid. Clearly, correction factors based on $t = .25$ and dependent on c/R , c'/R are only valid for specimens $.25$ " thick and new correction factors must be developed for different thicknesses. Developing new correction factors for each thickness would provide favorable results but would be much too tedious a task, involving experiments and analytical corrections each time a life prediction is necessary. Therefore, the development of correction factors that are independent of specimen thickness is highly desirable.

Rudd [42] suggested that the transition region after back surface penetration be corrected by transition correction factors based on the shape of the crack as it propagates from $a = t$ to a complete through-the-thickness crack. The shape of the crack can be dealt with by understanding how the front surface crack length (c) and the back surface crack length (c') vary with each other. When $c' = c$ (or $c'/c = 1$), the crack lengths on both surfaces are equal and a true through-

the-thickness crack exists (See Fig. 1.) If transition correction factors are based on c'/c , then the correction factors become thickness-independent.

5.2. Analytical/Experimental Correlations

Correlations were made of the experimental stress intensity factor ranges, using a form of the Walker equation, with the analytical predictions, based on the Grandt-Bowie solution, for 2024-T351 and 7075-T651 aluminum for the region from back surface penetration until the final fracture region. Experimental stress intensity factors were obtained using the James-Anderson backtracking technique, based on duplicate specimens for each of 6 different load conditions. The procedure used to obtain the appropriate correlations is outlined next:

- 1) Using the James-Anderson backtracking techniques, experimental data in the form of c vs N (and c' vs N for back surface) were converted to c vs dc/dN (and c' vs dc'/dN).
- 2) Results from 1) above for each duplicate set of specimens were curve-fitted using an ASTM-recommended polynomial regression scheme. The data were "best fitted" to 5th-order equations. This provided dc/dN and dc'/dN equations as functions of c and c' for each set of duplicate specimens.

- 3) The experimental stress intensity factor (K_E) was calculated from back surface penetration to final fracture using the Walker equation.
- 4) The analytical stress intensity factor (K_A) was calculated from back surface penetration to final fracture using the Grandt-Bowie solution.
- 5) Results are plotted in the form of c'/c vs K_A/K_E (See Figs. 27 to 30.)

The correlations show that at $c'/c = 1.0$, K_A/K_E approaches a constant. Therefore, the end of the transition region is where $c'/c = 0.9$ and the crack can be approximated as a through-crack. This result can favorably be compared to Johnson [34] who defined the end of the transition region to be $c'/c = .9$ for life prediction approximations.

5.3. Correction Factor Development

5.3.1. Back Surface Penetration Until Final Fracture. As noted in the previous section, correlations tend to become constant at K_A/K_E when $c'/c = 0.9$. Fig.31 shows the correlations for the back surface data. The polynomial regression curve fit for this data was found to be

$$(Ftr)_{bs} = [1/.609633 - .689614(c'/c) + 1.23275(c'/c)^2]$$

and it is plotted in Fig.31. It was found that a quadratic curve fit

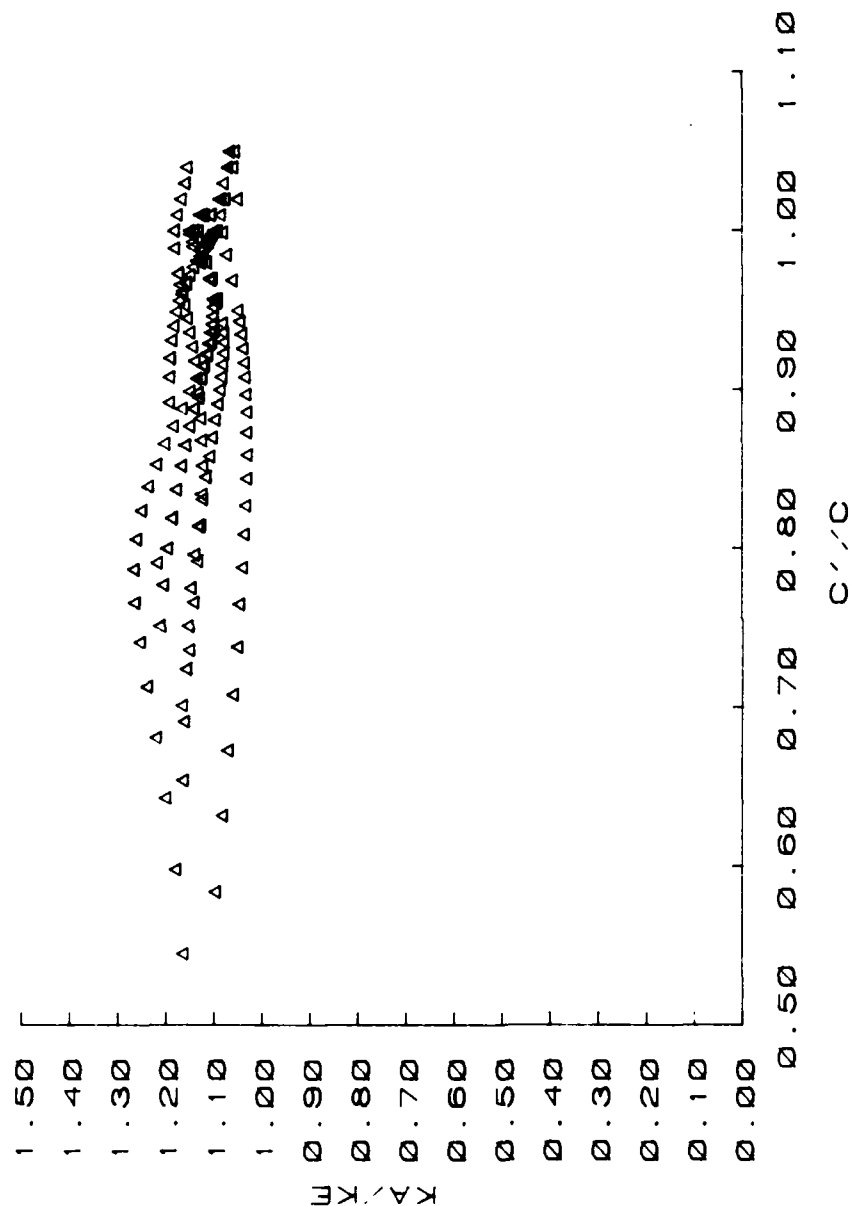


Figure 27: Correlation of Stress Intensity Factors Along the Front Surface of the 2024-T351 Aluminum Test in the Region of Interest

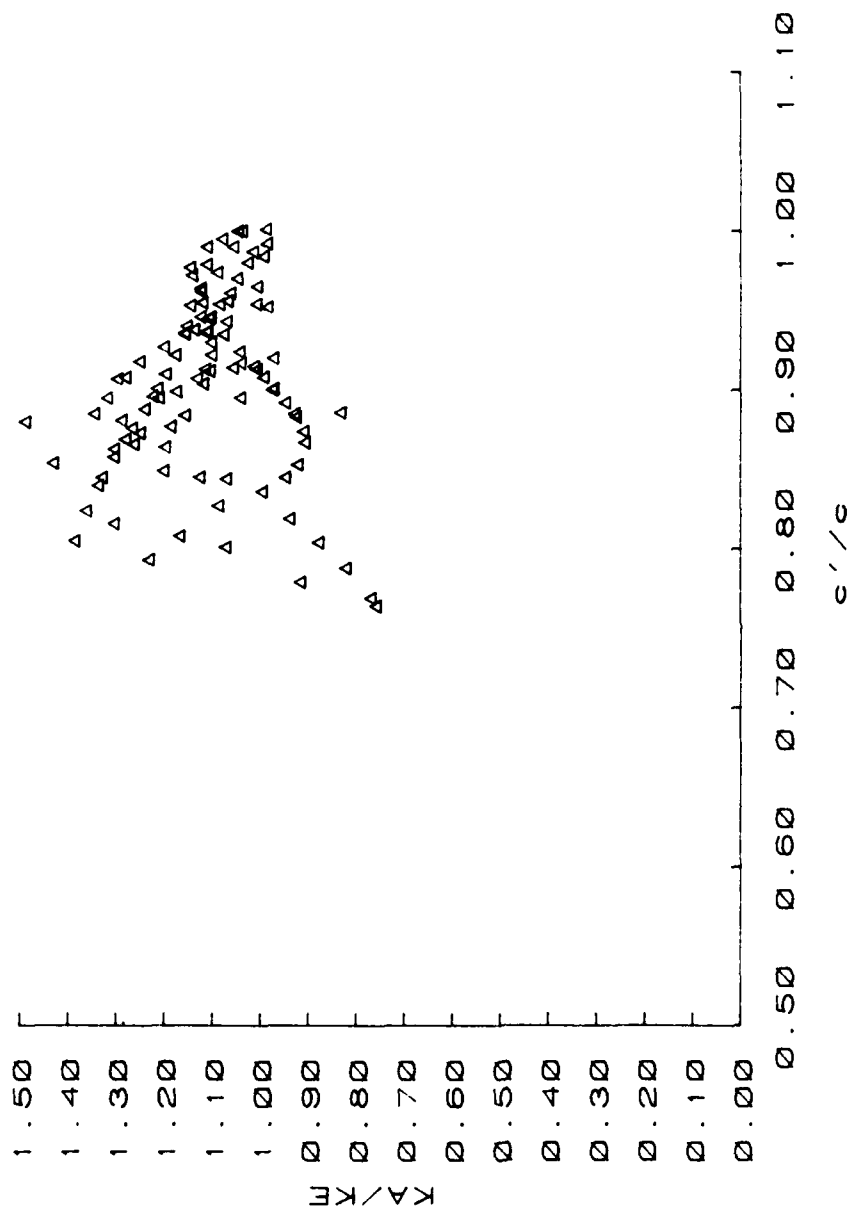


Figure 28: Correlation of Stress Intensity Factors Along the Front Surface of the 7075-T651 Aluminum Test in the Region of Interest

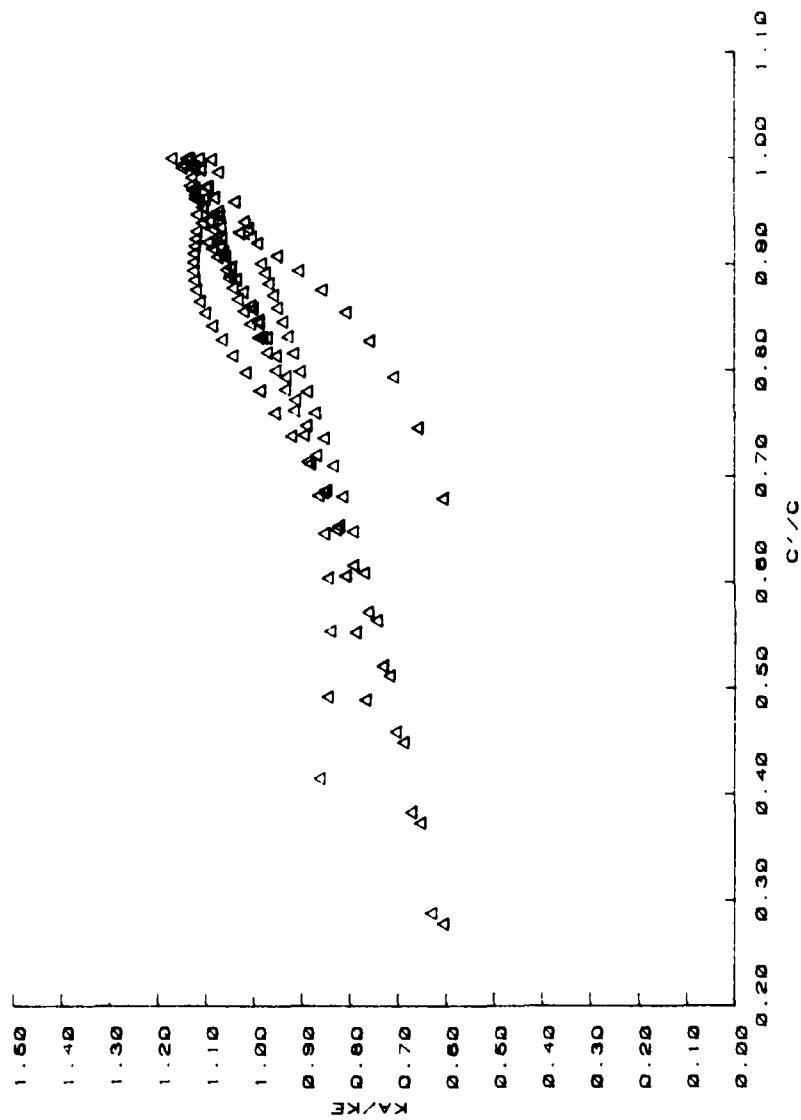


Figure 29: Correlation of Stress Intensity Factors Along the Back Surface of the 2024-T351 Aluminum Test in the Region of Interest

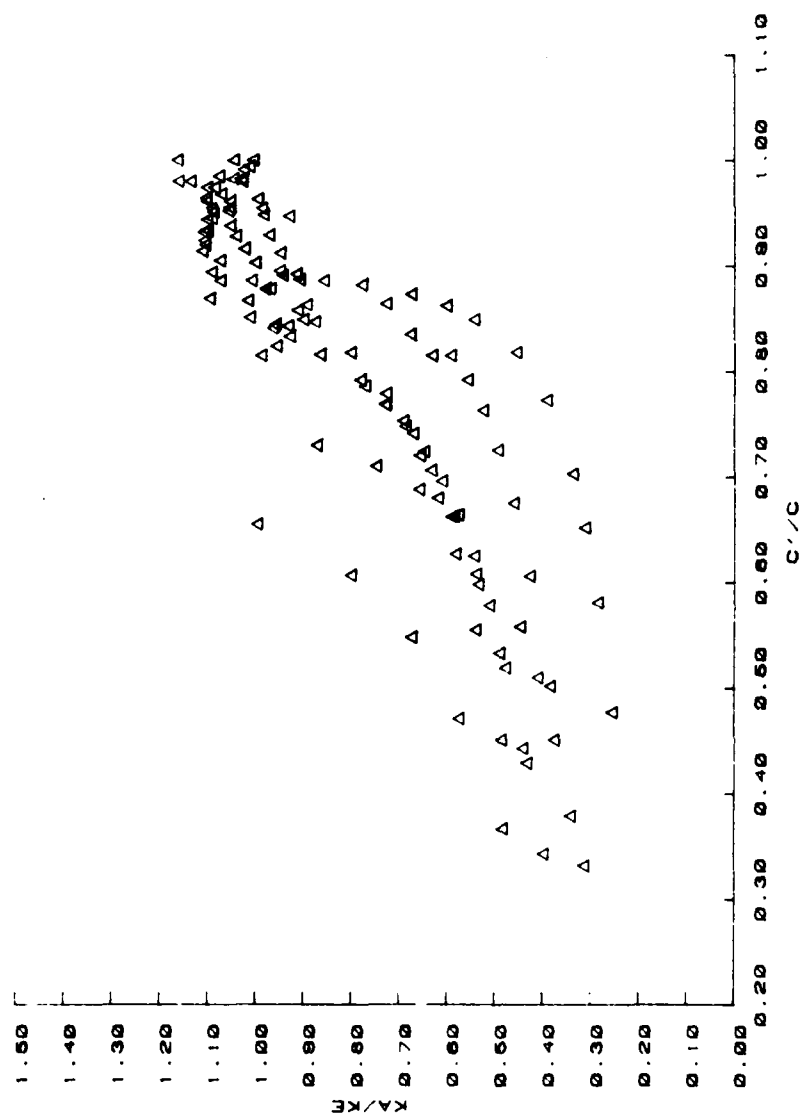


Figure 30: Correlation of Stress Intensity Factors Along the Back Surface of the 7075-T651 Aluminum Test in the Region of Interest

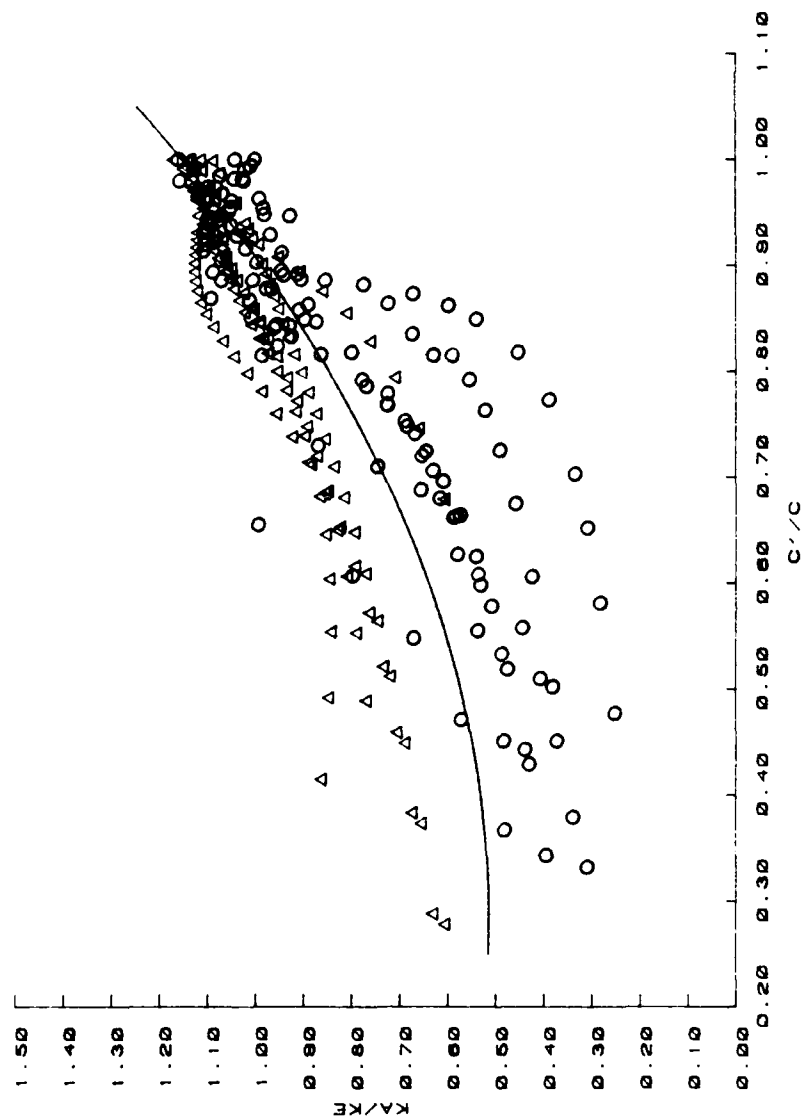


Figure 31: Superposition of Correlations of Stress Intensity Factors
Along the Back Surface for 2024-T351 and 7075-T651 Aluminum Tests.
(Correction Factor Plotted in the Transition Region.)

resulted in a good correlation for the data. Correlations did not improve significantly when higher order curve fits were attempted.

This correction is applied to the Grandt-Bowie solution after back surface penetration until final fracture. This correction, when applied to the correlation data, essentially brings all the data points to a constant value of $K_A/K_E = 1.0$. The effect would be to "speed up" the growth of the crack on the back surface, and "slow down" the growth of the crack on the front surface. Therefore more accurate life predictions will result when the correction factors are used to modify the stress intensity factors on the front and back surfaces.

5.3.2. Front Surface.

In a similar manner, the front surface correction factor based on the polynomial regression curve fit is:

$$(F_{tr})_{fs} = [1/1.24007 - .13564(c'/c)]$$

and it is plotted in Fig.32. Again, it was found that a linear curve fit resulted in a good correlation and did not improve significantly when higher order curve-fits were attempted.

The correction factors for the front and back surfaces were substituted into the Grandt-Bowie equation as follows:

$$(K_{max})_{cor} = (K_{max})_{G-B}/(F_{tr})_{bs}$$

$$(K_{max})_{cor} = (K_{max})_{G-B}/(F_{tr})_{fs}$$

where $(K_{max})_{cor}$ is the corrected stress intensity factor, $(K_{max})_{G-B}$ is the Grandt-Bowie solution and $(F_{tr})_{bs}$, $(F_{tr})_{fs}$ are the back and front surface correction factors respectively.

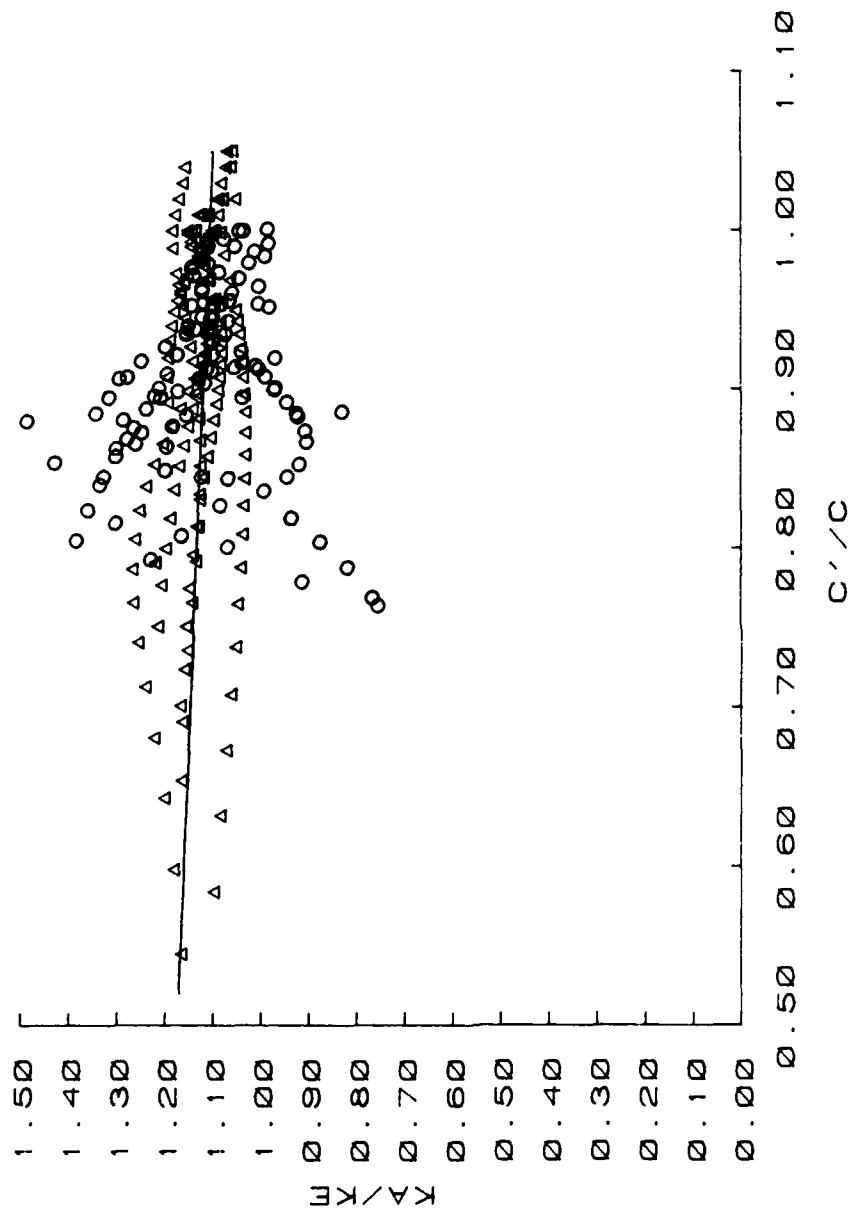


Figure 32: Superposition of Correlations of Stress Intensity Factors Along the Front Surface for 2024-T351 and 7075-T651 Aluminum Tests.
(Correction Factor Plotted in the Transition Region.)

5.4. Summary of Transition Region.

In summary, the growth of a crack as it grows from a corner-crack-at-a-hole to final fracture can be separated up into three phases:

- 1) Corner crack at a hole until back surface penetration ($a = t$); this phase is dealt with by evaluation for stress intensity factors along "imaginary" surfaces near the top surface and the surface at the base of the hole to preclude effects of fabrication (cold-rolling, hole drilling, etc.). No other corrections are necessary to the Newman-Raju solution.
- 2) Back surface penetration ($a = t$) until through-the-thickness crack ($c'/c = 0.9$); this is dealt with by applying front-and-back-surface correction factors, $(F_{tr})_{fs}$ and $(F_{tr})_{bs}$ respectively, to the Grandt-Bowie solution for through-the-thickness cracks.
- 3) Through the thickness crack until final fracture; use only the Grandt-Bowie solution, no corrections.

6.0 Evaluation of Transition Criteria.

6.1 Life Prediction Models Used

An evaluation is made of the accuracy of the transition criteria developed in this study as well as that of an instantaneous criterion [11], Opel's criterion [5], a criterion developed by Brussat et al. [8] and one developed by Collipriest and Ehret [7]. Life predictions are made using these criteria. These predictions are then compared with each other, as well as with the corner crack at a hole test results for 7075-T651 and 2024-T351 aluminum previously described.

Life predictions were made for corner crack at a hole specimens subject to constant amplitude loading. These life predictions were based on material characterization data obtained for 2024-T351 and 7075-T651 aluminum. This characterization data was used to derive the proper form of the Walker equation for each type of aluminum, see equations 2 through 3 for 2024-T351 aluminum and the following equations were used for 7075-T51 aluminum (from Opel [5]):

$$da/dN = 3.2624 \times 10^{-9} [(1-R) \cdot K_{\max}]^{3.3908} \quad (23)$$

for positive stress ratios and for negative stress ratios:

$$da/dN = 1.29 \times 10^{-8} [K_{\max}]^{2.89} \quad (24)$$

Using the Walker equations, the crack growth rate was calculated and then the new crack length was found by integrating after each cycle. Subsequent crack lengths were found by adding the change in crack length to the previous crack length.

Three different lives were considered for each life prediction model: (a) from the initial crack sizes specified in Tables 2 and 7 to back surface penetration ($a=t$), (b) from back surface penetration to final fracture and ($a=t \rightarrow C=C_c$), (c) total life ($C = C_c$). The instantaneous transition criterion predictions were made using the Newman-Raju corner crack at a hole solution [9] until back surface penetration occurred (i.e. $a = t$). The Grandt linearization of the Bowie solution for through the thickness cracks [10] was then used, assuming an initial back surface crack length equal to the front surface crack length at the time of back surface penetration. In addition to the transition criteria developed in this study, the Brussat, Opel and Collipriest-Ehret criteria were applied according to procedures outline in [8, 5, and 7] respectively.

6.2 Results.

6.2.1. Life Predictions Based on Corrected Stress Intensity Factors. (Note: Experimental results were obtained by Heckel & Rudd [25] and analytical predictions made by Opel [5] for a 7075-T651 aluminum. Experimental lives for 2024-T351 and 7075-T651 aluminum are shown in Tables 8 and 9, respectively.)

Analytical life predictions were made for the six 2024-T351 aluminum test conditions presented in Table 2 and the seven 7075-T651 aluminum test conditions presented in Table 7 using the criteria developed in this study. Each experimental life shown in these tables represents the average of duplicate specimens. The life predictions

Specimen Number	Load Ratio (R)	a_i (in)	c_i (in)	σ_{max} , ksi
FH-7	0.1	.074	.053	20.00
FH-8	0.3	.076	.051	20.00
FH-9	-0.5	.071	.050	20.00
FH-10	0.1	.089	.050	15.00
FH-11	0.3	.102	.050	15.00
FH-13	-0.3	.097	.053	15.00
FH-12	-0.5	.081	.051	15.00

TABLE 7: 7075-T651 Aluminum Test Conditions
 (a_i, c_i) are average of duplicate specimens,
data from Opel [5])

$\sigma_{\max} = 18 \text{ ksi}$		$\sigma_{\max} = 15 \text{ ksi}$	
	$R = 0.1$	$R = -0.5$	$R = -0.5$
$a = t$	24,250	11,550	27,150
$a=t \rightarrow C=Cc$	18,910	16,500	28,695
$C = Cc$	43,160	83,280	55,845

TABLE 8: Experimental Life for 2024-T351 Aluminum
(Average of duplicate specimens)

$$\sigma_{\max} = 2\sigma \text{ ksi}$$

$$\sigma_{\max} = 15 \text{ ksi}$$

	R = 0.1	R = 0.3	R = -0.5	R = 0.1	R = 0.3	R = -0.3	R = -0.5
a = t	7,980	13,600	6,390	12,780	14,510	8,450	13,410
a=t → C=Cc	11,260	18,500	9,350	29,180	39,850	18,580	28,880
C = Cc	19,240	32,100	15,740	41,960	54,360	27,030	42,290

TABLE 9: Experimental Life for 7075-T651 Aluminum
(Averages of duplicate specimens, from Opell [5])

based on the corrections developed in this thesis are shown in Tables 10 and 11 for 2024-T351 and 7075-T651 aluminum, respectively.

6.2.2 Life Predictions Based on Other Models.

6.2.2.1 Newman-Bowie. The Newman-Bowie (instantaneous) method was used as presented by Engle [11] to predict the fatigue life for the specimens referenced in the previous section. The important consideration for this model is the fact that it ignores the transition region altogether. It assumes a through-the-thickness crack once back surface penetration has occurred. The results are presented in Table 12 for 2024-T351 and Table 13 for 7075-T651 aluminums.

6.2.2.2 Opel. The development of Opel's correction factors are discussed in section 4.3. (See Opel [5] for more details). His transition region correction factors for the base of the hole were derived from PMMA data and based on $\Phi = 0^\circ$ and 90° . The transition correction factors for the front and back surfaces are based on analytical and experimental stress intensity factors as a function of c/R and c'/R for 7075-T651 aluminum. Life predictions using these transition region correction factors are shown for 2024-T351 aluminum and 7075-T651 aluminum in Tables 1 and 14, respectively.

6.2.2.3 Brussat. The Brussat method [8] was developed for quarter-circular cracks at holes, therefore the initial crack length used was the average of the initial crack lengths along the base of the hole and along the front surface. The procedure used for the

		$\sigma_{\max} = 18 \text{ ksi}$			$\sigma_{\max} = 15 \text{ ksi}$			
		R = 0.1	R = 0.3	R = -0.5	R = 0.1	R = 0.3	R = -0.5	Average
a = t		13,509 (55.71)	23,910 (65.69)	7,247 (62.74)	24,784 (53.01)	57,744 (68.34)	18,248 (67.21)	(62.12)
a=t \rightarrow c=c _c		12,694 (67.13)	24,500 (73.93)	11,854 (71.84)	25,102 (68.72)	43,187 (94.50)	20,830 (72.59)	(74.79)
c = c _c		26,203 (60.71)	48,410 (69.61)	19,101 (68.10)	49,886 (59.90)	105,931 (78.18)	39,078 (69.98)	(67.75)

() - indicates percent of experimental life

Table 10: Life Prediction (Corrected Newman-Bowie) 2024-T351 Aluminum

		$\sigma_{\max} = 20 \text{ ksi}$			$\sigma_{\max} = 15 \text{ ksi}$		
		R = 0.1	R = 0.3	R = -0.5	R = 0.1	R = 0.3	R = -0.3
		Average			Average		
a = t		6,282 (78.72)	9,613 (70.68)	5,289 (82.77)	15,551 (121.68)	22,127 (152.49)	10,382 (122.86)
a=t → c=c _c		7,407 (65.78)	11,356 (61.38)	7,593 (81.21)	19,951 (68.37)	30,725 (77.10)	17,859 (96.12)
c = c _c		13,689 (71.15)	20,969 (65.32)	12,882 (81.84)	35,502 (84.61)	52,852 (97.23)	28,241 (104.48)
							29,192 (69.03)
							17,750 (61.46)
							11,442 (85.32)
							(102.07)
							(73.06)
							(81.95)

() - indicates percent of experimental life

Table 11: Life Prediction (Corrected Newman-Bowie) 7075-T651 Aluminum

$\sigma_{\max} = 15 \text{ ksi}$

$\sigma_{\max} = 18 \text{ ksi}$

	R = 0.1	R = 0.3	R = -0.5	R = 0.1	R = 0.3	R = -0.5	Average
a = t	13,509 (55.71)	23,910 (65.69)	7,247 (62.74)	24,784 (53.01)	57,744 (68.34)	18,248 (67.21)	(62.12)
a=t → C=Cc	11,430 (60.44)	22,078 (66.62)	10,821 (65.58)	22,615 (61.91)	43,392 (85.10)	18,893 (65.84)	(67.58)
C = Cc	24,939 (57.78)	45,988 (66.13)	18,068 (64.41)	47,399 (56.91)	101,136 (74.64)	37,141 (66.51)	(64.40)

() - indicates percent of experimental life

TABLE 12: Life Prediction (Instantaneous)
2024-T351 Aluminum

$\sigma_{max} = 20 \text{ ksi}$

$\sigma_{max} = 15 \text{ ksi}$

	R = 0.1	R = 0.3	R = -0.5	R = 0.1	R = 0.3	R = -0.3	R = -0.5	Average
a = t	6,282 (78.72)	9,613 (70.68)	5,289 (82.77)	15,551 (121.68)	22,127 (151.49)	10,382 (122.86)	11,442 (85.32)	(102.07)
a=t → C=C ₀	6,703 (59.53)	10,280 (55.57)	6,925 (74.06)	18,100 (62.03)	27,915 (70.05)	16,351 (88.00)	16,225 (56.18)	(66.49)
C = C ₀	12,985 (67.50)	19,893 (61.97)	12,214 (77.60)	33,651 (80.20)	50,042 (92.06)	26,733 (98.90)	27,667 (65.42)	(77.66)

() - indicates percent of experimental life

TABLE 13: Life Predictions (Instantaneous)
7075-T651 Aluminum

	$\sigma_{\max} = 20 \text{ ksi}$			$\sigma_{\max} = 15 \text{ ksi}$		
	R = 0.1	R = 0.3	R = -0.5	R = 0.1	R = 0.3	R = -0.5
Average						
a = t	3,955 (49.59)	6,080 (44.71)	3,530 (55.24)	9,815 (76.82)	13,892 (95.74)	7,717 (57.55)
a=t \rightarrow c=c _t	9,256 (82.20)	14,263 (77.10)	8,123 (86.88)	24,881 (85.27)	38,454 (96.50)	20,036 (110.55)
c = c _t	13,211 (68.66)	20,343 (63.37)	11,653 (74.03)	34,696 (82.69)	52,346 (96.30)	27,753 (65.63)

Table 14. Life Prediction. Opel's Model for 7075-T651 Aluminum

AD-A151 835

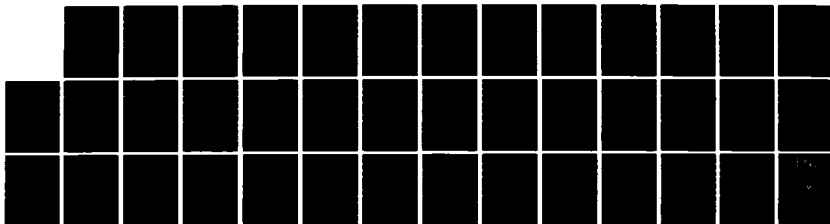
TRANSITION REGION FOR CORNER CRACKS AT HOLES(U) AIR
FORCE INST OF TECH WRIGHT-PATTERSON AFB OH SCHOOL OF
ENGINEERING P A CHANSLER DEC 84 AFIT/GAE/AA/84D-4

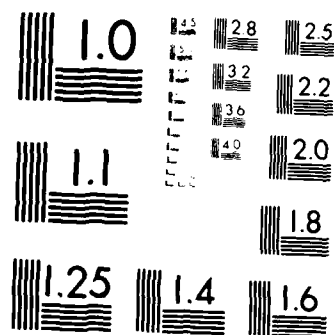
2/2

UNCLASSIFIED

F/G 11/6

NL





MICROCOPY RESOLUTION TEST CHART
NATIONAL BUREAU OF STANDARDS-1963-A

Brussat life predictions are the same as outlined in section A, except for calculating the stress intensity factors where Brussat used the following equation:

$$K_{\max} = \sigma_{\max} \sqrt{\pi c} f_w f_{tr} \quad (22)$$

$$\text{where } f_{tr} = 1 - [0.2886/(1 + 2(c/t)^2)]$$

and f_w is the finite width correction by equation (18).

The results of the Brussat predictions are shown in Table 15 for 2024-T351 aluminum and Table 16 for 7075-T651 aluminum.

6.2.2.4 Collipriest-Ehret. Collipriest and Ehret [7] suggested transition criteria based on the front and back surface crack lengths. Similar to the method developed in this study, Collipriest and Ehret did not use any correction until after back surface penetration. The Newman-Bowie prediction method was used as a basis for this life prediction. The Newman-Raju corner crack at a hole solution was used to calculate stress intensity factors until back surface penetration ($a = t$). Then an imaginary crack length along the base of the hole was used of the form:

$$a' = T[1 - (C_B/C_F)^2]^{-.5}$$

where C_F = front surface crack length

C_B = back surface crack length

T = specimen thickness

	$\sigma_{\text{max}} = 18 \text{ ksi}$				$\sigma_{\text{max}} = 15 \text{ ksi}$			
	R = 0.1	R = 0.3	R = -0.5	R = 0.1	R = 0.3	R = -0.5	Average	
a = t	20,080 (82.80)	35,856 (98.51)	10,659 (92.29)	37,149 (79.46)	84,000 (99.41)	25,706 (94.63)	(91.19)	
a=t → C=Cc	12,933 (68.39)	24,945 (75.27)	11,729 (71.08)	25,552 (69.96)	49,147 (96.39)	20,946 (73.00)	(64.87)	
C = Cc	33,013 (76.49)	60,801 (87.43)	22,388 (79.81)	62,701 (75.29)	133,147 (98.27)	46,652 (83.54)	(71.55)	

() - indicates percent of experimental life

TABLE 15: Life Prediction (Brussat)
2024-T351 Aluminum

$\sigma_{\text{min}} = 20 \text{ ksi}$

$\sigma_{\text{max}} = 15 \text{ ksi}$

	R = 0.1	R = 0.3	R = -0.5	R = 0.1	R = 0.3	R = -0.3	R = -0.5	Average
$\sigma = \tau$	9,684 (121.35)	14,077 (103.51)	7,386 (115.59)	22,929 (179.41)	32,875 (226.57)	14,833 (175.53)	16,350 (121.92)	(149.13)
$\sigma = \tau \rightarrow C=C_c$	7,626 (67.73)	12,473 (67.42)	7,531 (80.55)	21,627 (74.12)	33,129 (83.13)	18,924 (101.85)	18,691 (64.72)	(77.07)
$C = C_c$	17,310 (89.97)	26,550 (82.71)	14,917 (94.77)	44,556 (106.19)	66,004 (121.42)	33,757 (124.89)	35,041 (82.86)	(100.40)

() - indicates percent of experimental life

TABLE 16: Life Prediction (Brussat)
7075-T651 Aluminum (from Opel [1]).

This crack length was used in the Newman-Raju solution for the stress intensity factors along the front surface.

The stress intensity factors along the back surface were calculated using the Grandt-Bowie through crack solution of the form:

$$K_{I\max} = \sigma \max \sqrt{\pi c} F_{gr}(c/R) F_w f_{cec}$$

$$f_{cec} = [1/(1-(1-(C_B/C_F)^2))]^{.5}$$

and $F_{gr}(c/R)$ and f_w are given by equations 22 and 18.

When the back surface crack length equals the front surface crack length, only the uncorrected Grandt-Bowie equation was used until final fracture. (See Fig.33 for details of imaginary crack length.) The results of the Collipriest-Ehret models are shown in Tables 17 and 18 for 2024-T351 and 7075-T651 aluminum, respectively.

6.3. Discussion of Results

The model developed in this thesis is the most accurate and versatile. The average total lives for 2024-T351 and 7075-T651 aluminum are shown in Tables 19 and 20. All predictions, except for Opel's and Brussat's, have been made using the parametric angle ($\phi = 10^\circ, 80^\circ$) corrections. The new model shows an average improvement of 4% over the instantaneous model. This improvement is significant, considering that the transition region, where the new model differs from the instantaneous model, represents only a small portion of the specimen's total life. The new model also shows an improvement of 3% over the Opel model. However, it should also be pointed out that the Opel model is limited since the transition region

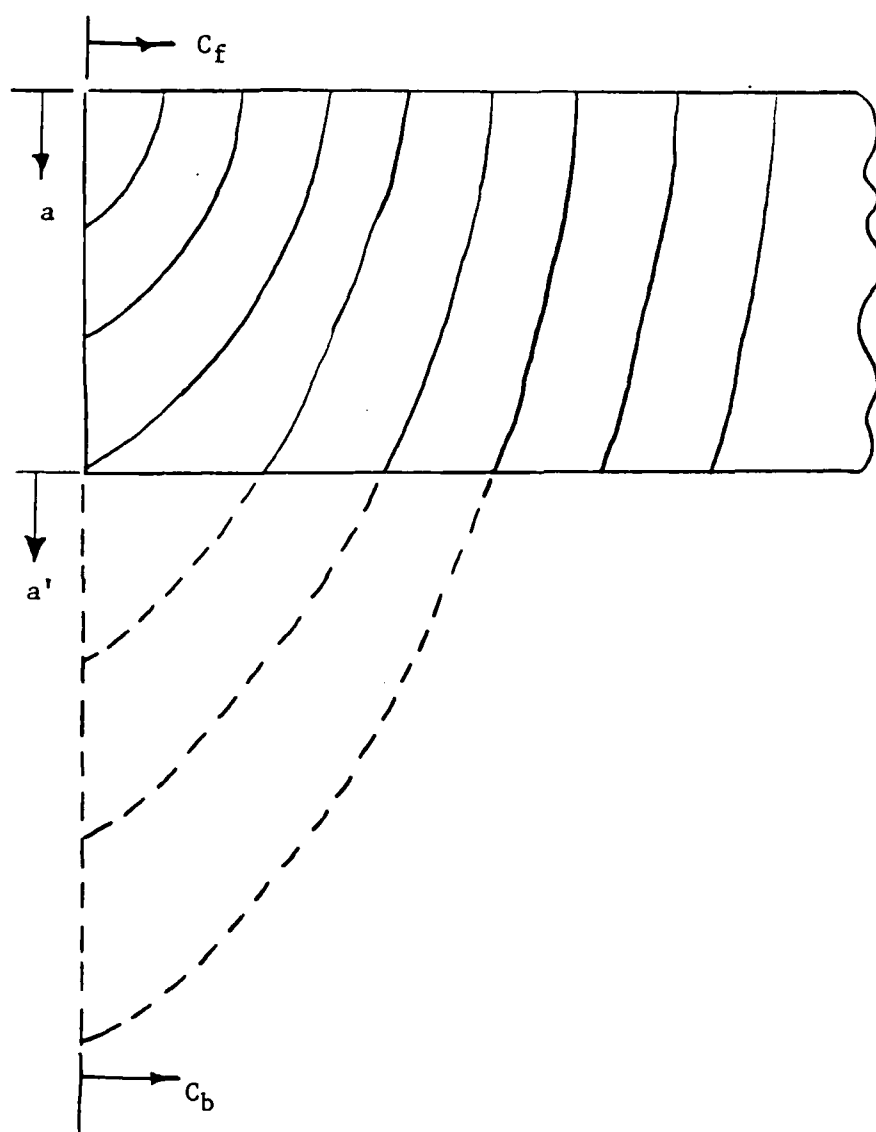


Figure 33: Collipriest-Ehret Transition Region

		$\sigma_{\max} = 18 \text{ ksi}$			$\sigma_{\max} = 15 \text{ ksi}$		
		$R = 0.1$	$R = 0.3$	$R = -0.5$	$R = 0.1$	$R = 0.3$	$R = -0.5$
		Average			Average		
$a = t$		13,509 (55.71)	23,910 (65.69)	7,247 (62.74)	24,784 (53.01)	57,744 (68.34)	18,248 (67.21)
$a = t$	$c = c_c$	11,463 (60.62)	22,179 (66.93)	10,865 (65.85)	22,720 (62.20)	43,605 (85.52)	19,002 (66.22)
$c = c_c$		24,972 (57.86)	46,089 (66.28)	18,112 (64.57)	47,504 (57.04)	101,349 (74.80)	37,250 (66.70)

() - indicates percent of experimental life

Table 17. Life Prediction. (Collipriest-Ehret) for 2024-T351 Aluminum

		$\sigma_{\max} = 20 \text{ ksi}$					$\sigma_{\max} = 15 \text{ ksi}$				
		R = 0.1	R = 0.3	R = -0.5	R = 0.1	R = 0.3	R = -0.3	R = 0.3	R = -0.5	Average	
a = t		6,282 (78.72)	9,613 (70.68)	5,289 (82.77)	15,551 (121.68)	22,127 (152.49)	10,382 (122.86)	11,442 (185.32)		(102.07)	
a=t → c=c _c		6,737 (59.83)	10,344 (55.91)	6,976 (74.61)	18,213 (62.42)	28,081 (70.47)	16,460 (88.59)	16,341 (56.58)		(66.92)	
c = c _c		13,019 (67.67)	19,957 (62.17)	12,265 (77.92)	33,764 (80.47)	50,208 (92.35)	26,842 (99.30)	27,783 (65.70)		(77.94)	

() - indicates percent of experimental life

Table 18: Life Prediction (Collipriest-Ehret) for 7075-T651 Aluminum

Test No.	PC 1/2	PC 3/4	PC 5/6	PC 7/8	PC 9/10	PC 11/12	Ave.
New Model	60.71	69.61	68.10	59.90	78.18	69.98	67.75
Instantaneous ($\phi = 10^\circ, 80^\circ$)	57.78	66.13	64.41	56.91	74.64	66.51	64.40
OPEL	57.70	67.22	67.95	57.51	73.27	65.83	64.91
BRUSSAT	76.49	87.43	79.81	75.29	98.27	83.54	71.55
COLLIPRIEST and EHRET	57.86	66.28	64.57	57.04	74.80	66.70	64.54

TABLE 19: Percent Total Life Ratios for All Models

Considered for 2024-T351 Aluminum

Test No.	FH-7	FH-8	FH-9	FH-10	FH-11	FH-13	FH-12	Ave.
New Model	71.15	65.32	81.84	84.61	97.23	104.48	69.03	81.95
Instantaneous ($\phi = 10^\circ, 80^\circ$)	67.50	61.97	77.60	80.20	92.06	98.90	65.42	77.66
OPEL	68.66	82.69	63.37	96.30	101.24	74.03	65.63	78.85
BRUSSAT	89.97	82.71	94.77	106.19	121.42	124.89	82.86	100.40
COLLIPRIEST and EHRET	67.67	62.17	77.92	80.47	92.36	99.30	65.70	77.94

TABLE 20: Percent Total Life Ratios for All Models

Considered for 7075-T651 Aluminum

correction factors it uses were derived specifically for specimens 0.25 inches thick, and must be rederived for other thicknesses.

The Brussat model seems to be more accurate than the new model, but a closer look will reveal that this is not true. As shown in Table 16, the Brussat model is unconservative for three out of seven tests. However, an examination of Table 16 reveals that the Brussat predictions for life until back surface penetration very unconservative, while those for the region from back surface penetration until final fracture are conservative. This accounts for the good average total life predictions. Table 15 shows that the Brussat predictions for 2024-T351 aluminum which is more ductile than the 7075-T651 aluminum are much more accurate. Therefore, these results seem to indicate that caution should be exercised in the application of the Brussat model to materials which are relatively brittle. On the other hand, the model put forth in this investigation seems to yield conservative predictions for both relatively ductile and brittle aluminum alloys.

The Collipriest-Ehret model was found to be limited when applied to thin specimens. As previously discussed, this model calculates the stress intensity factors for the front surface after back surface penetration using an imaginary crack length in the Newman-Raju corner-crack solution. Due to the form of the equation used to calculate the imaginary crack length, a relatively large initial back surface crack length (of the order of 0.1 inch) must be assumed. When this is done

for thin specimens, a good deal of the transition region is ignored, and therefore the predictions become almost identical to those of the instantaneous model. Therefore, there seems to be no advantage in applying this model to relatively thin specimens instead of the instantaneous model.

7.0 CONCLUSIONS AND RECOMMENDATIONS

This investigation showed that although Opel's model yielded more accurate life predictions for a new, more ductile material (2024-T351 aluminum), it was very conservative in predicting total life. The new model proposed in this work was shown to be considerably more effective.

The new model was developed by first considering the Hartranft and Sih suggestion to modify the Newman-Raju solution with a parametric angle $\phi = 10^\circ$ and 80° instead of 0° and 90° traditionally used. This correction eliminated the surface boundary effects and resulted in significant improvements in the life prediction obtained from all models that were investigated. As a result of using $\phi = 10^\circ$ and 80° , no transition correction factors were necessary for the bore of the hole in the life predictions from corner-crack to back surface penetration.

The Newman-Raju corner-crack and the Grandt linearization of the Bowie through-crack solutions were found to be accurate, but conservative in predicting the stress intensity factors for a corner-crack emanating from a hole as it grows until final fracture. However, neither of these solutions considers the transition region where the crack propagates neither as a corner-crack or a through-crack. This transition region was determined to

begin at back surface penetration and end when the back surface crack length equals the front surface crack length (i.e., $c'=c$). At this point the crack becomes a true through-the-thickness-crack. Transition correction factors based on correlations of analytical and experimental stress intensity factors were derived as a function of c'/c . Using transition factors based on c'/c instead of c/R , as Opel did, eliminated the thickness-dependence of the transition factors and as a result they are more versatile.

The life-prediction model developed in this thesis proved to be the most accurate and versatile. It accounts for the transition region while the Instantaneous model does not. It uses thickness-independent transitions correction factors while the Opel transition factors have to be re-derived when the thickness changes. The new model yields consistently conservative predictions, while the Brussat model is very unconservative for predicting life until back surface penetration and is conservative for life predictions from back surface penetration until final fracture. Finally it uses correction factors which apply over any thickness while the Collipriest-Ehret model seems to assume a relatively large initial back surface crack length which makes it inappropriate for thin specimens.

This study has demonstrated that the proposed corrections to the currently used stress intensity factor solutions have resulted in better life predictions for

constant amplitude loading. The life prediction model developed in this study showed a three or four percent improvement over the uncorrected life prediction model. Even though this does not seem like a sizable improvement, one must keep in mind the specimen thickness considered was only 0.25 inches. Therefore, the transition region is a very small part of the total life of the specimen. Further investigation using this prediction model and thicker specimens should be undertaken. Thicker specimens would have a larger transition region and the new model should result in greater improvements in the accuracy of the predictions. Applications of this model to lugs, for instance, may prove useful. Lugs have geometries such that there are thick specimen depths and narrow specimen widths. Therefore the transition region would account for a significant part of the total life after back surface penetration. Other follow-on topics should include the investigation of the effect of different parametric angles, ϕ , other than $\phi = 10^\circ$ and 80° as well as applying the new model to different types of material, such as steel. Should the correction factors developed in this thesis prove to be as effective as they seem to be, they should be considered for incorporation into the Air Force Damage Tolerance Design Handbook [44].

APPENDIX: Computer Programs Used

There were six major computer programs, written in Fortran 77, used for this study. A short discussion of what each program does, followed by complete program listings are included in this appendix. The input variables for the life prediction programs are:

- A - Initial crack length
- C - Initial crack depth
- R - Radius of hole
- S - Maximum stress
- T - Thickness of specimen
- W - Width of specimen
- ASTOP - Non-functional parameter
- RS - Stress ratio
- C1,N,FAC - Walker constants (mat'l dependant)

A. Newman-Bowie (Uncorrected)

Also known as the instantaneous model, this is the program upon which all of the other life prediction programs are based (except Brussat's model). It uses a Newman-Raju corner-crack solution for stress intensity factors until back surface penetration. After back surface penetration, the program uses a Grandt-Bowie through-crack solution until final fracture.

B. Newman-Bowie (New model)

This program is similiar to the program in A. above. From back surface penetration until a through-crack develops (i.e., $c'/c=1$), the Grandt-Bowie solution is corrected with the transition corrections developed in this study. These factors are functions of c'/c . After

$c'/c=0.9$, the uncorrected Grandt-Bowie solution for a through-crack is used until final fracture.

C. Newman-Bowie (Opel's model)

This program uses a Newman-Raju solution until $a/t=0.75$. At that point, Opel hole correction factors are applied to the Newman-Raju solution. The Opel model uses 0 and 90 for the parametric angle, . After back surface penetration, until $c/R=2.5$, surface correction factors are applied to the Grandt-Bowie solution. From $c/R=2.5$ until final fracture, the uncorrected Grandt-Bowie solution is used.

D. Newman-Bowie (Collipriest-Ehret model)

This program uses an uncorrected Newman-Raju corner-crack solution until back surface penetration. After back surface penetration until the end of the transition region, an imaginary crack length (FSC) is used in the Newman-Raju solution to calculate the front surface stress intensity factors. A correction factor (CEC) is applied to the Grandt-Bowie through-crack solution to calculate the back surface stress intensity factors. The transition region ends when the front and back surface crack lengths are equal. After this point, the uncorrected Grandt-Bowie solution is used until final fracture.

E. Brussat

This program uses an engineering approximation developed for a quarter-circular crack-at-a-hole. It uses an initial crack length that is the average of the actual initial test

specimen crack lengths along the bore of the hole and along the front surface. This model uses the Newman-Raju finite width correction.

F. Walker/Grandt-Bowie Surface Stress Intensity
Correlations

This program calculates the experimental stress intensity factors based on curve-fit data for c vs dc/dN experimental data. It also calculates analytical stress intensity factors using the Grandt-Bowie through-crack solution. The front and back surface crack length ratio, c'/c , is calculated based on curve-fit data from experimental results.

```

PROGRAM TRNSUN3(INPUT, OUTPUT, TAPE5=INPUT, TAPE6=OUTPUT)
INTEGER X, XX
REAL PI, PA, PC, K9, KA, KC, N, NC, L1, L2, M1, M2, M3, A, C, R, S, T, W,
&ASTOP, RS
DO 40 I=1,6
K9=53.5
PRINT*, 'INPUT MATERIAL AND GEOMETRY VARIABLES'
READ(5,*) A, C, R, S, T, W, ASTOP, RS
IF(RS.GT.0.0) GO TO 5
C1=4.31544E-09
N=3.2116
FAC=0.0
GO TO 6
5 C1=1.11616E-09
N=3.71797
FAC=0.7
6 CONTINUE
WRITE (6,35)A, C, R, S, T, W, ASTOP, RS
35 FORMAT(8F8.3)
PA=1.39626
PC=0.17453
NC=1.0
B=W/2.
PI=3.1416
XX=1
X=1
WRITE(6,130)

```

C This is the Newman-Raju corner crack solution with the
parametric angle = 10 & 80

```

10 F1=C/A
F2=A/T
Z3=A/C
L1=(1./((1.+(C/R)*COS(.85*(PA))))
L2=(1./((1.+(C/R)*COS(.85*(PC))))
Q1=(1.+1.464*F1**1.65)
M1=(F1**2.5)*(1.+0.04*F1)
M2=(.2*F1**4.)
M3=(-.11*F1**4.)
G1=(1.+(.1+.35*F1*F2**2.)*(1.-SIN(PA))**2.)
G2=(1.+(.1+.35*F1*F2**2.)*(1.-SIN(PC))**2.)
G3=((1.-.15*L1+3.46*L1**2.-4.47*L1**3.+3.52*L1**4.)/(1.
&+.13*L1**2.))
G4=((1.-.15*L2+3.46*L2**2.-4.47*L2**3.+3.52*L2**4.)/(1.
&+.13*L2**2.))
G5=(1.13-.09*F1)*(1.+1*(1.-COS(PA))**2.)*(.8+.2*F2**2.25)
G6=(1.13-.09*F1)*(1.+1*(1.-COS(PC))**2.)*(.8+.2*F2**2.25)
F3=((F1**2.)*(SIN(PA))**2.+(COS(PA))**2.)*.25
F4=((F1**2.)*(SIN(PC))**2.+(COS(PC))**2.)*.25
F5=(1/(COS((PI*R)/(2.*B))))
F6=(1/(COS((PI*(2.*R+NC*C)/(4.*(B-C)+2.*NC*C))*F2**2.5)))

```

```

F7=(F5*F6)**.5
F8=(M1+M2*F2**2.+M3*F2**4.)*G1*G3*G5*F3*F7
F9=(M1+M2*F2**2.+M3*F2**4.)*G2*G4*G6*F4*F7
D1=(S*SQRT(PI*A/Q1))*F8
D2=(S*SQRT(PI*A/Q1))*F9
KA=D1*((4./PI+(A*C)/(2.*T*R))/(4./PI+(A*C)/(T*R))**.5)
KC=D2*((4./PI+(A*C)/(2.*T*R))/(4./PI+(A*C)/(T*R))**.5)
130 FORMAT(2X,'A',5X,'C',5X,'A/T',3X,'A/C',6X,'KA',6X,'KC',9
&X,'DA',9X,'DC',9X,'CYCLES')
DA=((KA)*(1-RS)**(FAC))**N)*C1
DC=((KC)*(1-RS)**(FAC))**N)*C1
IF((X/(XX*500)).EQ.1.0) WRITE(6,15) A,C,F2,Z3,KA,KC,
&DA,DC,X
IF((X/(XX*500)).EQ.1.0) XX=XX+1
IF(X.EQ.1) WRITE(6,15) A,C,F2,Z3,KA,KC,DA,DC,X
IF(KA.GE.K9) GO TO 200
IF(KC.GE.K9) GO TO 200
A=A+DA
IF (A.GT.T) GO TO 200

```

C This signals back surface penetration. The remainder of the program is an uncorrected Grandt-Bowie through-crack solution.

```

C=C+DC
X=X+1
GO TO 10
15 FORMAT (3F6.3,F7.3,2F10.2,2E11.4,I8)
200 WRITE(6,15) A,C,F2,Z3,KA,KC,DA,DC,X
71 A=C
FWC=(COS(PI*(R+A)/4.))**(-.5)
AA=(.6762062+(.8733015/(.3245442+A/R)))*S*(PI*A)**.5
KA=AA*FWC
KC=KA
DA=((KA)*(1-RS)**(FAC))**N)*C1
DC=((KC)*(1-RS)**(FAC))**N)*C1
IF((X/(XX*500)).EQ.1.0) WRITE(6,15) A,C,F2,Z3,KA,KC,
&DA,DC,X
IF ((X/(XX*500)).EQ.1.0) XX=XX+1
IF (X.EQ.1) WRITE (6,15) A,C,F2,Z3,KA,KC,DA,DC,X
IF(KA.GE.K9) GO TO 600
IF (KC.GE.K9) GO TO 600
A=A+DA
C=C+DC
X=X+1
GO TO 71
600 WRITE (6,15) A,C,F2,Z3,KA,KC,DA,DC,X
40 CONTINUE
END

```

```

PROGRAM TRANCOR(INPUT, OUTPUT, TAPE5=INPUT, TAPE6=OUTPUT)
INTEGER X, XX
REAL PI, PA, PC, K9, KA, KC, N, NC, L1, L2, M1, M2, M3, A, C, R, S, T, W,
&ASTOP, RS
DO 40 I=1,6
K9=53.5
PRINT*, 'INPUT MATERIAL AND GEOMETRY VARIABLES'
READ(5,*) A, C, R, S, T, W, ASTOP, RS
IF(RS.GT.0.0) GO TO 5
C1=4.31544E-09
N=3.2116
FAC=0.0
GO TO 6
5 C1=1.11616E-09
N=3.71797
FAC=0.7
6 CONTINUE
WRITE (6,35)A, C, R, S, T, W, ASTOP, RS
35 FORMAT(8F8.3)
PA=1.39626
PC=0.17453
NC=1.0
B=W/2.
PI=3.1416
XX=1
X=1
WRITE(6,130)

```

C This is the beginning of the Newman-Raju solution,
uncorrected, with the parametric angle = 10 & 80

```

10 F1=C/A
F2=A/T
Z3=A/C
L1=(1./(1.+(C/R)*COS(.85*(PA))))
L2=(1./(1.+(C/R)*COS(.85*(PC))))
Q1=(1.+1.464*F1**1.65)
M1=(F1**.5)*(1.+.04*F1)
M2=(.2*F1**4.)
M3=(-.11*F1**4.)
G1=(1.+(.1+.35*F1*F2**2.)*(1.-SIN(PA))**2.)
G2=(1.+(.1+.35*F1*F2**2.)*(1.-SIN(PC))**2.)
G3=((1.-.15*L1+3.46*L1**2.-4.47*L1**3.+3.52*L1**4.)/(1.
&+.13*L1**2.))
G4=((1.-.15*L2+3.46*L2**2.-4.47*L2**3.+3.52*L2**4.)/(1.
&+.13*L2**2.))
G5=(1.13-.09*F1)*(1.+.1*(1.-COS(PA))**2.)*(.8+.2*F2**.25)
G6=(1.13-.09*F1)*(1.+.1*(1.-COS(PC))**2.)*(.8+.2*F2**.25)
F3=((F1**2.)*(SIN(PA))**2.+(COS(PA))**2.)*.25
F4=((F1**2.)*(SIN(PC))**2.+(COS(PC))**2.)*.25
F5=(1/(COS((PI*R)/(2.*B))))

```



```

F6=(1/(COS((PI*(2.*R+NC*C)/(4.*(B-C)+2.*NC*C))*F2**.5)))
F7=(F5*F6)**.5
F8=(M1+M2*F2**.2.+M3*F2**.4.)*G1*G3*G5*F3*F7
F9=(M1+M2*F2**.2.+M3*F2**.4.)*G2*G4*G6*F4*F7
D1=(S*SQRT(PI*A/Q1))*F8
D2=(S*SQRT(PI*A/Q1))*F9
KA=D1*((4./PI+(A*C)/(2.*T*R))/(4./PI+(A*C)/(T*R))**.5)
KC=D2*((4./PI+(A*C)/(2.*T*R))/(4./PI+(A*C)/(T*R))**.5)
130 FORMAT(2X,'A',5X,'C',5X,'A/T',3X,'A/C',6X,'KA',6X,'KC',9
&X,'DA',9X,'DC',9X,'CYCLES')
DA=((KA)*(1-RS)**(FAC))**N)*C1
DC=((KC)*(1-RS)**(FAC))**N)*C1
IF((X/(XX*500)).EQ.1.0) WRITE(6,15) A,C,F2,Z3,KA,KC,
&DA,DC,X
IF((X/(XX*500)).EQ.1.0) XX=XX+1
IF(X.EQ.1) WRITE(6,15) A,C,F2,Z3,KA,KC,DA,DC,X
IF(KA.GE.K9) GO TO 200
IF(KC.GE.K9) GO TO 200
A=A+DA
IF (A.GT.T) GO TO 200

```

C This signals back surface penetration and the Chansler correction factors are applied to the Grandt-Bowie through-crack solution until the end of the transition region

```

C=C+DC
X=X+1
GO TO 10
15 FORMAT (3F6.3,F7.3,2F10.2,2E11.4,I8)
200 WRITE(6,15) A,C,F2,Z3,KA,KC,DA,DC,X
A=.005
C=C+A
61 FWC=(COS(PI*(R+A)/4.))**(-.5)
AA=(.6762062+(.8733015/(.3245442+A/R)))*S*(PI*A)**.5
BCF1=-.689614*A/C
BCF2=1.23275*(A/C)**2
BCF=.609633+BCF1+BCF2
KA=AA*FWC/BCF
FWC=(COS(PI*(R+C)/4.))**(-.5)
AA=(.6762062+(.8733015/(.3245442+C/R)))*S*(PI*C)**.5
SCF1=-.13564*A/C
SCF=1.24007+SCF1
KC=AA*FWC/SCF
DA=((KA)*(1-RS)**(FAC))**N)*C1
DC=((KC)*(1-RS)**(FAC))**N)*C1
IF((X/(XX*500)).EQ.1.0) WRITE(6,15) A,C,F2,Z3,KA,KC,
&DA,DC,X
IF ((X/(XX*500)).EQ.1.0) XX=XX+1
IF (X.EQ.1) WRITE (6,15) A,C,F2,Z3,KA,KC,DA,DC,X
IF (KC.GE.K9) GO TO 600
A=A+DA

```

```
C=C+DC
IF ((A/C).GE.0.9) GO TO 400
```

C This signals the end of the transition region
The remainder of the program is an uncorrected
Grandt-Bowie through-crack solution

```
X=X+1
GO TO 61
400 WRITE (6,15) A,C,F2,Z3,KA,KC,DA,DC,X
71 A=C
FWC=(COS(PI*(R+A)/4.))**(-.5)
AA=(.6762062+(.8733015/(.3245442+A/R)))*S*(PI*A)**.5
KA=AA*FWC
KC=KA
DA=((KA)*(1-RS)**(FAC))**N)*C1
DC=((KC)*(1-RS)**(FAC))**N)*C1
IF((X/(XX*500)).EQ.1.0) WRITE(6,15) A,C,F2,Z3,KA,KC,
&DA,DC,X
IF ((X/(XX*500)).EQ.1.0) XX=XX+1
IF (X.EQ.1) WRITE (6,15) A,C,F2,Z3,KA,KC,DA,DC,X
IF(KA.GE.K9) GO TO 600
IF (KC.GE.K9) GO TO 600
A=A+DA
C=C+DC
X=X+1
GO TO 71
600 WRITE (6,15) A,C,F2,Z3,KA,KC,DA,DC,X
40 CONTINUE
END
```

```

PROGRAM TRANS3(INPUT, OUTPUT, TAPE5=INPUT, TAPE6=OUTPUT)
INTEGER X, XX
REAL PI, PA, PC, K9, KA, KC, N, NC, L1, L2, M1, M2, M3, A, C, R, S, T, W,
&ASTOP, RS
DO 40 I=1,6
K9=53.5
PRINT*, 'INPUT MATERIAL AND GEOMETRY VARIABLES'
READ(5,*) A, C, R, S, T, W, ASTOP, RS
IF(RS.GT.0.0) GO TO 5
C1=4.31544E-09
N=3.2116
FAC=0.0
GO TO 6
5 C1=1.11616E-09
N=3.71797
FAC=0.7
6 CONTINUE
WRITE (6,35)A, C, R, S, T, W, ASTOP, RS
35 FORMAT(8F8.3)
PA=1.570796
PC=0.0
NC=1.0
B=W/2.
PI=3.1416
XX=1
X=1
WRITE(6,130)

```

C This begins the Newman-Raju corner-crack solution

```

10 F1=C/A
F2=A/T
Z3=A/C
L1=(1./((1.+(C/R)*COS(.85*(PA))))
L2=(1./((1.+(C/R)*COS(.85*(PC))))
Q1=(1.+1.464*F1**1.65)
M1=(F1**5)*(1+.04*F1)
M2=(.2*F1**4)
M3=(-.11*F1**4)
G1=(1.+(.1+.35*F1*F2**2.)*(1.-SIN(PA))**2.)
G2=(1.+(.1+.35*F1*F2**2.)*(1.-SIN(PC))**2.)
G3=((1.-.15*L1+3.46*L1**2.-4.47*L1**3.+3.52*L1**4.)/(1.
&+.13*L1**2.1))
G4=((1.-.15*L2+3.46*L2**2.-4.47*L2**3.+3.52*L2**4.)/(1.
&+.13*L2**2.1))
G5=(1.13-.09*F1)*(1+.1*(1.-COS(PA))**2.)*(1+.2*F2**
&.25)
G6=(1.13-.09*F1)*(1+.1*(1.-COS(PC))**2.)*(1+.2*F2**
&.25)
F3=((F1**2.)*(SIN(PA))**2.+(COS(PA))**2.)*.25
F4=((F1**2.)*(SIN(PC))**2.+(COS(PC))**2.)*.25

```

```

F5=(1/(COS((PI*R)/(2.*B))))
F6=(1/(COS((PI*(2.*R+NC*C)/(4.*(B-C)+2.*NC*C))*F2**.5)))
F7=(F5*F6)**.5
F8=(M1+M2*F2**2.+M3*F2**4.)*G1*G3*G5*F3*F7
F9=(M1+M2*F2**2.+M3*F2**4.)*G2*G4*G6*F4*F7
D1=(S*SQRT(PI*A/Q1))*F8
D2=(S*SQRT(PI*A/Q1))*F9
IF (F2.LE..75) GO TO 100

```

C If this conditon is met, Opel's hole bore corrections take effect here

```

TF1=1.468068*F2
TF2=-1.275787*F2**2
TCF=.573924+TF1+TF2
KA=D1*((4./PI+(A*C)/(2.*T*R))/(4./PI+(A*C)/(T*R))**.5)
&/TCF
SC1=-.362863*F2
SCF=1.316867+SC1
KC=D2*((4./PI+(A*C)/(2.*T*R))/(4./PI+(A*C)/(T*R))**.5)
&/SCF
GO TO 101
100 KA=D1*((4./PI+(A*C)/(2.*T*R))/(4./PI+(A*C)/(T*R))**.5)
    KC=D2*((4./PI+(A*C)/(2.*T*R))/(4./PI+(A*C)/(T*R))**.5)
101 CONTINUE
130 FORMAT(2X,'A',5X,'C',5X,'A/T',3X,'A/C',6X,'KA',9X,'KC',9
&X,'DA',9X,'DC',9X,'CYCLES')
DA=((KA)*(1-RS)**(FAC))**N)*C1
DC=((KC)*(1-RS)**(FAC))**N)*C1
IF((X/(XX*500)).EQ.1.0) WRITE(6,15) A,C,F2,Z3,KA,KC,
&DA,DC,X
IF((X/(XX*500)).EQ.1.0) XX=XX+1
IF(X.EQ.1) WRITE(6,15) A,C,F2,Z3,KA,KC,DA,DC,X
IF(KA.GE.K9) GO TO 200
IF(KC.GE.K9) GO TO 200
A=A+DA
IF (A.GT.T) GO TO 200

```

C If this condition is met, back surface penetration has occurred and Opel's surface corrections are applied to the Grandt-Bowie through-crack solution

```

C=C+DC
X=X+1
GO TO 10
15 FORMAT (3F6.3,F7.3,2F10.2,2E11.4,I8)
200 WRITE(6,15) A,C,F2,Z3,KA,KC,DA,DC,X
61 A=R*(-1.9311+1.70076*C/R)
FWC=(COS(PI*(R+A)/4.))**(-.5)
AA=(.6762062+(.8733015/(.3245442+A/R)))*S*(PI*A)**.5
BCF1=.724961*A/R
BCF2=-.158451*(A/R)**2

```

```

BCF=.191601+BCF1+BCF2
KA=AA*FWC/BCF
FWC=(COS(PI*(R+C)/4.))**.5
AA=(.6762062+(.8733015/(.3245442+C/R)))*S*(PI*C)**.5
SCF1=-.106745*C/R
SCF2=.018451*(C/R)**2
SCF=1.279537+SCF1+SCF2
KC=AA*FWC/SCF
DA=((((KA)*(1-RS)**(FAC))**N)*C1
DC=((((KC)*(1-RS)**(FAC))**N)*C1
IF((X/(XX*500)).EQ.1.0) WRITE(6,15) A,C,F2,Z3,KA,KC,
&DA,DC,X
IF ((X/(XX*500)).EQ.1.0) XX=XX+1
IF (X.EQ.1) WRITE (6,15) A,C,F2,Z3,KA,KC,DA,DC,X
IF (KC.GE.K9) GO TO 600
A=A+DA
C=C+DC
IF ((A/R).GT.2.5) GO TO 400

```

C Meeting this condition signals the end of Opel's transition region and the rest of the program is an uncorrected Grandt-Bowie through-crack solution

```

X=X+1
GO TO 61
400 WRITE (6,15) A,C,F2,Z3,KA,KC,DA,DC,X
71 A=C
FWC=(COS(PI*(R+A)/4.))**.5
AA=(.6762062+(.8733015/(.3245442+A/R)))*S*(PI*A)**.5
KA=AA*FWC
KC=KA
DA=((((KA)*(1-RS)**(FAC))**N)*C1
DC=((((KC)*(1-RS)**(FAC))**N)*C1
IF ((X/(XX*500)).EQ.1.0) WRITE (6,15) A,C,F2,Z3,KA,KC,
&DA,DC,X
IF ((X/(XX*500)).EQ.1.0) XX=XX+1
IF (X.EQ.1) WRITE (6,15) A,C,F2,Z3,KA,KC,DA,DC,X
IF (KA.GE.K9) GO TO 600
IF (KC.GE.K9) GO TO 600
A=A+DA
C=C+DC
X=X+1
GO TO 71
600 WRITE (6,15) A,C,F2,Z3,KA,KC,DA,DC,X
40 CONTINUE
END

```

```

PROGRAM COLEHR2(INPUT, OUTPUT, TAPE5=INPUT, TAPE6=OUTPUT)
INTEGER X, XX
REAL PI, PA, PC, K9, KA, KC, N, NC, L1, L2, M1, M2, M3, A, C, R, S, T, W,
&ASTOP, RS
DO 40 I=1,6
K9=53.5
PRINT*, 'INPUT MATERIAL AND GEOMETRY VARIABLES'
READ(5,*) A, C, R, S, T, W, ASTOP, RS
IF(RS.GT.0.0) GO TO 5
C1=4.31544E-09
N=3.2116
FAC=0.0
GO TO 6
5 C1=1.11616E-09
N=3.71797
FAC=0.7
6 CONTINUE
WRITE (6,35)A, C, R, S, T, W, ASTOP, RS
35 FORMAT(8F8.3)
PA=1.39626
PC=0.17453
NC=1.0
B=W/2.
PI=3.1416
XX=1
X=1
WRITE(6,130)

```

C This is the beginning of the uncorrected Newman-Raju corner-crack solution with parametric angle = 10 & 80

```

10 F1=C/A
F2=A/T
Z3=A/C
L1=(1./((1.+(C/R)*COS(.85*(PA))))
L2=(1./((1.+(C/R)*COS(.85*(PC))))
Q1=(1.+1.464*F1**1.65)
M1=(F1**5)*(1.+.04*F1)
M2=(.2*F1**4.)
M3=(-.11*F1**4.)
G1=(1.+(.1+.35*F1*F2**2.)*(1.-SIN(PA))**2.)
G2=(1.+(.1+.35*F1*F2**2.)*(1.-SIN(PC))**2.)
G3=((1.-.15*L1+3.46*L1**2.-4.47*L1**3.+3.52*L1**4.)/(1.
&+.13*L1**2.))
G4=((1.-.15*L2+3.46*L2**2.-4.47*L2**3.+3.52*L2**4.)/(1.
&+.13*L2**2.))
G5=(1.13-.09*F1)*(1.+.1*(1.-COS(PA))**2.)*(1.+.2*F2**
&.25)
G6=(1.13-.09*F1)*(1.+.1*(1.-COS(PC))**2.)*(1.+.2*F2**
&.25)
F3=((F1**2.)*(SIN(PA))**2.+(COS(PA))**2.)*.25

```

```

F4=((F1**2.)*(SIN(PC))**2.+(COS(PC))**2.）**.25
F5=(1/(COS((PI*R)/(2.*B))))
F6=(1/(COS((PI*(2.*R+NC*C))/(4.*(B-C)+2.*NC*C)))*F2**.5)))
F7=(F5*F6)**.5
F8=(M1+M2*F2**2.+M3*F2**4.)*G1*G3*G5*F3*F7
F9=(M1+M2*F2**2.+M3*F2**4.)*G2*G4*G6*F4*F7
D1=(S*SQRT(PI*A/Q1))*F8
D2=(S*SQRT(PI*A/Q1))*F9
KA=D1*((4./PI+(A*C)/(2.*T*R))/(4./PI+(A*C)/(T*R))**.5)
KC=D2*((4./PI+(A*C)/(2.*T*R))/(4./PI+(A*C)/(T*R))**.5)
130 FORMAT(2X,'A',5X,'C',5X,'A/T',3X,'A/C',6X,'KA',6X,'KC',9
&X,'DA',9X,'DC',9X,'CYCLES')
DA=((KA)*(1-RS)**(FAC))**N)*C1
DC=((KC)*(1-RS)**(FAC))**N)*C1
IF((X/(XX*500)).EQ.1.0) WRITE(6,15) A,C,F2,Z3,KA,KC,
&DA,DC,X
IF((X/(XX*500)).EQ.1.0) XX=XX+1
IF(X.EQ.1) WRITE(6,15) A,C,F2,Z3,KA,KC,DA,DC,X
IF(KA.GE.K9) GO TO 200
IF(KC.GE.K9) GO TO 200
A=A+DA
IF (A.GT.T) GO TO 200

```

C This signals back surface penetration. The Collipriest-Ehret corrections are applied from here to the end of the transition region. An imaginary crack length (FSC) is used with the Newman-Raju corner-crack solution to calculate the front surface stress intensity factors and a correction factor (CEC) is applied to the Grandt-Bowie through-crack solution to calculate the back surface stress intensity factors.

```

C=C+DC
X=X+1
GO TO 10
15 FORMAT (3F6.3,F7.3,2F10.2,2E11.4,I8)
200 WRITE(6,15) A,C,F2,Z3,KA,KC,DA,DC,X
CB=.020
CF=C
PA=0.17453
71 FSC=T*((1.0-(CB/CF)**2.0)**(-.5))
A=FSC
FWC=(COS(PI*(R+CB)/4.))**(-.5)
AA=(.6762062+(.8733015/(.3245442+CB/R)))*S*(PI*CB)**.5
CEC=(1.0/(1.0-(1.0-(CB**2.0/CF**2.0))**.5))**.5
F1=CF/A
F2=1.0
Z3=A/CF
L1=(1./((1.+(CF/R)*COS(.85*(PA))))
Q1=(1.+1.464*F1**1.65)
M1=(F1**.5)*(1.+0.4*F1)

```

```

M2=(.2*F1**4.)
M3=(-.11*F1**4.)
G1=(1+.1+.35*F1*F2**2.)*(1.-SIN(PA))**2.)
G3=((1.-.15*L1+3.46*L1**2.-4.47*L1**3.+3.52*L1**4.)/(1.
&+.13*L1**2.))

G5=(1.13-.09*F1)*(1+.1*(1.-COS(PA))**2.)*(.8+.2*F2**
&.25)
F3=((F1**2.)*(SIN(PA))**2.+(COS(PA))**2.)*.25
F5=(1/(COS((PI*R)/(2.*B))))
F6=(1/(COS((PI*(2.*R+NC*CF)/(4.*(B-CF)+2.*NC*CF))*F2**
&.5)))
F7=(F5*F6)**.5
F8=(M1+M2*F2**2.+M3*F2**4.)*G1*G3*G5*F3*F7
D1=(S*SQRT(PI*A/Q1))*F8
KC=D1*((4./PI+(A*CF)/(2.*T*R))/(4./PI+(A*CF)/(T*R)))
&**5)
KA=AA*FWC*CEC
DA=((KA)*(1-RS)**(FAC))**N)*C1
DC=((KC)*(1-RS)**(FAC))**N)*C1
IF((X/(XX*500)).EQ.1.0) WRITE(6,15) A,CF,F2,Z3,KA,KC,
&DA,DC,X
IF ((X/(XX*500)).EQ.1.0) XX=XX+1
IF (X.EQ.1) WRITE (6,15) A,CF,F2,Z3,KA,KC,DA,DC,X
CB=CB+DA
CF=CF+DC
X=X+1
IF(CB.GE.CF) GO TO 400

```

C When this conditon is met, the front and back surface crack lengths are equal and this signals the end of the transition region. The rest of the program is an uncorrected Grandt-Bowie through-crack solution.

```

GO TO 71
400 WRITE (6,15) A,CF,F2,Z3,KA,KC,DA,DC,X
75 A=CF
FWC=(COS(PI*(R+A)/4.))**(-.5)
AA=(.6762062+(.8733015/(.3245442+A/R)))*S*(PI*A)**.5
KA=AA*FWC
KC=KA
DA=((KA)*(1-RS)**(FAC))**N)*C1
DC=((KC)*(1-RS)**(FAC))**N)*C1
IF ((X/(XX*500)).EQ.1.0) WRITE (6,15) A,CF,F2,Z3,KA,KC,
&DA,DC,X
IF ((X/(XX*500)).EQ.1.0) XX=XX+1
IF (X.EQ.1) WRITE (6,15) A,CF,F2,Z3,KA,KC,DA,DC,X
IF (KA.GE.K9) GO TO 600
IF (KC.GE.K9) GO TO 600
A=A+DA
CF=CF+DC
X=X+1

```


GO TO 75
600 WRITE (6,15) A,CF,F2,Z3,KA,KC,DA,DC,X
40 CONTINUE
END

```

PROGRAM BRUSS(INPUT, OUTPUT, TAPE5=INPUT, TAPE6=OUTPUT)
INTEGER X, XX
REAL PI, PA, PC, K9, KA, KC, N, NC, L1, L2, M1, M2, M3, A, C, R, S, T, W,
&ASTOP, RS
DO 40 I=1,6
K9=53.5
READ (5,*) A, C, R, S, T, W, ASTOP, RS
IF (RS.GT.0.0) GO TO 5
C1=4.31544E-09
N=3.2116
FAC=0.0
GO TO 6
5 C1=1.11616E-09
N=3.71797
FAC=0.7
6 CONTINUE
WRITE (6,35) A, C, R, S, T, W, ASTOP, RS
35 FORMAT (8F8.3)
PI=3.1416
XX=1
X=1
WRITE (6,130)
A=(C+A)/2
C=A
10 F1=C/A
F2=A/T
Z3=A/C
FAC1=S*(PI*A)**.5
FAC2=(1/COS(PI*(A+2*R)/(2*(W-A))))**.5
FAC3=1-(.2886/(1+2*(C/T)**2))
FAC4=1.2133-2.205*(A/(A+R))+.6451*(A/(A+R))**2
FAC5=EXP(FAC4)
KA=FAC1*FAC2*FAC3*FAC5
KC=KA
130 FORMAT (2X,'A',5X,'C',5X,'A/T',3X,'A/C',6X,'KA',6X,'KC',
&9X,'DA',9X,'DC',9X,'CYCLES')
DA=((KA)*(1-RS)**(FAC))**N)*C1
DC=((KC)*(1-RS)**(FAC))**N)*C1
IF ((X/(XX*500)).EQ.1.0) WRITE(6,15) A, C, F2, Z3, KA, KC,
&DA, DC, X
IF ((X/(XX*500)).EQ.1.0) XX=XX+1
IF (X.EQ.1) WRITE(6,15) A, C, F2, Z3, KA, KC, DA, DC, X
IF(KA.GE.K9) GO TO 200
IF(KC.GE.K9) GO TO 200
A=A+DA
C=C+DC
X=X+1
GO TO 10
15 FORMAT(3F6.3,F7.3,2F10.2,2E11.4,I8)
200 WRITE(6,15) A, C, F2, Z3, KA, KC, DA, DC, X
40 CONTINUE
END

```

```

PROGRAM INT7T(INPUT,OUTPUT,TAPE5=INPUT,TAPE6=OUTPUT)
REAL PI,N,M,KE,KA,R,T1,T2,C0,C1,C2,C3,C4,C5,B1,B2,MAXS
PI=3.1416
DO 20 I=1,7
PRINT*, 'INPUT R, COEFS AND MAX STRESS'
READ(5,*) R,T1,T2,C0,C1,C2,C3,C4,C5,B1,B2,MAXS
IF (R.GT.0.0) GO TO 100
C=1.29E-08
N=2.89
FAC=0.0
GO TO 101
100 C=3.2624E-09
N=3.3908
FAC=0.5
101 CONTINUE
D=.20
WRITE (6,32)
32 FORMAT (4X,'C',8X,'C/C',8X,'K EXPERIMENTAL',8X,
&'K ANALYT',8X,'ACCURACY')
DO 10 J=1,70
A=.015*J+D
T=T1*A+T2

```

C This part uses fifth-order polynomial regression curve fit data based on experimental results to calculate the experimental stress intensity factor using a Walker equation.

```

DADN=C0+C1*T+C2*T**2+C3*T**3+C4*T**4+C5*T**5
FACTOR=DADN/C
COEF=ABS(FACTOR)**(1/N)
KE=COEF*(1-R)**(-FAC)
33 FORMAT(2X,F5.3,5X,F7.3,5X,F8.3,15X,F8.3,12X,F6.3)

```

C This part calculates the analytical stress intensity factor using the Grandt-Bowie through-crack solution

```

RAD=.125
FWC=(COS(PI*(RAD+A)/4.))**(-.5)
AA=(.6762062+(.8733015/(.3245442+A/RAD)))*MAXS*(PI*A)
&**5
KA=AA*FWC
ACCUR=KA/KE

```

C The next line calculates the back surface crack length based on linear curve fit data using experimental results

```

B=B1+B2*A
AT=B/A
10 WRITE(6,33)A,AT,KE,KA,ACCUR
20 CONTINUE
END

```

BIBLIOGRAPHY

1. Gran, R.J., Orazio, F.D., Paris, P.C., Irwin, G.R. and Hertzberg, R., "Investigation and Analysis Development of Early Life Aircraft Structural Failures," AFFDL-TR-70-149, Air Force Flight Dynamics Laboratory, March 1971.
2. Wood, H.A. and Engle, R.M., Jr., "Damage Tolerant Design Handbook, Guidelines for the Analysis and Design of Damage Tolerant Aircraft," AFFDL-TR-79-3021, Air Force Flight Dynamics Laboratory, March 1979.
3. Williams, M.L., "Surface Stress Singularities Resulting from Various Boundary Conditions in Angular Corners of Plates Under Bending," U.S. Nat'l. Congress of Applied Mechanics, Illinois Institute of Technology, Chicago, IL., June 1957.
4. Williams, M.L., "Stress Singularities Resulting from Various Boundary Conditions in Angular Corners of Plates in Extension," Journal of Applied Mechanics, Vol. 19, TRANS. ASME Vol. 74, Summer 1952.
5. Opel, S.W., "Transition of Corner Cracks at Holes into Through-the-Thickness Cracks," Master's Thesis, Air Force Institute of Technology, Wright-Patterson AFB, OH, 1983.
6. Opel, S.W., Rudd, J.L. and Haritos, G.K., "Transition of Corner Cracks at Holes into Uniform Through-the-Thickness Cracks," Seventeenth National Symposium on Fracture Mechanics, ASTM STP xxx, J.H. Underwood, Ed., American Society for Testing and Materials, 1984, pp. xx-yy.
7. Collipriest, J.E., Jr. and Ehret, R.M., "Computer Modeling of Part-Through Crack Growth," SD 72-CE-0015B, Space Division, Rockwell Int'l. Corp., Downey, CA., October 1973.
8. Brussat, T.R., Chiu, S.T. and Creager, M., "Flaw Growth in Complex Structure," AFFDL-TR-77-79, Vol. I, Air Force Flight Dynamics Laboratory, September 1977.
9. Newman, J.C., Jr. and Raju, I.S., "Stress Intensity Factor Equations for Cracks in Three-Dimensional Finite Bodies," NASA Technical Memorandum 83200, National Aeronautics and Space Administration, August 1981.

10. Grandt, A.F., Jr., "Stress Intensity Factors for Some Through-Cracked Fastener Holes," Seventh National Congress of Applied Mechanics, University of Colorado, June 1974.
11. Engle, R.M., Jr., "CRACKS II User's Manual," Technical Report AFFDL-TM-74-173, Wright-Patterson AFB, OH, July 1974.
12. Bowie, O.L., "Analysis of an Infinite Plate Containing Radial Cracks Originating at the Boundary of an Internal Circular Hole," Journal of Mathematics and Physics, Vol. 35, 1956, pp. 60-71.
13. Liu, A.F., "Stress Intensity Factor for a Corner Flaw," Engineering Fracture Mechanics, Vol. 4, 1972, pp.175-179.
14. Smith, F.W., Emery, A.F. and Kobayashi, A.S., "Stress Intensity Factors for Semicircular Cracks," Journal of Applied Mechanics, Vol. 34, December 1967.
15. Kobayashi, A.S. and Moss, W.L., "Stress Intensity Magnification Factors for Surface-Flawed Tension Plate and Notched Round Tension Bar," Fracture 1969, Chapman and Hall, London, 1969.
16. Tweed, J. and Rooke, D.P., "The Distribution of Stress Near the Tip of a Radial Crack at the Edge of a Circular Hole," International Journal of Engineering Science, Vol. 11, 1973, pp. 1185-1195.
17. Rice, J.R., "Some Remarks on Elastic Crack-Tip Stress Fields," International Journal of Solids and Structures, 6 June 1972, pp. 751-758.
18. Paris, P.C. and Sih, G.C., "Stress Analysis of Cracks, Fracture Toughness Testing and its Applications, ASTM STP 381, American Society for Testing and Materials, 1965, pp. 30-81.
19. Kullgren, T.E, Smith, F.W. and Ganong, G.P., "Quarter Elliptical cracks Emanating From Holes in Plates," Journal of Engineering Materials and Technology, Vol. 100, April 1978.
20. Browning, W.M. and Smith, F.W., "An Analysis for Complex Three-Dimensional Crack Problems," Proceedings of the Eighth Southeastern Conference on Theoretical and Applied Mechanics, Blacksburg, VA., 1976.

21. Kullgren, T.E. and Smith, F.W., "Part-Elliptical Cracks Emanating From Open and Loaded Holes in Plates," Journal of Engineering Materials and Technology, Vol. 101, January 1979.
22. Howland, R.C.J., "On the Stresses in the Neighbourhood of a Circular Hole in a Strip Under Tension," Philos. Trans. Royal Society, London, Series A, Vol 229, January 1930.
23. Tada H., Paris, P.C. and Irwin, G.R., "The Stress Analysis of Cracks Handbook," Del Research Corporation, 1973.
24. Hall, L.R., Shah, I.S. and Engstrom, W.L., "Fracture and Fatigue Crack Growth Behavior of Surface Flaws and Flaws Originating at Fastener Holes," AFFDL-TR-74-47, Vol. I, Air Force Flight Dynamics Laboratory, Wright-Patterson AFB, OH., May 1974.
25. Heckel, J.B and Rudd, J.L., "Assessment of Stress Intensity Factors for Corner Cracks at Holes," AFWAL-TM-82-201-FIBE, Wright-Patterson AFB, OH, August 1982.
26. James, L.A. and Anderson, W.E., "A Simple Experimental Procedure for Stress Intensity Calibration," Engineering Journal of Fracture Mechanics, Vol. 1, No. 3, April 1969, pp.565-568.
27. Schijve, J., "Interpolation Between Calculated Stress-Intensity Factors of Semi- and Quarter Elliptical Cracks," Dept. of Aerospace Engineering Report LR-368, Delft University of Technology, Delft, The Netherlands, January 1983.
28. Raju, I.S. and Newman, J.C., Jr., "Stress-Intensity Factors for a Wide Range of Semi-Elliptical Surface Cracks in Infinite Plates," Engineering Fracture Mechanics, Vol. 11, 1979, pp. 817-829.
29. Raju, I.S. and Newman, J.C., Jr., "Stress Intensity Factors for Two Symetric Corner Cracks," ASTM STP 677, American Society for Testing and Materials, 1979, pp. 411-430.
30. Chang, J.B., editor, Part-Through Crack Fatigue Life Prediction, ASTM STP 687, American Society for Testing and Materials, October 1979.

31. Peterson, D.E. and Vroman, G.A., "Computer-Aided Fracture Mechanics Life Prediction Analysis," Part-Through Crack Fatigue Life Prediction, ASTM STP 687, J.B. Chang, Ed., American Society for Testing and Materials, 1979, pp. 129-142.
32. Forman, R.G., Kavanaugh, H.C. and Stuckey, B., "Computer Analysis of Two-Dimensional Fatigue Flaw-Growth Problems," NASA Technical Memorandum TMX-58086, NASA Manned Spacecraft Center, Houston, TX. 1972.
33. Paris, P.C., The Growth of Cracks Due to Variations in Load. PhD Dissertation. School of Engineering Mechanics, Lehigh University, Bethlehem, PA., September 1962.
34. Johnson, W. S., "Prediction of Constant Amplitude Fatigue Crack Propagation in Surface Flaws," Part-Through Crack Fatigue Life Prediction, ASTM STP 687, J. B. Chang, Ed., American Society for Testing and Materials, 1979, pp. 143-155.
35. Grandt, A.F. and Snow, J.R., "A Stress Intensity Factor Calibration for Corner Flaws at an Open Hole," AFML-TR-74-282, Air Force Materials Laboratory, Wright-Patterson AFB, OH., May 1975.
36. Heckel, J.B. and Rudd, J.L., "Evaluation of Analytical Solutions for Corner Cracks at Holes," Sixteenth National Symposium on Fracture Mechanics, American Society for Testing and Materials, Columbus, Ohio, August 1983.
37. Hartranft, R.J. and Sih, G.C., "An Approximate Three-Dimensional Theory of Plates with Application to Crack Problems," International Journal of Engineering Science, Vol. 8, No. 8, 1970, pp. 711-729.
38. Grimsley, F., "Crack Rate Analysis and Walker Equation Solver Using the Method of Least Squares (CRAWLS)," Technical Report AFWAL-TM-82-151-FIBE, Wright-Patterson AFB, OH, November 1981.
39. Walker, K., "The Effect of Stress Ratio During Crack Propagation and Fatigue for 2024-T3 and 7075-T6 Aluminum," Effects of Environment and Complex Load History on Fatigue Life, ASTM STP 462, M.S. Rosenfeld, Ed., American Society for Testing and Materials, 1970, pp.1-14.

40. Hudar, S.J. Jr., Saxena, A., Bucci, R.J. and Malcolm, R.C., "Development of Standard Methods of Testing and Analyzing Fatigue Growth Rate Data," AFWAL-TR-78-40, 1978.
41. Chang, J.B., Hiyama, R.M. and Szamosi, M., "Improved Methods for Predicting Spectrum Loading Effects - Final Report, Vol. I - Technical Summary," AFFDL-TR-79-3036, Rockwell International, May 1981.
42. Rudd, J.L., Private Communication, Air Force Flight Dynamics Laboratory, Wright-Patterson AFB, OH., 29 October 1984.
43. Chung, J.H., "Life Predictions for Corner-Cracks-at-a-Hole Considering Different Parametric Angles," Presentation at ASTM Task Group E24.06.01 Meeting for Analytical Round-Robin for Corner-Crack Solutions, Pittsburgh, PA., November 1983.
44. Wood, H.A. and Engle, R.M., Jr., "Damage Tolerant Design Handbook, Guidelines for the Analysis and Design of Damage Tolerant Aircraft," AFFDL-TR-79-3021, Air Force Flight Dynamics Laboratory, Wright-Patterson AFB, OH., March 1979.

VITA

Captain Phillip A. Chansler was born in Winter Haven, Florida on March 6, 1958. The son of an Air Force officer, William A. Chansler, LTC, USAF (Ret), he lived on military bases throughout the United States, England, and Japan. He graduated from Ann Arundel County High School in Gambrills, Maryland in June 1976. He received a Bachelor of Science degree in Mechanical Engineering from the University of Colorado, Boulder, Colorado in May 1980, and a Master of Science degree in Systems Management from the University of Southern California in December 1982. He received a commission through Air Force ROTC at University of Colorado and was assigned to the 6595th Shuttle Test Group, Vandenberg AFB, California. In March 1983, he attended Squadron Officer's School at Maxwell AFB, Alabama and was subsequently assigned to the Air Force Institute of Technology, Wright-Patterson AFB, Ohio to work on a Master of Science degree in Aeronautical Engineering. He will be assigned to the 6595th Shuttle Test Group Operating Location at Kennedy Space Center, Florida beginning January 1985.

Permanent address: 568 Williamsburg Lane
Odenton, Maryland 21113

6c. ADDRESS (City, State and ZIP Code) Air Force Institute of Technology Wright-Patterson AFB, Ohio 45433			7b. ADDRESS (City, State and ZIP Code)		
8a. NAME OF FUNDING/SPONSORING ORGANIZATION AFWAL/AFFDL		8b. OFFICE SYMBOL (If applicable) FIBEC	9. PROCUREMENT INSTRUMENT IDENTIFICATION NUMBER		
8c. ADDRESS (City, State and ZIP Code) See Box 6c			10. SOURCE OF FUNDING NOS.		
			PROGRAM ELEMENT NO.	PROJECT NO.	TASK NO.
			WORK UNIT NO.		
11. TITLE (Include Security Classification) See Box 19					
12. PERSONAL AUTHOR(S) Phillip A. Chansler, B.S., M.S., Capt, USAF					
13a. TYPE OF REPORT MS Thesis		13b. TIME COVERED FROM _____ TO _____		14. DATE OF REPORT (Yr., Mo., Day) 1984 December	
				15. PAGE COUNT 132	
16. SUPPLEMENTARY NOTATION					
17. COSATI CODES			18. SUBJECT TERMS (Continue on reverse if necessary and identify by block number)		
FIELD	GROUP	SUB. GR.			
20	11		Cracks		
			Crack Propagation		
			Cracking (Fracturing)...		

This study develops correction factors for currently used stress intensity factor equations to more accurately predict stress intensity factors for a corner-crack emanating from a hole as it transitions to a uniform through-the-thickness crack. These correction factors resulted in an increase in accuracy for total life prediction and much better correlation between analytical stress intensity factor predictions and experimental results in the transition region for 2024-T351 and 7075-T651 aluminum alloys. An experimental program was undertaken to generate all 2024-T351 aluminum test data used in this investigation. The 7075-T651 aluminum test data was generated during earlier work. Correction factors developed by Opel for 7075-T651 aluminum were evaluated for 2024-T351 aluminum and found to be excessively conservative.

Hartranft and Sih suggested the stress intensity factors be evaluated at an imaginary surface at an angle ϕ away from the front and hole-bore surfaces. These stress intensity factors could then be used in the life prediction models for life from a corner-crack until back surface penetration. Evaluating stress intensity factors at $\phi = 10^\circ$ and 80° eliminate surface boundary effects caused by fabrication processes like cold rolling and hole drilling, thereby improving life predictions to back surface penetration significantly. It is shown that with $\phi = 10^\circ$ and 80° , no other corrections are necessary for life prediction to back surface penetration.

A transition region is postulated to effect life prediction from back surface penetration until final fracture. Correlations were made between experimental results for 2024-T351 and 7075-T651 aluminum test data and the Grandt linearization of the Bowie solution for a through-the-thickness crack. These correlations were plotted from back surface penetration until final fracture. The plot yields the end of the transition region and the required correction factors. The life prediction model incorporating these transition correction factors are shown to be the most accurate and versatile of all models investigated.

Life predictions were made using the new model, an instantaneous model (which assumes a through-crack at back surface penetration), Opel's model, Brussat's model and the Collipriest-Ehret model.

END

FILMED

5-85

DTIC